Strong matter-light coupling with organic molecules and inorganic semiconductors

Artem Strashko

University of
St Andrews

This thesis is submitted in partial fulfilment for the degree of

Doctor of Philosophy (PhD)

at the University of St Andrews

July 2019

Candidate's declaration

I, Artem Strashko, do hereby certify that this thesis, submitted for the degree of PhD, which is approximately 22,000 words in length, has been written by me, and that it is the record of work carried out by me, or principally by myself in collaboration with others as acknowledged, and that it has not been submitted in any previous application for any degree.

I was admitted as a research student at the University of St Andrews in August 2015.

I received funding from an organisation or institution and have acknowledged the funder(s) in the full text of my thesis.

Date Signature of candidate

Supervisor's declaration

I hereby certify that the candidate has fulfilled the conditions of the Resolution and Regulations appropriate for the degree of PhD in the University of St Andrews and that the candidate is qualified to submit this thesis in application for that degree.

Date Signature of supervisor

Permission for publication

In submitting this thesis to the University of St Andrews we understand that we are giving permission for it to be made available for use in accordance with the regulations of the University Library for the time being in force, subject to any copyright vested in the work not being affected thereby. We also understand, unless exempt by an award of an embargo as requested below, that the title and the abstract will be published, and that a copy of the work may be made and supplied to any bona fide library or research worker, that this thesis will be electronically accessible for personal or research use and that the library has the right to migrate this thesis into new electronic forms as required to ensure continued access to the thesis.

I, Artem Strashko, confirm that my thesis does not contain any third-party material that requires copyright clearance.

The following is an agreed request by candidate and supervisor regarding the publication of this thesis:

Printed copy

No embargo on print copy.

Electronic copy

Embargo on all of electronic copy for a period of 1 year on the following ground(s):

- Publication would preclude future publication

Supporting statement for electronic embargo request

Some of the results presented in my thesis may be used for a journal publication

Title and Abstract

- I agree to the title and abstract being published.

Date Signature of candidate

Date Signature of supervisor

Underpinning Research Data or Digital Outputs

Candidate's declaration

I, Artem Strashko, understand that by declaring that I have original research data or digital outputs, I should make every effort in meeting the University's and research funders' requirements on the deposit and sharing of research data or research digital outputs.

Date Signature of candidate

Permission for publication of underpinning research data or digital outputs

We understand that for any original research data or digital outputs which are deposited, we are giving permission for them to be made available for use in accordance with the requirements of the University and research funders, for the time being in force.

We also understand that the title and the description will be published, and that the underpinning research data or digital outputs will be electronically accessible for use in accordance with the license specified at the point of deposit, unless exempt by award of an embargo as requested below.

The following is an agreed request by candidate and supervisor regarding the publication of underpinning research data or digital outputs:

Embargo on all of electronic files for a period of 1 year on the following ground(s):

- Publication would preclude future publication

Supporting statement for embargo request

Some of the digital outputs may be used for a journal publication

Title and Description

- I require an embargo on the title and description

Date Signature of candidate

Date Signature of supervisor

Abstract

This dissertation studies the effects of strong matter-light coupling on properties of organic molecules and inorganic semiconductors. The interplay of complex intramolecular dynamics and strong coupling of a photon to molecular transitions results in new physics having no counterparts in other systems. In contrast, low-energy optically active excitations of semiconductors (excitons) usually do not feature such complexity. However, the combination of strong electronic correlations and strong matter-light coupling leads to new physics.

Firstly, the effect of strong coupling between molecular vibrations and infrared photons on Raman scattering (RS) is considered. This is motivated by the experiment of Ref. [1] showing up to 10^3 enhancement of RS signal under strong coupling. While the exact analytical results of this dissertation predict around 100% enhancement of total RS signal, they cannot explain orders of magnitude enhancement, leaving the question open for further studies.

Next, the effects of strong coupling of an optical photon and a molecular electronic transition on molecular lasing properties are discussed. Starting from a microscopic description of a driven–dissipative system, an exact (in the thermodynamic limit) mean-field solution is developed. It allows to uncover the mechanism of molecular lasing in the weak and strong coupling regime and to obtain a non-equilibrium lasing phase diagram.

Finally, a semiconductor with different densities of electrons and holes, strongly coupled to a microcavity photon, is studied. While finite electron–hole density imbalance is detrimental for excitonic condensation, it may still lead to a condensed state of excitons with finite centre of mass momentum coexisting with unpaired electrons. On the other hand, due to its low mass, a photon favours zero center of mass momentum condensation. The variational mean-field calculations reveal that the interplay of these effects leads to a variety of novel states with coexisting polariton condensate and unpaired electrons.

Acknowledgements

Over the last four years I have had a great privilege, luck and pleasure to work under supervision of Jonathan Keeling, to whom I wish to express my sincere gratitude. I want to thank him for his incredible support, patience, advice, always having time for me, comprehensive emails and in-person discussions, for rigorous scientific approaches, for his remarkable QFT lectures, and for opening a door to the world of numerical physics for me.

I would like to thank Peter Kirton for his invaluable support with scientific computing and for discussing physics with me. I would also very much like to acknowledge my close friend Alexander Katrutsa who helped me with Python and LaTeX so much. I also want to express my gratitude to the Stack Exchange community, which helps me to resolve most of computing issues I have.

This all would not be possible without the priceless support from EPSRC, which allowed me to work in live in this wonderful country, to visit so many different places and to meet such amazing people. This experience shaped and reshaped my personality, allowed me to open my eyes wider and to change my mind about many questions, made me much more flexible in science and beyond. I wish to express my gratitude to the administrators of CDT, particularly to Julie Massey, Christine Edwards, Wendy Clark and Debra Thompson, who made me forget what bureaucracy is and were always ready to help with any issues.

Over my PhD I have also had a remarkable opportunity to stay in Madrid working with Francesca Marchetti, to whom I wish to express my gratitude for hosting me, discussing the physics and making my visit so enjoyable. I also want to thank Allan MacDonald, who visited us in St Andrews and hosted us in Austin, for his advise and long thorough discussions of physics, from which I leaned a lot.

My experience would not be so enjoyable without other St Andrews PhD students and postdocs, whom I also want to thank, particularly Veronika Sunko, Maja Bachmann, Scott Taylor, Michael Lynch-White, Rhea Stewart, Dainius Kilda, Kristin Arnardottir and Peter Kirton.

I wish to thank my teachers from MIPT, particularly Alexey Barabanov, Yakov Fominov, Nikolay Kirichenko and Andrey Gavrikov for their amazing lectures, invaluable seminars and particularly for sharing their passion for physics. I want to thank my MIPT friends, with whom we went through MIPT

challenges and had a lot of fun together, particularly Alexander Gagloev, Evgeniy Gaiduk, Matvey Pochechuev, Anton Baranikov, Timur Yagafarov, Maria Usoltseva and Alexander Katrutsa. I also want to thank my school physics teacher Elena Yanovskaya, who ran additional physics classes attended by my school friend and myself only, for teaching us to solve difficult problems, for her patience and guidance, and for friendship we have since then.

Finally, I would particularly like to thank my family, my parents for their love and continuous support. I would like to give my special thanks to my wife Sofia, who has been my love, colleague and my closest friend for the last ten years, for her love, for her support, for sharing my happiness, for her understanding of how much science requires. I would also like to thank her for adding another layer of meaning and joy to our life — for our daughter Alice.

Funding

This work was supported by the Engineering and Physical Sciences Research Council, the Scottish Doctoral Training Centre in Condensed Matter Physics (grant number EP/L015110/1).

Research Data

Research data underpinning this thesis are available at:

https://doi.org/10.17630/e8d899d3-7c86-4919-8076-5e7ea746e5cf

Contents

Chapter 1

Introduction

Nature generously supplies us with new materials which demonstrate unusual properties, set up new challenges, widen our knowledge horizons and sometimes lead to technological advances. However, the search for material with desired properties is not a trivial task, which requires extensive theoretical calculations, a lot of experimental data and statistical analysis (for example [2]) to guide the hunt. A recent triumph of finding a material with unprecedented properties was the discovery of a topological insulator [3], which was preceded by theoretical calculations [4].

A different approach to obtain new material properties is to engineer them by means of external handles. For example, lowering temperature led to the discovery of superconductivity [5], application of high pressure — to almost room T_c superconductivity [6], application of strong magnetic field to a two-dimensional electron gas — to the Quantum Hall Effect [7, 8]. More recent examples include Floquet Engineering [9] of material properties and driving by strong laser pulses, leading, for example, to transient superconducting-like states [10, 11]. However, the last two approaches suffer an ubiquitous problem of heating, which seems to be the main problem for practical long time-scale applications. In contrast, strong coupling of material excitations to quantum light does not have such an issue.

Recent experimental advances in fabrication of optical microcavities opened up an avenue to study how strong coupling of light to excitations of matter can affect various material properties [12, 13]. A list of already experimentally demonstrated effects includes polariton-assisted chemistry [14–16], modified magneto-transport of two-dimensional electron gas in magnetic field [17, 18], enhanced conductivity of an organic semiconductor [19], polaritonically-enhanced Förster energy transfer [20, 21], room-temperature polariton condensation (lasing) [22, 23] and superfluidity [24], polaritonically-enhanced Raman scattering [1].

It is the aim of this thesis to model some of these experimental systems and extend the list of effects driven by strong coupling of light and mate-

rial excitation. Chapters 2 and 3 concern the effects of strong-matter light coupling on properties of organic molecules featuring strong coupling between their intramolecular electronic and vibrational excitations (which will be called exciton-vibron coupling), while Chapter 4 discusses how a phase diagram of an imbalanced electron-hole system is affected by strong coupling of an excitonic transition to a photon.

In particular, Chapter 2 discusses how strong matter-light coupling between an infrared cavity photon and intramolecular vibrons affects Raman scattering with organic molecules [25], which is motivated by the experiment [1]. In contrast to the experimental results, which showed three orders of magnitude enhanced Raman scattering under stong matter-light coupling, the results of theoretical modeling show only a moderate enhancement of Raman scattering in the ultra-strong matter-light coupling regime matching the outcomes of other theoretical calculations [26].

Next, Chapter 3 considers a similar system of organic molecules in a microcavity and discusses the effects of strong coupling between a microcavity photon and electronic excitations of molecules, which also feature strong exciton-vibron coupling. This chapter is motivated by experiments on exciton-polariton lasing (condensation) with organic molecules, e.g. [22, 23], and aims to understand the microscopic mechanism of polariton lasing, how it depends on the various system parameters, and to uncover the connection between an ordinary dye laser operating in a weak matter-light coupling regime and a more exotic polaritonic laser. This chapter presents the exact (in the thermodynamic limit) non-equilibrium phase diagram of a system of organic molecules strongly coupled to a single photon mode. It shows a smooth transition from a usual dye laser to a strongly-coupled polariton laser, and so for the first time explains the physics of organic polariton lasing [27].

The final chapter, Chapter 4, discusses a more conventional setup of semiconductor Wannier-Mott excitons coupled to microcavity photons. The new physics discussed in this chapter comes from considering a charged (imbalanced) semiconductor with tunable electron and hole density difference set up by applying bias voltage akin to a field-effect transistor (FET). This chapter predicts and discusses new phases emerging from the interplay of polaritonic physics and charge imbalance. It shows how the new phases compete and intertwine with each other upon tuning experimentally-controlled parameters such as temperature, photon cutoff frequency and charge density, thus enriching the physics of imbalanced correlated many-body systems due to additional photon-mediated interaction, which has no counterparts in more conventional setups such as (imbalanced) superconductors in a strong magnetic field.

The remainder of the current chapter introduces these topics in more detail. Section 1.1 discusses the physics of Raman scattering, Section 1.2 concerns polariton lasing with organic molecules, and Section 1.3 discusses condensation of imbalanced Fermi-systems and conventional polaritonic condensation with inorganic semiconductors.

1.1 Raman scattering

Raman scattering (RS) spectroscopy is a powerful technique to address (usually infrared) transitions, which are not optically active. For example, it is widely used to study low-lying ro-vibrational molecular levels [28]. It can be also used to probe optically forbidden single-band excitations of superconductors [29].

The physics of Raman scattering is straightforward and can be summarized by a single formula for a transition amplitude between two states via an infinite number of virtual states, which follows from the second order perturbation theory [30] and reads:

$$f_{eg} = \sum_n \frac{\langle g|V|n\rangle\langle n|V'|e\rangle}{E_n - (E_g + \hbar\omega)}. \tag{1.1}$$

In this expression $|g\rangle$ stands for the ground (initial) state, which may represent, for example, a molecule in its ground electronic and vibrational state and a photon before it gets absorbed, thus $E_g + \hbar\omega$ is the energy of this state. Next, $|n\rangle$ is an intermediate excited state (after photon absorption) with energy E_n, and $|e\rangle$ is the final state, which may correspond to, e.g. a vibrationally excited state of a molecule in the ground electronic state. In this expression V is a matter-light coupling term, while $V' = \alpha V$ with α is some numerical prefactor which depends on polarisation of an emitted photon.

Due to naturally small matter-light coupling strength and a two-photon nature of the RS process (1.1), in linear spectroscopy RS signal is usually rather weak, which thus required long signal collection in pioneering RS experiments. This led to the development of various non-linear RS enhancement techniques [31] such as resonant RS, where excitation laser wavelength is tuned close to energy of some electronic transition, or stimulated RS, where a transition from excited to a final state is stimulated by another laser beam, or coherent anti-Stokes RS, where two lasers are used to drive both transition from the ground to excited and from the excited to the final states. Another technique is to put molecules close to metallic surface and so to employ the effect of strong surface plasmon electric field (usually called surface-enhanced RS) [31–34].

In many experimental works, strong coupling of an infrared (IR) microcavity photon and a molecular vibrational mode was demonstrated [35–39] and then in Ref. [1] a fundamentally new method to enhance RS was discovered, which, in contrast to the techniques discussed above, is not based on resonant excitation of molecules, on any fine-tuned laser driving or strong (plasmonic) surface field effects. The effect demonstrated in Ref. [1] is claimed to originate from strong coupling of an infrared photon and a molecular vibron only (i.e. from formation of vibron-polariton). Although this requires a vibrational transition to be active both in RS and IR (and also strong enough IR absorption and emission to allow strong matter-light coupling), thus hardly motivating

such a setup for a linear RS spectroscopy, nevertheless it provides an example of how single molecule properties may be tuned by collective strong coupling, i.e. by engineering the properties of environment (microcavity). Therefore, the nature of this effect is of fundamental interest.

Let us now discuss the experiment of Ref. [1] in more detail. The experiment of Ref. [1] demonstrated that when molecules are placed into an infrared microcavity, the formation of vibron-polaritons leads to peculiar consequences in Raman scattering (RS). Particularly, the Raman transition signal from the scattering between the ground and the first vibron excited state splits between scattering to lower and upper vibron-polariton states. Also, quite surprisingly, Rabi splitting in RS signal turned out to be about twice larger than in IR absorption measurement. However, the most remarkable result of that experiment is the enhancement of the total RS cross-section by up to 3 orders of magnitude in the strong coupling regime. To prove that this effect originates from strong matter-light coupling only, experiments were performed with and without an upper mirror. While in a microcavity strong RS enhancement was observed, without an upper mirror no notable enhancement was detected. Also, when a cavity photon was out of resonance with the molecular vibrational transition (and so when strong coupling was not achieved), no enhancement was observed as well. For these reasons it was then concluded that this effect occurs due to strong light-matter coupling only.

To understand the nature of this remarkable effect, we [25] and a group in Madrid [26] proposed and solved similar models resulting in the same conclusion that vibron-polariton formation does lead to redistribution of RS signal between upper and lower polaritons, but does not lead to any notable enhancement of RS cross-section even under artificially ultra-strong matter-light coupling. In both papers [25, 26] the electronic excitation of a molecule was treated as a two-level system, while a local molecular vibrational mode (vibron) — as an harmonic oscillator; strong coupling of a fundamental cavity mode and a molecular vibron was the considered in both papers. In our paper [25] we derived an exact analytical expression for the probability of Raman scattering at any strength of matter-light coupling with an arbitrary number of molecules. We showed that RS probability to the upper polariton goes down and to the lower polariton goes up under increasing polariton Rabi splitting, thus concluding that RS enhancement or reduction originates from the softening or "hardening" of the final mode respectively. While we did find around 100% overall enhancement of RS signal at reasonable experimental conditions, our results do not show more than three time RS enhancement even at currently experimentally impossible matter-light coupling, which is far below the $10^2 - 10^3$ enhancement reported in [1]. In the paper [26] a different approach based on numerical solution of a small driven-dissipative system (with the same system Hamiltonian) was employed. While the authors considered a system of only a few molecules below ultra-strong coupling, they did consider not only Hamiltonian, but also driven-dissipative dynamics. However, their

results are basically identical to ours.

Overall, the current conclusion is that we do not understand the giant polaritonic RS enhancement observed in [1] and so we need a better theory and more experimental checks. However, while two theoretical papers already exist [25, 26], the giant polaritonic RS enhancement was reported in literature only once — although with quite convincing details — in one particular setup [1] in 2015, which thus hardly motivates further theoretical investments.

Chapter 2, which is based on the results of Ref. [25], discusses the model and the solution in details, showing how RS scattering probability evolves from weak to ultra-strong vibron-photon coupling.

1.2 Polariton lasing

Bose-Einstein statistics is a necessary ingredient of Bose-Einstein condensation [40], which leads to remarkable phenomena such as superconductivity, superfluidity and lasing. Examples of quantum condensates span from liquid $He_{3,4}$, superconductors, magnons [41, 42], cold atoms [43] to excitons [44], Quantum Hall excitons in double-layer structures in strong magnetic fields [45], exciton-polaritons in inorganic semiconductors [22] and organic molecules [22, 23] and even photons [46].

Bosonic condensation usually requires low temperature to prevent thermal depletion of a condensate or ionization (unbinding) of composite bosons (such as Cooper pairs or excitons) and to allow strong overlap of De Broglie waves of constituent bosons. The most prominent example is the condensation of cold atoms, which requires temperatures as low as nano-Kelvins. In contrast, exciton-polaritons (which are superpositions of a photon and an optically-active matter excitation) in organic materials allow to reach condensation even at room temperatures [22], which is not surprising due to large polariton de Broglie wavelength (because of small mass of a photon) and strong binding energy of excitons in organic molecules. Moreover, from the observed experimental results it is seen that low temperature may even prevent condensation of polaritons in organic materials by suppressing thermalisation due to freezing out of low-energy degrees of freedom, while high temperature activates them and allows thermalisation leading to condensation at high enough density of polaritons [22].

The manifestations of polariton condensation is straightforward: it is the development of spatial and temporal coherence and non-linear increase of photon emission, which signals emergence of a condensate [22, 47]. Condensation is known to break the U(1) symmetry, which then leads to increased spatial coherence, seen via fringes in interferometric pictures of a polariton cloud. The fact that in a condensed regime a single mode is macroscopically populated readily leads to very narrow emission spectrum, i.e. to temporal coherence. Another manifistation of polariton condensation is the appearance of vortices

[48] (which can be seen as dislocations in interferometric pictures), which try to restore the U(1) symmetric state. Until recently, a blue shift of emission has been believed to be another signature of condensation in organic materials and has been associated with repulsive interaction of a macroscopically large number of excitons. However, it is now clear that a blue shift in organic polaritons originates simply from the reduction of polariton Rabi splitting upon increasing pumping [49, 50], which happens far below the value of external pumping required for polariton condensation.

In spite of numerous experiments on exciton-polariton condensation (or lasing) with organic materials [22, 23, 47, 51–54], until recently a detailed picture of the microscopic nature of organic polariton condensation (lasing) mechanism has not been understood. A relatively widely accepted story of polariton condensation is that as soon as the number of the lowest energy polaritons exceeds some critical value, it stimulates scattering of polaritons from a reservoir, thus leading to low-threshold polariton condensation, which does not require electronic inversion, in contrast to ordinary optical lasers. The role of molecular vibrons in the process of polariton condensation with organic molecules is believed to assist scattering from a reservoir to the lowest energy polariton mode.

Although this story sounds reasonable, it immediately leads to a number of questions. For example, how does an ordinary laser at weak matter-light coupling, which requires inversion, transform to a polaritonic laser, which is believed to be inversionless? Is there a continuous or an abrupt transition between these two regimes? Also, if a molecular vibron is strongly coupled to an electronic transition (local intramolecular exciton), then it cannot be considered perturbatively (i.e. as a polariton scattering-assisted mechanism only), while it must be treated on equal footing with a molecular exciton coupled to a cavity photon, i.e. a full strongly-coupled driven-dissipative vibron-exciton-photon system must be considered. Another question is how to optimise the system parameters, such as exciton-photon detuning and polariton Rabi splitting to have as low-threshold lasing as possible? And does a polariton laser really outperform an ordinary laser in terms of pumping threshold as widely believed?

To answer these questions, standard macroscopic approaches used in the physics of polariton condensates based on the complex Gross-Pitaevskii (GP) equation [12, 55, 56], which describes evolution of polariton condensate density under pumping, decay along with a phenomenological polariton-polariton interaction (which is usually of contact type), are not adequate. Indeed, a phenomenological GP equation is universal for any condensates independently on their microscopic details because microscopic degrees of freedom are integrated out and phenomenologically included in different incoherent processes to model condensate dynamics.

In contrast, our aim here is to describe the dynamics of a strongly coupled vibron-exciton-photon system under different incoherent mechanisms, to study

the interplay of coherent and incoherent dynamics, to uncover lasing mechanism from weak to strong matter-light coupling, in other words going from photon to polariton lasing, where the very nature of a condensate changes. Therefore, a fully miscroscopical approach is required.

Chapter 3, which is based on the results of Ref. [27], introduces a microscopic model of N molecules in a microcavity, where each molecule has a single electronic transition (intramolecular exciton) and a vibron (local intramolecular vibrational mode) strongly coupled to an exciton. All molecules are coupled to a single cavity mode via their electronic transition. Incoherent processes are included within the Markovian second-order perturbation theory, conventionally written in terms of a Lindblad master equation [57] for a system (vibron-exciton-photon) density matrix. The reminder of Chapter 3 provides an exact (in the thermodynamic limit $N \to \infty$) solution of this model and for the first time answers all the questions outlined above.

1.3 Imbalanced polariton condensates

1.3.1 Fermionic pairing

The ground state of non-interacting electrons (and, in general, fermions) is a Fermi sea, where electrons occupy all states with energies below the Fermi energy E_F. In the second quantized notation, the Fermi sea state is $|FS\rangle = \prod_{k<k_F} c^\dagger_{k\uparrow} c^\dagger_{k\downarrow}|0\rangle$, where $|0\rangle$ is a fermionic vacuum, i.e. $c_k|0\rangle = 0, \forall k$ and $k_F = \sqrt{2mE_F/\hbar^2}$ — Fermi momentum (m is a particle mass). However, arbitrary small interaction is enough to make a Fermi sea unstable and induce superconductivity (the Kohn-Luttinger argument [58]), which — at the mean-field level — is described by the BCS wavefunction

$$\prod_k (u_k + v_k c^\dagger_{k\uparrow} c^\dagger_{-k\downarrow})|0\rangle, \tag{1.2}$$

which is believed to work well in both strong and weak interaction limits [59]. The phenomenon of fermionic pairing and condensation is universal and goes far beyond electronic superconductivity, spanning condensation of pairs of cold atoms [60], liquid He_3 [61], color superconductivity in high-energy physics [62], exciton condensation [44], Quantum-Hall exciton condensation [45], and condensation of exciton-polaritons in microcavities [63]. However, independently on the microscopic nature of interacting fermions, the mean-field ground state is described by the same wavefunction (1.2). For example, the condensed state of excitons in a semiconductor with a conduction and a valence band is $\prod_k (u_k + v_k e^\dagger_{k,c} e_{k,v})|0\rangle$, where $e_{c/v}$ annihilates an electron in a conduction or a valence band. Making a particle-hole transformation of electrons in the valence band, this can be rewritten as $\prod_k (u_k + v_k e^\dagger_k h^\dagger_{-k})|0\rangle$, which is formally identical to the BCS wavefunction (1.2). This is why the

description of excitons in semiconductors and Cooper pairs in superconductors is formally identical. The mean-field wavefuntion of a quasi-equilibrium condensate of polaritons has one extra component, namely a coherent state of a photon: $e^{\lambda a^\dagger}\prod_k(u_k + v_k e_k^\dagger h_{-k}^\dagger)|0\rangle$ [64].

1.3.2 Imbalanced condensates

While the physics of a simple condensed state is relatively well understood, the interplay of fermionic condensation, e.g. superconductivity, with other possible states, such as charge or magnetically ordered states, is a broad and vibrant subject of ongoing research. Of particular interest is the possibility of tuning states of matter externally by such standard means as chemical doping and cooling [65] widely used in the field of high T_c superconductors, or by tuning an external electric field [66], by more recent techniques as laser pulse excitation [10, 67], or by recently proposed strong matter-light coupling for changing matter properties (e.g., [68–71]).

A well known example of changing an ordered state of electrons is application of a strong magnetic field to a superconductor. Its effect can be modeled by a term $h\sum_k(c_{k\uparrow}^\dagger c_{k\uparrow} - c_{k\downarrow}^\dagger c_{k\downarrow})$, which favours a polarised state with all electrons spins pointing along the applied field, i.e. it makes a system spin-imbalanced. Strong enough magnetic field breaks superconductivity, thus bringing a system from a superconducting to a normal state, which is probably the last thing one wants to do. Fortunately, this is not the end of the story. Finite imbalance introduces frustration to the system and before ending up in a normal state, the system adjusts itself to stay partially coherent, i.e. to have finite density of paired electrons, and at the same time to accommodate finite density of unpaired electrons. The most prominent candidate of such state is a so-called FFLO (Fulde-Ferrel-Larkin-Ovchinnikov) state [72, 73], which has finite density of paired electrons with finite centre of mass pairing momentum (or a superposition of pairing momenta) and also unpaired electrons. This state is proposed to be the ground imbalanced condensed state in many different contexts ranging from superconductors and imbalanced QCD systems [74] to cold atoms [75, 76] and bi-layer excitons [77]. Due to simultaneously present bosonic (fermionic pairs) and fermionic (unpaired fermions) degrees of freedom, the FFLO state can be considered as a Bose-Fermi mixture, which beyond mean-field fate is yet to be explored, although considerable steps have been made [78, 79].

A new platform for studying imbalanced condensates is currently emerging from a recently developed system of electrically biased semiconductor monolayers (a field-effect transistor with a grounded layer being the "system") in optical microcavities [80–84], which will allow to experimentally access the physics of imbalanced exciton and exciton-polariton condensates. The phase diagram of an imbalanced exciton-polariton system is expected to be much different from, e.g. a phase diagram of a superconductor in magnetic field or an

imbalanced system of fermionic cold atoms, due to strong long-range Coulomb interaction and extra photon-mediated interaction. Due to low mass of a photon, imbalanced polariton condensates with pairing wavevector near zero may also be stable at large temperatures akin to a usual polaritonic condensate.

1.3.3 Polaritonic Bose-Fermi mixtures

While in the field of excitons and exciton-polaritons in inorganic semiconductors, mostly balanced electron-hole systems have been studied, there are a few notable exceptions. Firstly, there is the Fermi-Edge singularity (FES) effect in doped semiconductors, which manifests itself in strongly enhanced spectral function of electrons near conduction bang edge, thus leading to an absorption peak at corresponding interband transition (rather than vanishing or constant absorption in 3D and 2D respectively) [85–88]. Secondly, there is the physics of trions (bound states of an exciton and an electron or hole) which has been discussed in the context of doped or biased semiconductors [89–92]. Thirdly, in a pioneering experiment [80] it was shown that dressing of exciton-polaritons by itinerant electrons in biased semiconductors leads to the formation of Fermi-polaron-polaritons. It is not difficult to see that all the phenomena mentioned above originate from precisely the same system, which is an imbalanced semiconductor (with unequal densities of electrons and holes) and so they probably discuss the same physics using different language. Therefore, to understand the physics of imbalanced polaritonic systems and so to be able to reliably predict new effects, it is of great importance to develop a unified approach to these systems and then to systemise the language of this field to get rid of the present confusion.

On the other hand, the ground state of a strongly enough (but not too strongly) imbalanced fermionic system is known to be the FFLO state. However, so far the transition from the FES/trion/polaron regime to an FFLO regime is not well understood (although the first step has been recently made [93]), so these phenomena remain relatively disconnected. It is the aim of future theory and experiments to unify them.

Another proposal of polariton-electron Bose-Fermi mixtures includes the effects of interaction of polariton condensate in one semiconductor layer with a two-dimensional electron gas (2DEG) in another layer. There are theoretical works showing that such a setup can be used to drive high T_c (up to room temperature) superconductivity in 2DEG [94, 95]. On the other hand, there is a paper showing the formation of a supersolid in the polaritonic subsystem [96]. A recent paper [97] (devoted to unify these phenomena) showed that superconductivity in 2DEG and supersolidity in polaritonic condensate are closely intertwined and that superconducting T_c is expected to be of the order of a few kelvins, which also suggests that non-self-consistent approaches applied in Ref. [94, 95] may overestimate T_c.

1.3.4 Imbalanced polariton condensates

It is the aim of Chapter 4 to provide a firm foundation for studies of imbalanced (with different densities of electrons and holes) polaritonic systems, which belong to a more general class of Bose-Fermi mixtures. Particularly, an electrically biased layer of a semiconductor in a microcavity is considered and then a finite temperature mean-field phase diagram of an imbalanced polariton system is obtained. On the one hand, a number of different phases are presented, switching between which may be done by tuning temperature, applied voltage or changing the distance between microcavity mirrors. On the other hand, a mean-field phase diagram covers a wide range of system parameters within a single approach and so for the first time provides a clear map to study the effects of fluctuations (e.g., such as polaron dressing of polaritons or emergence of new phases) and interplay between different phases in search of new effects in imbalanced polaritonic condensates.

Chapter 2

Raman scattering with strongly coupled vibron-polaritons

The calculations presented in this section are inspired by the experiment [1], where a new technique of increasing Raman scattering (RS) based on strong coupling of a cavity photon and molecular vibration mode (vibron) was proposed. This new effect is fundamentally different from the known ways of enhancing RS, such as plasmonic (near-field) assisted RS [32, 33], Purcell-enhanced scattering [98] or stimulated RS [31], as it is based on matter-light hybridization rather than on various kinds of stimulated emission.

In the experiment [1] polyvinyl acetate (PVAc) molecules, which have a symmetric CO bond stretching frequency at 215 meV (wavelength 5.7 μm), were used. The choice of molecules is motivated by the fact that their CO vibrational transition is strong and active both in infra-red (IR) absorption and in RS. This allowed to perform two different measurements to characterise the system. To study the physics of strong coupling, these molecules were embedded into an Ag metal-metal cavity with fundamental frequency in or out of resonance with a molecular vibron.

The results of IR absorption measurements demonstrated strong coupling of light with molecular vibrons, i.e. formation of lower and upper vibron-polariton modes. While polaritonic Rabi splitting was also detected in the RS signal, it turned out to be around two times larger than in the IR measurements. The most striking and unexpected consequence of strong coupling was a giant enhancement (around three orders of magnitude) of the total RS cross section.

It is the aim of this section to model polariton-enhanced Raman scattering. Section 2.1 introduces the model and discusses Hamiltonian eigenstates. Section 2.2 presents the details and results of Raman scattering calculations in the rotating wave approximation (RWA) when matter-light coupling is not

very strong, while Section 2.3 presents ultra-strong coupling generalisation and dependence of vibron frequency on the electronic state. In Section 2.4 the results of the probability of Raman transition to final higher-excited states are discussed.

The results of calculations show only moderate enhancement of scattering to the lower polariton mode and suppression of scattering to the upper one. While this conclusion agrees well with the results of numerical modelling [26], which takes into account incoherent dynamics, it strongly contradicts the experimental results [1]. Therefore, the question of the origin of the observed effect remains open. The fact that the results [1] are the only existing results of polariton-enhanced RS since 2015 is warning and so hardly motivates further theoretical efforts.

2.1 RWA Hamiltonian and its eigenstate structure

The experimental setup — a cartoon of which is presented in Fig. 2.1(b) — consists of a microcavity containing molecules at the center. To model the physics of strong coupling, we consider only a single cavity mode, which is in resonance (or close to resonance) with a vibron transition of a molecule. In each molecule only the ground and the first excited electronic states are taken into account, which leads to a two-level system description of an electronic subspace. This assumption is reasonable if other transitions are far from the resonance with the frequency of excitation laser light and are not strongly couple to light. Both conditions are usually satisfied experimentally. Vibrational excitation of a molecule is modeled by a single bosonic mode. Although nuclear potential is not parabolic in general, which leads to anharmonicity and so a dense level structure near ionization level, in the vicinity of potential minimum it may replaced by a simple parabola. This simplification is reasonable because the physics we want to explore is apparently (and as will be shown below) dominated by the lowest vibrational states. On top of this, this assumption allows to obtain closed-form results for scattering probabilities and so to gain deeper understanding of the model. The assumption of a single vibrational mode is also reasonable as in a typical experimental absorption or emission spectra may be well modeled using a single vibronic mode, which is strongly coupled to an electronic transition. The effect of other weakly coupled molecular vibrations may taken into account phenomenologically by introducing electronic state dephasing and thermalisation of a strongly coupled vibrational mode [26] within a master equation approach. Also, assuming that direct molecule-molecule coupling is much weaker than cavity-enhanced exciton-photon coupling, the former is neglected. This assumption is reasonable for molecules which do not have a static dipole moment, thus which interact via Van der Waals potential.

Starting from the rotating wave approximation with respect to a cavity

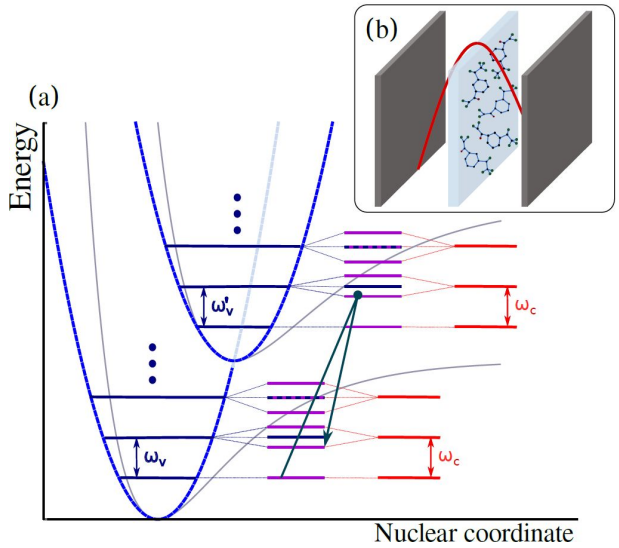

Figure 2.1: a) Energy diagram of coupled vibron-photon system, b) System cartoon

mode and vibration excitation interaction, the Hamiltonian reads

$$H = \omega_c \hat{a}^\dagger \hat{a} + \sum_n \left(\frac{1}{2}\omega_e \sigma_n^z + \omega_v [\hat{b}_n^\dagger \hat{b}_n + \sqrt{S}(\hat{b}_n^\dagger + \hat{b}_n)\sigma_n^z] + G(\hat{b}_n^\dagger \hat{a} + \hat{b}_n \hat{a}^\dagger) \right), \quad (2.1)$$

where a sum is over all molecules, ω_c - cavity photon frequency, $\hat{a}$ - a photon annihilation operator, ω_e - energy of an electronic transition, ω_v - frequency of a molecular oscillation, $\hat{b}$ - corresponding annihilation operator, S - a Huang Rhys factor, which describes coupling between vibrational and electronic modes (a displacement of the vibrational mode in the electronically excited state with respect to the ground state). G is a vibration–cavity photon interaction strength, σ_n^z is 0 or 1, describing whether the n-th molecule is in its ground or excited electronic state. Raman transitions are caused by external laser field $(\sigma_n^+ + \sigma_n^-)E$, which is treated perturbatively.

Within the second-order perturbation theory, probability of Raman scattering into a polaritonic mode is given by [30]:

$$P_{0\to f} = \left| \sum_n \frac{\langle 0|\hat{V}_1|n\rangle\langle n|\hat{V}_2|f\rangle}{(E_n - E_0) - \hbar\omega} \right|^2, \quad (2.2)$$

where ω is the frequency of the excitation field, E_0 is initial state energy, E_n - intermediate state energy. The interaction term is $\hat{V}_1 = (\boldsymbol{de}_{exc})\sigma_n^- \hat{A}_{exc}^\dagger, \hat{V}_2 = (\boldsymbol{de}_{emit})\sigma_m^+ \hat{A}_{emit}$. $\hat{A}^\dagger, \hat{A}$ - are (non-cavity) photon creation and annihilation operators, $\boldsymbol{d}$ - vibron dipole moment, e - polarisation of emitted/absorbed light. Polarisation effects are not important in the current context, thus will be ignored hereafter.

In order to calculate a sum over all virtual transitions in (2.2), we need to find Hamiltonian (2.1) eigenstates. In general, this is a non-trivial problem requiring extensive numerical calculations. However, what we want to calculate is a probability of a spontaneous Raman scattering in a linear-spectroscopy regime. This means that the system contains either one or no electronically excited molecules, which simplifies calculations significantly. In a state where only an m^{th} molecule is electronically excited, the Hamiltonian (2.1) reads

$$H_{\text{eff,m}} = \omega_c \hat{a}^\dagger \hat{a} + \sum_n \left(\omega_v \hat{b}_n^\dagger \hat{b}_n + G(\hat{b}_n^\dagger \hat{a} + \hat{b}_n \hat{a}^\dagger) \right) + \omega_v \sqrt{S}(\hat{b}_m^\dagger + \hat{b}_m). \quad (2.3)$$

The eigenstates of this Hamiltonian play the role of intermediate states $|n\rangle$ in (2.2). This Hamiltonian is readily diagonalized by the unitary transformation $\hat{\xi}_i = \hat{a}\upsilon_i + \sum_n \hat{b}_n U_{n,i} + \beta_{m,i}$ (requiring $[\hat{\xi}_i, \hat{\xi}_j^\dagger] = \delta_{i,j}$). This leads to $N+1$ eigenmodes: 2 polaritonic ones and $N-1$ dark modes (which are orthogonal to polaritonic ones and do not contain photonic part, i.e. for which $\upsilon_i \equiv 0$).

Polaritonic mode energies are:

$$\omega_i \equiv \omega_{1,2} = \frac{\omega_c + \omega_v}{2} \pm \sqrt{\left(\frac{\omega_c - \omega_v}{2}\right)^2 + NG^2}, \quad (2.4)$$

This expression suggests a definition of Rabi splitting as a splitting between upper and lower polariton at resonance $\Omega_R = 2G\sqrt{N}$. Then using the requirement $[\hat{\xi}_i, \hat{\xi}_j^\dagger] = \delta_{i,j}$, the fraction of a photon and exciton in the polaritonic mode are:

$$\upsilon_i = \frac{\omega_i - \omega_v}{\sqrt{(\omega_i - \omega_v)^2 + NG^2}}, \quad (2.5)$$

$$U_{n,i} \equiv U_i = \frac{G}{\sqrt{(\omega_i - \omega_v)^2 + NG^2}}. \quad (2.6)$$

A Hamiltonian without electronically excited molecules is diagonalised by the same transformation, but with $\beta_{m,i} = 0$, i.e. $\hat{\eta}_i = \hat{a}\upsilon_i + U_i \sum_n \hat{b}_n$, and so it leads to the following relation between annihilation operators for intermediate (with an electronically excited molecule) and initial or final (all molecules in their electronic ground state) states: $\hat{\eta}_i + \beta_i = \hat{\xi}_i$.

Let us now consider the remaining $N-1$ solutions, i.e. dark modes ($\upsilon_i \equiv 0$) with $\omega_{3,4,...,N+1} = \omega_v$ and $\hat{\xi}_m = \sum_n U_{n,m} \hat{b}_m$ with $U_{n,m}$ such that $\sum_n U_{n,i} = 0$, $\sum_n U_{n,i} U_{n,j}^* = \delta_{i,j}$. Firstly, it is clear that there are not enough equations to determine eigenvectors unambiguously, so there are many ways to chose them. However, observables cannot depend on the specific form of eigenvectors, so we should just choose a convenient set of eigenvectors. For example, $U_{n,m} = \frac{1}{\sqrt{N}} \exp\left(i\frac{2\pi nm}{N}\right)$, where $n = 0, ..., N-1$ - the number of a molecule, $m = 1, ..., N-1$ - the number of a dark mode.

The last ingredient $\beta_{j,m}$ is given by

$$\beta_{j,m} = \begin{cases} \frac{U_j \omega_v \sqrt{S}}{\omega_j}, & \text{j=1,2 (or UP and LP),} \\ U_{j,m}\sqrt{S}, & \text{j=3,4,...,N+1,} \end{cases} \quad (2.7)$$

where m is a number of an electronically excited molecule, j - the mode number. For polaritonic modes $\beta_{j,m}$ does not depend on the number of a molecule m because polariton is delocalised over all molecules, i.e. it is a superposition of a photon and a delocalised excitation of all molecules.

Now the ground state of a Hamiltonian without electronically excited molecules is $|0\rangle = |\Downarrow, 0_L, 0_U, 0_1, ..., 0_{N-1}\rangle$ and an intermediate state with an excited molecule is $|0_{int,j}\rangle = |\Uparrow_j, 0_L, 0_U, 0_1, ..., 0_{N-1}\rangle$ ($\Uparrow_j$ means electronically excited j-th molecule, the first number — number of lower polaritons, second — upper polaritonic, all others — numbers of dark states). Due to the relation $\tilde{\eta}_j + \beta_{j,m} = \tilde{\xi}_j$, the connection between these two is

$$|0_{int,j}\rangle = e^{-\sum_i \left(\beta_{j,i}\hat{\eta}_i^\dagger - \beta_{j,i}^* \hat{\eta}_i\right)} |0\rangle. \tag{2.8}$$

2.2 Transition probability calculation in RWA

Transition probability from the ground to the final state via all virtual states is $P_{|0\rangle\to|f_k\rangle} = \gamma\,|M_k|^2$ (γ combines various factors, which do not depend on matter-light interaction strength, such as an electronic matrix element and density of final photon states), where a transition matrix element is

$$M_k = \sum_n \frac{\langle 0|\sigma_n^-|n\rangle\langle n|\sigma_n^+|f_k\rangle}{(E_{int,n} - E_0 - \hbar\omega)}. \tag{2.9}$$

In this expression $|f_k\rangle$ is the final state (index k labels which state is excited), which may be an upper (UP) or lower (LP) polariton mode or a dark state, $E_{int,n}$ is the energy of a virtual (intermediate) state

Operators σ_n only change the electronic state of an n-th molecule, so now we can write

$$M_k = \sum_{\substack{n;\\ p_1,\ldots,p_{N+1}}} \frac{e^{-\sum_i |\beta_{n,i}|^2}\mathcal{M}_{int,0}(n;p_1,\ldots,p_{N+1})\mathcal{M}_{f_k,int}(n;p_1,\ldots,p_{N+1})}{p_1!\ldots p_2!\Big(E_{el} - \hbar\omega + p_1\omega_{UP} + p_2\omega_{LP} + \omega_v(p_3 + \cdots + p_{N+1})\Big)}, \tag{2.10}$$

where p_i describes the number of excitations in a corresponding polariton or dark mode, E_{el} - energy of the electronic transition, ω_{UP} and ω_{LP} are the UP and LP frequencies respectively. Also, ω_v is the energy of a dark mode.

Now let us consider matrix elements in (2.10). The first matrix element is trivial:

$$\begin{aligned}\mathcal{M}_{int,0} &= \langle 0|(\hat{\eta}_1^\dagger + \beta_1)^{p_1}(\hat{\eta}_2^\dagger + \beta_2)^{p_2}\ldots(\hat{\eta}_{N+1}^\dagger + \beta_{n,N+1}^*)^{p_{N+1}} e^{-\sum_i \beta_{n,i}\eta_i^\dagger}|0\rangle = \\ &= \beta_1^{p_1}\beta_2^{p_2}(\beta_{n,3}^*)^{p_3}\ldots(\beta_{n,N+1}^*)^{p_{N+1}}.\end{aligned} \tag{2.11}$$

Here $\beta_{1/2}$ are real as they refer to polaritonic states (see Eq. 2.6). The second matrix element describing the transition from the intermediate state to one of

$N+1$ single excited (polariton or dark) states in electronic ground state is:

$$\mathcal{M}_{f_k,int} = \mathcal{M}^*_{int,0}\frac{p_k - |\beta_{n,k}|^2}{\beta_{n,k}}. \tag{2.12}$$

The difference between these matrix elements comes simply from the fact that the first one (2.11) originates from an expression like $\langle 0|(\xi^\dagger + \beta^*)^p e^{-\beta\xi^\dagger}|0\rangle$, while the second one (2.12) – from $\langle 0|\xi(\xi^\dagger + \beta^*)^p e^{-\beta\xi^\dagger}|0\rangle$. Now we can rewrite Raman transition matrix element (2.10) in a more compact form:

$$M_k = \sum_n \frac{1}{\beta_{n,k}} \sum_{\{p_i\}} \prod_i e^{-|\beta_{n,i}|^2} \frac{|\beta_{n,i}|^{2p_i}}{p_i!} \frac{p_k - |\beta_{n,k}|^2}{\Delta + \sum_j p_j\omega_j}, \tag{2.13}$$

where $\Delta = E_{el} - \hbar\omega$ is the laser field–electronic transition energy detuning and $\sum_{\{p_i\}} \equiv \sum_{p_1,\ldots,p_{N+1}}$. As energy levels can be degenerate (dark modes), calculation of a scattering probability with a definite Stokes shift, requires summation over all final states with the same energy, i.e.

$$P(\nu) \propto \sum_k \delta(\nu - \omega_k) P_{|0\rangle\to|f_k\rangle}. \tag{2.14}$$

However, this should be applied only for dark modes because polaritonic modes are not degenerate.

Summation over the number of excitations of all modes $\{p_i\}$ in (2.13) can be performed analytically. To do this, we can rewrite the denominator as an integral of an exponential and get

$$\begin{aligned} M_k &= \int_0^\infty dz e^{-z\Delta} \sum_n \frac{1}{\beta_{n,k}} \sum_{\{p_i\}} \left(p_k - |\beta_{nk}|^2\right) \times \left(\prod_j \frac{\left(|\beta_{nj}|^2 e^{-z\omega_j}\right)^{p_j} e^{-|\beta_{nj}|^2}}{p_j!}\right) = \\ &= \int_0^\infty e^{-z\Delta} \sum_n \frac{(e^{-z\omega_k} - 1)}{\beta_{n,k}} |\beta_{nk}|^2 \prod_j e^{|\beta_{nj}|^2\left(e^{-z\omega_j} - 1\right)}, \end{aligned} \tag{2.15}$$

thus we get

$$M_k = \int_0^\infty dz e^{-z\Delta} \sum_n \beta^*_{n,k} \left(e^{-z\omega_k} - 1\right) \exp\left[\sum_j |\beta_{nj}|^2 \left(e^{-z\omega_j} - 1\right)\right]. \tag{2.16}$$

This expression together with (2.14) and a dark mode condition $\sum_n \beta_{ni} = 0$ clearly shows that there is no transition to a single-excited dark state, which has a simple interpretation. Indeed, dark state is a highly degenerate state, so the transition matrix elements to every dark state is the same up to a phase factor, therefore if we consider a transition to the dark state, we should

sum up over all transition amplitudes to the dark states, which cancel due to destructive interference.

For the bright states $\beta_{n,k}$ does not depend on n (and it is real), so for the transition to polaritonic states we have $\sum_n \to N$, where N is a total number of molecules. Also, for dark states $|\beta_{n,j}|$ does not depend on j, therefore $\sum_{j\in dark} \to N-1$ or just N for a large number of molecules. So, we get the final expression for the transition amplitude to the polaritonic mode

$$M_k = \frac{N\alpha_k}{\sqrt{2}} \int_0^\infty dz e^{-z\Delta} \left(e^{-z\omega_k} - 1\right) \exp\left[-\frac{1}{2}\sum_j |\alpha_{nj}|^2 \left(1 - e^{-z\omega_j}\right)\right], \quad (2.17)$$

where for polariton transition $k = 1$ or 3; $i = 1, 2, 3$ and in resonance $\omega_c = \omega_v$ we have $\alpha = \sqrt{\frac{S}{N}}\omega_v \left(\frac{1}{\omega_{UP}}, \frac{\sqrt{2N}}{\omega_v}, \frac{1}{\omega_{LP}}\right)$.

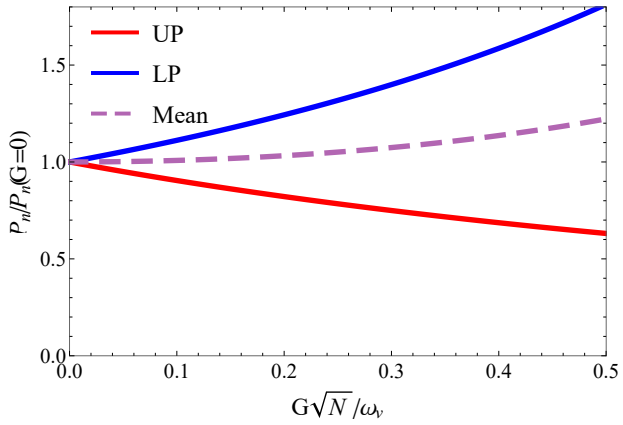

Figure 2.2: Transition probability to the upper and lower polariton in RWA; $\omega_c = \omega_v$, $S = 0.3$, $N = 10^6$, and $\Delta = \omega_v$.

Fig. 2.2 shows Raman scattering probability (normalized by the probability in the absence of light-matter coupling) as a function of dimensionless coupling (half Rabi splitting $G\sqrt{N} = \Omega_R/2$ divided by the bare vibron frequency ω_v). As RWA approximation is valid only at quite small coupling strength, we can conclude that in this limit the total Raman scattering cross-section is almost unaffected by the strong vibron-cavity photon coupling.

Fig. 2.3 demonstrates the dependence of Raman scattering probability on detuning $(\omega_c - \omega_v) = \delta$. Thick lines on this figure describe the scattering into the 1st and 2nd polaritonic mode for a half Rabi splitting $\Omega_R = 20meV$, dashed - for $\Omega_R = 5meV$. So, the signal just splits between polaritonic levels.

If in (2.17) we suppose a large laser field–electron excitation energy detuning $s \ll \Delta$, we can notice that only small values of z contribute to the integral, so we can expand exponents and keeping only first non-vanishing terms calculate the integral. For the corresponding transition probability to

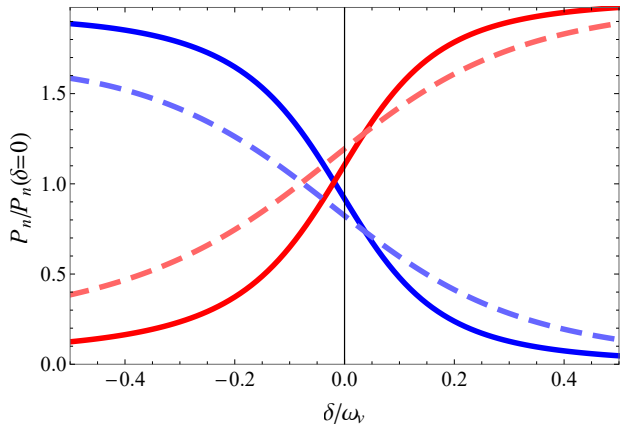

Figure 2.3: Transition probability to the LP and UP dependence on the vibron-cavity photon detuning in RWA. Red - lower polariton, blue - upper polariton; solid line - $G\sqrt{N} = 0.1\omega_v$, dashed - $G\sqrt{N} = 0.2\omega_v$

the UP or LP we get

$$P_{1,2} \simeq \gamma \frac{SN}{2} \frac{\omega_v^2}{\left[\Delta + \frac{S}{N}\omega_v \left(N + 1 + \frac{1}{1-\zeta^2}\right)\right]^2}, \tag{2.18}$$

where $\zeta = G\sqrt{N}/\omega_v$, thus it almost does not depend on ζ for $\zeta \ll 1$, but starts getting smaller at $\zeta > \zeta_0$, where $\zeta_0 \simeq 1 - \frac{1}{2N}$, i.e. when divergent part of the denominator dominates on a big but non-divergent part. This means that for a macroscopic number of molecules, we reach this regime only at $G\sqrt{N} \simeq \omega_v$, and eventually the transition probability vanishes at $\zeta = 1$, i.e. at $G\sqrt{N} = \omega_v$. However, at such strong coupling RWA is not valid. It is simple to further expand (2.17) to get a more accurate analytical expression, but, as we will see below, (2.18) already contains an important result, namely that the transition probability depends weakly on the coupling strength in RWA and that the total signal is almost independent on light-matter coupling.

2.3 Ultra-strong coupling & ω_v dependence of the electronic state

In the ultra-strong coupling regime RWA breaks down, so we should change $G(\hat{b}_n^\dagger \hat{a} + \hat{b}_n \hat{a}^\dagger)$ by an exact expression $G(\hat{b}_n^\dagger + \hat{b}_n)(\hat{a}^\dagger + \hat{a})$ and add a diamagnetic $\hat{A}^2$ term, i.e. $\frac{G^2 N}{\omega_v}(\hat{a}^\dagger + \hat{a})^2$. The prefactor of this term can be derived following the Thomas-Reiche-Kuhn sum rule (for details see A.1). Also, using $\hat{x} = \sqrt{\frac{\hbar}{2m\omega}}\left(\hat{b}_n^\dagger + \hat{b}_n\right)$ for the molecular oscillator coordinate, we can include the term originating from the vibration frequency difference in the ground and excited electronic state $\delta\omega_v$. It should be noted that we would get the term of

the same form if also considered the second order expansion in exciton-vibron coupling over oscillator displacement (but we will show that this does not play a big role in Raman scattering). Overall, we have

$$\begin{aligned} H = \ & \omega_c \hat{a}^\dagger \hat{a} + \sum_n \left(\frac{1}{2}\omega_e \sigma_n^z + \omega_v [\hat{b}_n^\dagger \hat{b}_n + \sqrt{S}(\hat{b}_n^\dagger + \hat{b}_n)\sigma_n^z] + \right. \\ & \left. + G(\hat{b}_n^\dagger + \hat{b}_n)(\hat{a}^\dagger + \hat{a}) + \frac{1}{2}\sigma_n^z \nu (\hat{b}_n^\dagger + \hat{b}_n)^2 \right) + \frac{G^2 N}{\omega_v}(\hat{a}^\dagger + \hat{a})^2, \end{aligned} \tag{2.19}$$

where $\nu = \frac{1}{4}\omega_v \left[2\frac{\delta\omega_v}{\omega_v} + \left(\frac{\delta\omega_v}{\omega_v}\right)^2 \right]$

In contrast with the case considered before (2.1), the new Hamiltonian includes non number conserving terms, therefore the Fock basis is not convenient here as it causes significant difficulties in matrix elements calculations. At the same time, the Hamiltonian is still quadratic, so it can be diagonalized analytically. However, even before it we can simplify the Hamiltonian considerably, rewriting it in terms of three modes, which is explained in the Appendix A.3. The main idea is that we have 2 polaritonic and N-1 identical dark modes, so there is a way to change the basis in order to have only 3 distinct modes (one photonic and two vibrational modes, one of which — will be called b below — describes vibrational excitation on the m-th molecule and other — excitation delocalized over $N-1$ molecules except the m-th one, which will be called c). Therefore, we will get a Hamiltonian which describes three coupled Harmonic oscillators with different frequencies.

We want to connect eigenstates of a Hamiltonian when we have an electronically excited molecule $H_\uparrow$ and a Hamiltonian with all molecules in an electronically ground state $H_\downarrow$:

$$H_\downarrow = \omega_c \hat{a}^\dagger \hat{a} + \omega_v (\hat{b}^\dagger \hat{b} + \hat{c}^\dagger \hat{c}) + \frac{G^2 N}{\omega_v}(\hat{a}+\hat{a}^\dagger)^2 + (\hat{a}+\hat{a}^\dagger)\left(\hat{b} + \hat{b}^\dagger + \sqrt{N-1}\left(\hat{c} + \hat{c}^\dagger\right)\right) \tag{2.20}$$

and

$$H_\uparrow = H_\downarrow + \delta(\hat{b} + \hat{b}^\dagger)^2 + \omega_v \sqrt{S}(\hat{b} + \hat{b}^\dagger).$$

As the Fock basis makes it difficult to calculate overlappings, but the Hamiltonian is quadratic, spatial and momentum representation is more appropriate in this situation. We can now introduce coordinates $\hat{x}_i$, and corresponding momentum $\hat{p}_i$ and ($\hbar = 1$) we write: $\hat{a} = \sqrt{\frac{\omega_c}{2}}\left(\hat{x}_a + \frac{i\hat{p}_a}{\omega_c}\right)$, $\hat{b} = \sqrt{\frac{\omega_v}{2}}\left(\hat{x}_b + \frac{i\hat{p}_b}{\omega_v}\right)$, and similarly for c. As the problem is isotropic in momentum, we can diagonalize it by solving the classical problem. If we write:

$$\hat{H}_\sigma = \frac{1}{2}\left(\mathbf{p}^\dagger \mathbf{p} + \mathbf{x}^\dagger \mathbf{V}_\sigma \mathbf{x} + 2\mathbf{h}_\sigma^\dagger \mathbf{x}\right), \tag{2.21}$$

where $\mathbf{h} = \left(0, \omega_v\sqrt{2\omega_v S}, 0\right)$ and

$$\mathbf{V}_\downarrow = \begin{pmatrix} \omega_c^2 + 4G^2N & \xi & \xi\sqrt{N-1} \\ \xi & \omega_v^2 & 0 \\ \xi\sqrt{N-1} & 0 & \omega_v^2 \end{pmatrix} \tag{2.22}$$

$$\mathbf{V}_\uparrow = \mathbf{V}_\downarrow + \begin{pmatrix} 0 & 0 & 0 \\ 0 & 4\varepsilon_v\nu & 0 \\ 0 & 0 & 0 \end{pmatrix} \tag{2.23}$$

where $\xi = 2G\sqrt{\omega_v\omega_c}$, we can clearly diagonalize $\hat{H}_\sigma$ by writing: $\mathbf{x} = \mathbf{U}_\sigma\mathbf{X}_\sigma - \mathbf{V}_\sigma^{-1}\mathbf{h}_\sigma$ where $\mathbf{U}_\sigma^\dagger\mathbf{V}_\sigma\mathbf{U}_\sigma = \Omega_\sigma^2$ is diagonal. Note that $\mathbf{V}$ is a real symmetric matrix, and so although we write Hermitian conjugates, these are all equivalent to transposes, as eigenvalues and vectors are all real. After diagonalization one has the eigenstates, which are products of three harmonic oscillator wave-functions:

$$\begin{aligned}\Psi_{lmn,\sigma}(x_a, x_b, x_c) = \sqrt[4]{\omega_{1,\sigma}\omega_{2,\sigma}\omega_{3,\sigma}}\psi_l\left(X_{1,\sigma}\sqrt{\omega_{1,\sigma}}\right) \\ \psi_m\left(X_{2,\sigma}\sqrt{\omega_{2,\sigma}}\right)\psi_n\left(X_{3,\sigma}\sqrt{\omega_{3,\sigma}}\right),\end{aligned} \tag{2.24}$$

where $\omega_{i\sigma}$ are the diagonal elements of Ω_σ and the components X_i are related to x_i by Eq. (2.3) and $\psi_n(x)$ are Gauss-Hermite functions:

$$\psi_n(x) = \frac{1}{\sqrt{\sqrt{\pi}2^n n!}}H_n(x)e^{-x^2/2} \tag{2.25}$$

Using the fact that $\mathbf{h}_\downarrow = \mathbf{0}$ we can relate the two basis coordinates as: $\mathbf{X}_\downarrow = \mathbf{U}_\downarrow^\dagger\left[\mathbf{U}_\uparrow\mathbf{X}_\uparrow - \mathbf{V}_\uparrow^{-1}\mathbf{h}_\uparrow\right]$.

Now, as in (2.9), we need to calculate M_k, which is a sum over all transition amplitudes from the ground to final state over all intermediate states divided by corresponding energy differences. The transition matrix elements can now be calculated as overlaps of position-basis wavefunctions (2.24). Rewriting the denominator as an integral of the exponent as before, for a transition matrix element to a single excited bright (polaritonic) mode k we get

$$\begin{aligned}M_k = N\sqrt{2\omega_{k,\downarrow}\prod_i \omega_{i,\uparrow}\omega_{i,\downarrow}}\int_0^\infty ds e^{-s\Delta}\int d^3x d^3x' \\ \prod_i\left[\psi_0\left(\sqrt{\omega_{i,\downarrow}}X_{i,\downarrow}\right)\sum_{l_i}\psi_{l_i}\left(\sqrt{\omega_{i,\uparrow}}X_{i,\uparrow}\right)\psi_{l_i}\left(\sqrt{\omega_{i,\uparrow}}X'_{i,\uparrow}\right)\psi_0\left(\sqrt{\omega_{i,\downarrow}}X'_{i,\downarrow}\right)e^{-sl_i\omega_{i,\uparrow}}\right]X_{k,\downarrow}\end{aligned} \tag{2.26}$$

where a factor of N came from the summation over the number of molecules and a coordinate $X_{k,\downarrow}$ came from the relation between the first excited and ground Hermite modes $\psi_1(x) = \sqrt{2}x\psi_0(x)$. The coordinate integrals in (2.26)

can be calculated by first making a unitary transformation of coordinates using the relation between $\boldsymbol{x}$ and $\boldsymbol{X}_\sigma$ and then identifying known overlaps of Gauss-Hermite functions (for further details of calculations see the Appendix A.4). The result is

$$M_k = 8N\sqrt{2\omega_{k,\downarrow}}\left[\mathbf{U}_\downarrow^\dagger\mathbf{U}_\uparrow\right]_{kr}\int ds e^{-s\Delta}\prod_i\left(\sqrt{\frac{\omega_{i,\downarrow}\omega_{i,\uparrow}}{1-\exp(-2s\omega_{i,\uparrow})}}\right)\times \\ \times\frac{(\mathbf{A}^{-1}\mathbf{q}-\mathbf{l})_r}{\sqrt{\det(\mathbf{A})}}\exp\left(\frac{1}{2}\mathbf{q}^\intercal\mathbf{A}^{-1}\mathbf{q}-\mathbf{l}^\intercal\mathbf{R}\mathbf{l}\right), \tag{2.27}$$

where

$$\mathbf{A} = \left(\begin{array}{c|c} \mathbf{P}+\mathbf{R} & -\mathbf{Q} \\ \hline -\mathbf{Q} & \mathbf{P}+\mathbf{R} \end{array}\right), \tag{2.28}$$

$\mathbf{R} = \mathbf{U}_\uparrow^\intercal\mathbf{U}_\downarrow\boldsymbol{\Omega}_\downarrow\mathbf{U}_\downarrow^\intercal\mathbf{U}_\uparrow$, $\mathbf{P} = \mathrm{diag}\left(\frac{\omega_{i,\uparrow}}{\tanh(s\omega_{i,\uparrow})}\right)$ and $\mathbf{Q} = \mathrm{diag}\left(\frac{\omega_{i,\uparrow}}{\sinh(s\omega_{i,\uparrow})}\right)$, $\mathbf{l} = \boldsymbol{\Omega}_\uparrow^{-2}\mathbf{U}_\uparrow^\dagger\mathbf{h}_\uparrow$, $\mathbf{q}^\intercal = (\mathbf{l}^\intercal\mathbf{R}, \mathbf{l}^\intercal\mathbf{R})$. This result contains a 6×6 matrix A, which naturally comes after computing the 6 dimensional Gaussian integral in (2.26) over coordinates of both 3D oscillators.

From Fig. 2.4 we can see that the detuning between upper and lower vibration energies $\delta\omega_v$ does not play a big role in Raman scattering, but non-RWA and A^2 terms are crucial at large coupling strength, which is clear from the comparison with the results of RWA calculations — Fig. 2.2. Therefore, we can conclude that changes in the ground electronic state of the molecule due to the strong coupling with light primarily affect the properties of Raman scattering, but transformations in the intermediate states affect RS negligibly.

Thus, let us then concentrate on a situation when the detuning $\delta\omega_v$ is zero. In this case the general expression (2.27) can be simplified considerably because $\nu = 0$, so $V_\uparrow = V_\downarrow$, consequently $U_\uparrow = U_\downarrow$ and $\Omega_\uparrow = \Omega_\downarrow$. If so, we get exactly the same expression as (2.17), but with a new α_j (again in resonance $\omega_c = \omega_v$): $\alpha_j = \sqrt{\frac{S}{N}}\omega_v^{3/2}\left(\frac{1}{\omega_{UP}^{3/2}}, \frac{\sqrt{2N}}{\omega_v^{3/2}}, \frac{1}{\omega_{LP}^{3/2}}\right)$.

As before, the integrand contributes to the integral only at $s \ll \Delta$, so we can suppose very large detuning Δ, and expand exponents. If we do it, we can clearly see that $M_{1,2}$ does not have singularities, but $M_3 \equiv M_{LP}$ (transition amplitude to LP) has, so let us consider the corresponding transition probability

$$P_{LP} \simeq \frac{SN}{2}\frac{\omega_v^3}{\omega_{LP}}\frac{1}{\left[\Delta + \frac{\omega_v^3 S}{2N}\left(\omega_{UP}^{-2}+\omega_{LP}^{-2}+2N\omega_v^{-2}\right)\right]^2}, \tag{2.29}$$

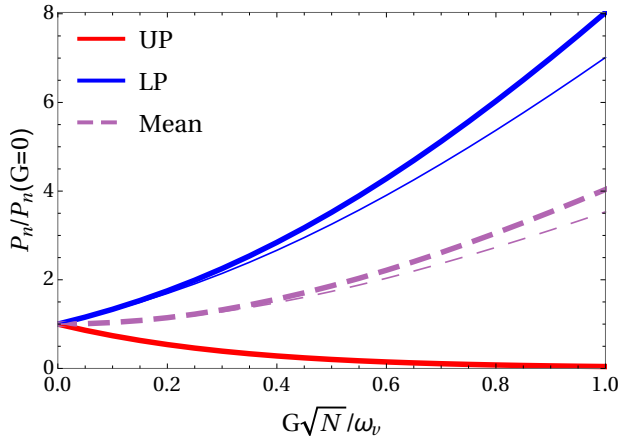

Figure 2.4: Probability of the transition to the upper and lower polariton beyond RWA, including A^2 term. Thick lines correspond $\delta\omega_v = 0$, thin ones — to $\delta\omega_v = -0.5\,\omega_v$

At relatively small values of matter-light coupling, $P_{LP} \propto 1/\omega_{LP}$ goes up when coupling increases because of softening of the lower polariton mode. This is different from the result obtained in RWA (2.18), where we did not have such a prefactor. In contrast, at very strong coupling, where $\omega_{LP} \ll \omega_v/\sqrt{N}$, the probability goes down as $P_{LP} \propto \omega_{LP}^3$. However, for an experimentally reasonable number of molecules $N \approx 10^6 - 10^{10}$ this regime of a "super-strong" coupling is hardly achievable. On the other hand, in a context of single strongly-coupled emitters (for example, in [99] single molecule exciton-plasmon strong coupling was demonstrated), this effect may arise.

It should be noted that the A^2 term plays a crucial role at ultra-strong coupling regime because it prevents the LP energy from abrupt plunge to zero (i.e. from a quantum phase transition to a superradiant state). With this term, LP energy approaches zero asymptotically as coupling increases, so Raman probability is a smooth function of the coupling strength.

2.4 Raman scattering to higher-excited states

While transition probabilities to only single excited states (one lower or upper polariton) were derived in previous sections, a more general formula describing the transition amplitude to the n-th UP or LP state can be obtained:

$$M_k^n = N\frac{\alpha_k^n}{\sqrt{2^n n!}}\int ds e^{-s\Delta}\left(e^{-s\omega_k}-1\right)^n \exp\left[-\frac{1}{2}\sum_i |\alpha_i|^2\left(1-e^{-s\omega_i}\right)\right]. \tag{2.30}$$

From this formula we can see that scattering probability to the LP state increases faster (as $1/\omega_{LP}^n$ comparing with (2.29)) when coupling grows. This

result is not surprising, because we can guess it qualitatively as the probability of the simultaneous excitation of two modes equals to the product of corresponding probabilities (if these are independent). However, it is also damped by a factor of $1/N^n$ (which comes from α_k^{2n}) as in this case we create n delocalized excitations over all N molecules.

The most general formula for a transition amplitude to a state $\{q_i\}$ reads

$$M_{\{q_i\}} = \sum_m \int_0^\infty ds e^{-s\Delta} \prod_i (\alpha_{m,i}^*)^{q_i} \frac{(e^{-s\omega_i} - 1)^{q_i}}{\sqrt{q_i!}} e^{-|\alpha_{m,i}|^2(1-e^{-s\omega_i})} \qquad (2.31)$$

This result is quite interesting because it shows that dark states can be excited as a result of Raman scattering because, while $\sum_m \alpha_{m,i} = 0$, the sum $\sum_m (\alpha_{m,i}^*)^{q_i}$ is not necessarily zero. Indeed, the reason of vanishing probability of scattering to a single-excited dark state is a momentum conservation, i.e. as the ground state momentum is zero, the final state momentum must also be zero, while dark states have finite momentum (thus they do not couple to a zero-momentum photon). However, a final state with two excited dark modes with opposite momenta is possible. In general, any final state is possible as soon as its total momentum is zero. Considering all final states with two excitations, one can see that a corresponding transition probability scales like N, i.e. the same as for a single-excitation final state. Therefore, in the strong coupling regime in the Raman emission one should see three peaks: a strong one due to a transitions to a single-excited LP state, a weaker one — to a double-excited dark state, and the weakest one — to a single-excited UP state. Other signals should clearly be much weaker (for a macroscopic number of molecules).

Chapter 3

Organic polariton lasing

Dye lasers are known to feature low-threshold lasing. In contrast to simple two-level systems, where electronic state inversion is necessary for lasing, the existence of ro-vibrational levels in molecules allows an inversionless lasing. Two basic components needed for lasing are an optically active inverted transition and an optical cavity to collect photons into a given mode. If we consider only ground and the first excited electronic state, and on top of this a single vibrational molecular mode, we can enumerate all the states by a the following pair $(\uparrow / \downarrow, n)$, where $\uparrow / \downarrow$ represents an excited or a ground electronic state and n - the number of phonons in this state. While in a two-level system we always have $n = 0$ and so lasing may be driven by $(\uparrow, 0) \rightarrow (\downarrow, 0)$ transition only (where $(\uparrow, 0)$ is incoherntly populated via excitation and subsequent relaxation of higher-energy states), in a molecule $(\uparrow, 0) \rightarrow (\downarrow, 1)$ is usually responsible for lasing (hereafter $(\downarrow, n) \rightarrow (\uparrow, m)$ is replaced by just $(n - m)$), thus requiring inversion between $(\uparrow, 0)$ and $(\downarrow, 1)$ states, which is easy to reach at temperatures lower than corresponding frequency of a molecular transition ω_v because at $k_B T \ll \hbar\omega_v$ the state $(\downarrow, 1)$ is almost empty. Therefore, tuning cavity frequency to a $(1-0)$ transition, it is possible to reach a lower-threshold lasing with respect to a two-level system due to softening of the electronic state inversion requirement [100].

In the very same system polaritonic physics can explored. Indeed, increasing the number of molecules and/or improving a cavity quality factor, a regime of strong matter coupling is routinely achieved in experiments. Increasing external pumping of such a system, polariton lasing can be reached. It is widely believed that polariton lasing is low-threshold because its mechanism is based on stimulated scattering from the reservoir to the polariton condensate, which does not require inversion, in contrast to an ordinary laser, which does require inversion. This is considered to be one of the main advantages of a polariton laser (from the results of this chapter it follows that this argument is not quite right).

However, until recently, there has been no systematic investigation of how

strong matter-light coupling modifies the physics of a dye laser, so these two inherently connected systems have been considered apart from each other. Moreover, the effect of polariton formation on lasing threshold has never been studied, although speculated frequently.

Therefore, the aim of this chapter is to describe the transition from a well-known regime of a molecular laser (weak matter-light coupling) to the regime of polariton laser (strong coupling), to understand similarities and differences, to propose a unified framework for the description of these systems, and to find optimal parameters for low-threshold lasing. To address these points, a microscopic model will be introduced in Section 3.1. Section 3.2 describes an exact (in the thermodynamic limit) solution of this model. In Section 3.3 the results are discussed.

3.1 Model

To describe lasing we need a theory of a driven-dissipative system. A widely used approach is to separate the full system into a "system", the physics of which we want to reveal, and a "bath", the effect of which on the "system" we want to understand, and which is not affected by the system. So, let us consider a Hamiltonian $H = H_S + H_B + H_{int}$, where H_S represents molecules in a microcavity coupled to its photon mode (system), H_B is responsible for incoherent driving, dissipation and dephasing of the system, and H_{int} is the system-bath interaction.

3.1.1 System Hamiltonian

Let us consider the system Hamiltonian first. Although molecules usually feature a huge number of transitions, to make calculations possible, we need to have some simplified model. The main ingredients we need to describe a molecular polariton laser are an electronic transition with finite optical matrix element and a molecular vibrational mode. Thus, we have

$$\begin{aligned} H_S = \sum_n \left\{ \frac{1}{2}\varepsilon\sigma_n^z + \omega_v \left[b_n^\dagger b_n + \sqrt{S}\sigma_n^z (b_n^\dagger + b_n) \right] \right\} \\ + \omega_c a^\dagger a + g\left(a^\dagger + a\right) \sum_n \sigma_n^x + \frac{g^2 \mathcal{N}_m}{\varepsilon} (a^\dagger + a)^2, \end{aligned} \tag{3.1}$$

where there is a sum over all molecules n, $\sigma^{x,y,z}$ are Pauli matrices, ε is the energy of an electronic transition, ω_v is the frequency of a vibrational mode, b_n is an annihilation operator of a molecular phonon (a quanta of local/internal molecular vibrational mode), S characterizes the coupling strength of the electronic and molecular transitions, $\mathcal{N}_m$ is the total number of molecules, g is the matter-light coupling strength, a is a photon annihilation operator. The last

term is a so-called A^2-term, which must be kept to avoid unphysical superradiant transition in the strong-coupling regime as it renormalises the lower polariton mode. The Hamiltonian (3.1) contains only a single photon mode with energy ω_c. This serves as a simplification to understand the basics of a very complex model of a molecular polariton laser and to provide a foundation for further calculations with more realistic models containing multiple photon modes.

3.1.2 Incoherent processes

There are a number of incoherent processes that needed be taken into account to model lasing of a system of molecules coupled to a microcavity photon. The most obvious one is the leakage of photons out of a cavity due to finite transmission of cavity mirrors. This may be described by introducing a Hamiltonian of free-space — non-cavity — photons $H_{nc} = \sum_{\boldsymbol{k},n} \hbar\omega_k \tilde{a}^\dagger_{\boldsymbol{k},n} \tilde{a}_{\boldsymbol{k},n}$ and coupling them to a cavity photon $H_{leak} = \sum_{\boldsymbol{k},n} \xi_{\boldsymbol{k},n} \left(a\tilde{a}^\dagger_{\boldsymbol{k},n} + a^\dagger \tilde{a}_{\boldsymbol{k},n} \right)$. Supposing that the density of non-cavity modes is constant in the range of cavity photon frequencies (which differ from ω_c in the strong matter-light coupling regime), that the state of non-cavity photons is not affected by a cavity photon, and that in-out cavity photon coupling may be treated perturbatively, then the dynamics of a cavity photon may be described by the Lindblad master equation:

$$\partial_t \rho_S = -i \left[H, \rho_S \right] + \kappa \mathcal{L}[a] \tag{3.2}$$

(neglecting small Lamb shift of system frequencies) where ρ_S is a system density matrix (a microcavity photon here), $H = \omega_c a^\dagger a$ — system Hamiltonian, κ — photon leakage rate and $\mathcal{L}[X] = X\rho X^\dagger - \frac{1}{2}\left[X^\dagger X, \rho\right]_+$ — Lindblad operator, describing photon leakage. However, in the strong coupling regime the assumption of constant density of non-cavity modes is not well justified. While removing this assumption requires numerically complicated non-Markovian treatment of an already complex system, its effect is not expected to change the results considerably. Indeed, while increased frequency of the upper polariton may lead to enhanced leakage, reduced lower polariton frequency competes with this effect due to corresponding lowered leakage.

Supposing that all incoherent processes satisfy the assumptions of the Lindblad master equation derivation (system-bath coupling is small in comparison with inter-system interactions, bath is not affected by the system), we can write the most general master equation describing evolution of the system (molecules and a microcavity photon) density matrix:

$$\partial_t \rho(t) = -i \left[H, \rho \right] + \sum_n \gamma_i \mathcal{L}[O^i_n] \tag{3.3}$$

where γ_i are rates of incoherent processes, O_n^i — corresponding jump operators and $\sum_n$ is the sum over all molecules. The cartoon Fig. 3.1(a) illustrates the system and all incoherent processes considered.

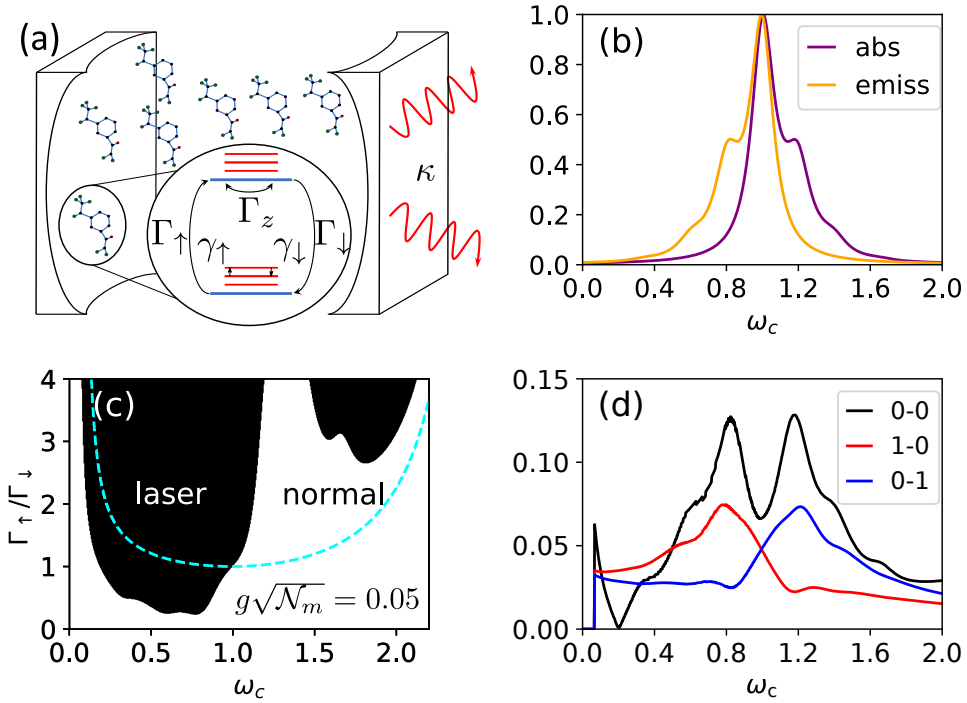

Figure 3.1: (a) Cartoon illustrating the model: many molecules (N-level systems) are coupled to a cavity mode. (b)–(d) Weak coupling behavior. (b) Emission and absorption spectra of the molecules. (c) Weak coupling phase diagram. The cyan dashed line marks the phase boundary without vibrational dressing ($S = 0$). (d) Dominant molecular transitions coupled into the lasing mode at threshold. Parameters used: $\varepsilon \equiv 1.0$, $S = 0.1$, $\omega_v = 0.2$, $\Gamma_\downarrow = \kappa = 10^{-4}$, $\Gamma_z = 0.03$, $\gamma_v = 0.02$, $k_B T_v = 0.025$, $N_v = 4$

First, as discussed above, photon leakage is modelled by the term $\kappa\mathcal{L}[a]$. Next, incoherent excitation of an electronic subsystem is described by the term $\Gamma_\uparrow\mathcal{L}[\sigma^+]$. Incoherent decay of an electronic excitation into non-cavity modes (which is responsible for a less than 100% quantum yield) is modelled by the term $\Gamma_\downarrow\mathcal{L}[\sigma^-]$. Interaction of an electronic subsystem with bath modes, which do not lead to real electronic transitions, is modeled phenomenologically by including a term $\Gamma_z\mathcal{L}[\sigma^z]$ describing dephasing. Scattering of intramolecular phonons (vibrons) with low-energy bath modes leads to thermalisation of molecular oscillations, which is described by the sum of terms $\gamma_\uparrow\mathcal{L}[b^\dagger - \sqrt{S}\sigma^z]$ and $\gamma_\downarrow\mathcal{L}[b - \sqrt{S}\sigma^z]$ accounting for the electronic-state-dependent vibrational displacement with $\gamma_\uparrow = \gamma_v n_B$ and $\gamma_\downarrow = \gamma_v\,(n_B + 1)$, $n_B = [\exp(\omega_v/k_B T) - 1]^{-1}$. From the form of these terms, it is clear that the

the first one describes absorption of a bath phonon by a molecule, while the second one — stimulated emission.

3.1.3 Absorption and emission spectrum

In the previous section, a rather large number of parameters describing incoherent rates was introduced, which warns that such a theory may describe anything upon tuning these parameters. However, the way to choose these parameters is to have physically motivated absorption and emission molecular spectra, which strongly narrows the region of possible parameter regimes. Moreover, as shown in [27], the main conclusions of this theory are robust with respect to fine tuning of parameters. Below we will be using $\varepsilon \equiv 1.0$ by the definition (so measuring energies in units of the electronic transition energy; while typical physical values are $\varepsilon \simeq 1 - 2$ eV), numerical values of other parameters are given in a caption of the Fig. 3.1. With these parameters using the Quantum Regression theorem [57], one can get emission and absorption spectrum of a molecule (essentially in the weak molecule-light coupling limit) — Fig. 3.1(b). These spectra make perfect sense. Indeed, there is a zero-phonon line at $\omega \simeq \varepsilon$ and absorption (emission) mirror-symmetric shoulders with clear one and two phonon peaks.

3.2 Method

The goal is to obtain a non-equilibrium phase diagram of a system described above in the thermodynamic limit taking into account both strong matter-light coupling (hereafter — exciton-photon coupling) and strong coupling of an electronic transition to intramolecular vibration (hereafter — exciton-phonon coupling).

If exciton-phonon coupling is weak, one can integrate intramolecular phonons out and get just an extra term in the Lindblad equation for a two-level system coupled to a photon. For weak coupling to light, one can make a polaron transformation and then treat matter-light coupling perturbatively, which leads to rate equations [101, 102], describing photon condensation. For a small number of molecules, exact numerical methods are available, which treat the vibrational modes as a non-Markovian dissipation process [103, 104]. However, the thermodynamic limit with many molecules and both strong matter-light and exciton-phonon coupling has not been addressed before, so the aim of this section is to solve this problem [27].

The solution is based on two crucial ideas. The first idea, which is illustrated in the Fig. 3.2, is to switch from a two-level system plus a phonon description to a new "molecular" basis, so to describe a molecule as an N-level system, rather than as a combination of an electronic and vibrational subsystems. Here $N = 2N_v$, where N_v is a number of molecular vibrational levels taken into account (i.e. states with zero, one, ..., $(N_v - 1)$ phonons). This

allows to avoid any exciton-phonon decoupling and so to treat exciton-phonon coupling exactly. As shown in an appendix of [27], in practical calculations, for $S = 0.1$ inclusion of as few as $N_v = 4$ vibrational levels already leads to convergent results.

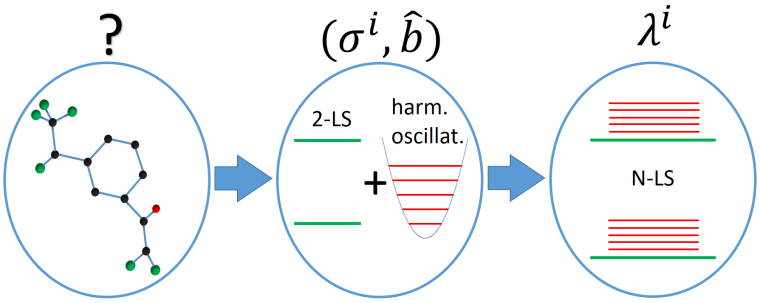

Figure 3.2: From 2-level system plus a phonon to an N-level system

For the description of a general N-level system, one can use a basis of Generalised Gell-Mann matrices λ_i [105], satisfying $\mathrm{Tr}\,(\lambda_i\lambda_j) = 2\delta_{ij}$ (which generalize a set of Pauli matrices serving a basis of Hermitian traceless two-by-two matrices). This allows to rewrite any operator (represented as N-by-N matrix) as follows $O = \frac{1}{2}\lambda_i\,\mathrm{Tr}\,(O\lambda_i)$ (with $\lambda_0 = \sqrt{(2/N)}\mathbf{1}_N$). Therefore, the Hamiltonian (3.1) can be rewritten in terms of new operators:

$$H = \omega_c a^\dagger a + \sum_n \left[A_i + B_i(a^\dagger + a)\right]\lambda_i^{(n)} + \frac{g^2\mathcal{N}_m}{\varepsilon}(a^\dagger + a)^2 \tag{3.4}$$

and the Lindblad equation (3.3) as well:

$$\partial_t\rho(t) = -i\,[H,\rho] + \kappa\mathcal{L}[a] + \sum_{\mu n}\mathcal{L}\left[c_i^\mu\lambda_i^{(n)}\right] \tag{3.5}$$

where n is a number of a molecule, μ is the number of one of the five molecular dissipative channels in Eq. (3.3), summarized in Fig. 3.1. Rewriting dissipative terms in Eq. (3.3) as $\sum_\mu \Gamma_\mu\mathcal{L}[J_\mu]$, the coefficients in Eq. (3.5) are $c_i^\mu = \sqrt{\Gamma_\mu}\,\mathrm{Tr}\,(J_\mu\lambda_i)/2$.

Having introduced a tool for non-perturbative description of exciton-phonon coupling, we now need to find a way to treat strong exciton-photon coupling. This leads to the second crucial idea of employing a mean-field matter-light decoupling, which was shown to be exact in the thermodynamic limit [106]. This can be done simply by deriving equations of motion for variables $\alpha = \langle a\rangle$ and $\ell_i = \langle\lambda_i\rangle$, where $\langle O\rangle = \mathrm{Tr}(\rho O)$, and then assuming $\langle a\lambda_i\rangle = \langle a\rangle\langle\lambda_i\rangle$ (mean-field decoupling). This leads to a set of coupled differential equations:

$$\partial_t\alpha = -\left(i\omega_c + \frac{\kappa}{2}\right)\alpha - 4i\frac{g^2\mathcal{N}_m}{\varepsilon}Re[\alpha] - i\mathcal{N}_m B_i\ell_i \tag{3.6}$$

$$\partial_t\ell_i = \left(\xi_{ik} + 4f_{ijk}B_j Re[\alpha]\right)\ell_k + \frac{4i}{N}c_j^\mu c_k^{\mu *}f_{ijk} \tag{3.7}$$

where $\xi_{ik} = 2f_{ijk}A_j + ic_l^\mu c_m^{\mu *}(f_{ilp}\zeta_{pmk} + f_{mip}\zeta_{plk})$ with $\zeta_{ijk} \equiv \mathrm{Tr}(\lambda_i\lambda_j\lambda_k)/2$, and $f_{ijk} = \mathrm{Tr}([\lambda_i, \lambda_j]\lambda_k)/4i$.

Mean-field theory shows a phase transition between a normal state with $\alpha = 0$, and a symmetry-broken state with $\alpha \neq 0$ which is denoted as a laser (but which may be either a photon or polariton laser depending on the interplay of coherent and incoherent processes). One can time evolve the equations for α and ℓ_i (starting from some small but finite α) or even simpler — study linear stability of equations of motion. Writing the variables as combinations of normal state solution and fluctuations $\alpha = \delta\alpha$, $\ell_i = \ell_{i,ns} + \delta\ell_i$, where $\ell_{k,ns} = -\frac{4i}{N} c_j^\mu c_k^{\mu *} f_{ijk}\xi_{ik}^{-1}$ (with $\xi_{ik}\xi_{ik}^{-1} = \delta_{ik}$), and linearising equations, one can obtain equations for fluctuations $\partial_t \upsilon = \mathcal{M}\upsilon$, where $\upsilon = (\delta\alpha, \delta\alpha^*, \delta\ell)^\intercal$, and then find the eigenmodes $\mathcal{M}\upsilon^k = \xi^k\upsilon^k$. Analysing eigenvalues ξ^k one can find regimes where the systems is stable or unstable (fluctuations proliferate or decay) and so deduce a system phase diagram. Indeed, $Re[\xi^k]$ gives the growth (positive) or decay (negative) rate of a mode, while $Im[\xi^k]$ gives its oscillation frequency. From the eigenvectors υ^k one can also find the contributions of different molecular transitions to the given unstable mode (for the details see Appendix B.1).

3.3 Results

3.3.1 Weak coupling

Before attempting to understand the effect of strong matter light coupling, it is instructive to consider a weak coupling limit first. The strength of matter-light coupling is usually characterized by a ratio of a "bare" Rabi frequency $g\sqrt{\mathcal{N}_m}$ (which is the splitting between the lower and upper polariton in the absence of vibrational dressing $S = 0$) and electronic transition energy ε. So, a weak coupling limit corresponds to $g\sqrt{\mathcal{N}_m}/\varepsilon \ll 1$.

Fig. 3.1 shows a summary of weak coupling results at $g\sqrt{\mathcal{N}_m} = 0.05$ (so it basically describes how an ordinary molecular laser operates) and a system cartoon. The weak coupling phase diagram, Fig. 3.1(c), is straightforward to understand. The cyan dashed line shows the lasing-normal phase boundary for 2-level molecules (without exciton-phonon coupling $S = 0$), while black and white regions represent lasing and normal phases when considering the full model. The lasing threshold at $S \neq 0$ is reduced with respect to $S = 0$ case in the region $\omega_c < \varepsilon$, where emission is stronger than absorption, and increased in an opposite region, which makes perfect sense. Indeed, for lasing with a two-level system one needs inversion, which requires pumping to be stronger than decay $\Gamma_\uparrow > \Gamma_\downarrow$. However, as discussed in the beginning of this section, in the case of vibrational dressing, a different transition may be employed for lasing, e.g. $(1 - 0)$ which is already inverted at much lower pumping $\Gamma_\uparrow$ because of exponentially small population of the state $(\downarrow, 1)$ at $k_B T_v \ll \omega_v$. Therefore the peaks of reduced lasing threshold at $\omega_c < \varepsilon_0$ originate from

transitions to final states with non-zero number of phonons. The anti-peaks at $\omega_c > \varepsilon$ correspond to maxima of absorption, where it is much stronger than emission. At $\omega_c = \varepsilon_0$ pumping threshold with vibrational dressing is the same as without it, i.e. $\Gamma_\uparrow^{th} = \Gamma_\downarrow$.

Next, Fig. 3.1(d) shows the composition of the unstable mode at the lasing threshold, i.e., along the boundary between lasing and normal states shown in Fig. 3.1(c). In the region where the threshold is low (around $\omega_c = \varepsilon - \omega_v$), the $(1-0)$ transition contributes most, while where the threshold is high (around $\omega_c = \varepsilon + \omega_v$), the $(0-1)$ transition dominates. Other transitions are not shown as they weight is generally much lower.

3.3.2 Strong coupling

Having understood the physics in the weak coupling limit, we can now explore how strong exciton-photon coupling modifies the phase diagram, and understand the physics behind. Fig. 3.3 shows the evolution of a $(\omega_c, \Gamma_\uparrow)$ phase diagram as exciton-photon coupling $g\sqrt{\mathcal{N}_m}$ goes up, in the low pumping regime to see whether strong coupling is a direct route to low threshold lasing. As the system enters the strong coupling regime $g\sqrt{\mathcal{N}_m} = 0.1$ (roughly speaking when $g\sqrt{\mathcal{N}_m}$ exceeds molecular transition linewidth, which is mostly controlled by dephasing Γ_z in our model), the form of a phase diagram basically remains the same as in the weak coupling limit. However, as $g\sqrt{\mathcal{N}_m}$ increases, the most striking feature is that the lobe at $\omega_c = \varepsilon - \omega_v$ (due to $(1-0)$ transition) bends and, at weak pumping around $\Gamma_\uparrow \simeq 0.5\Gamma_\downarrow$, extends to significantly higher cavity frequencies, which finally leads to a re-entrant behaviour.

To understand the mechanism responsible for the extension of low threshold lasing region to higher cavity frequency, we need to explore the nature of unstable modes. Again, to make a firm foundation for strong coupling analysis, it is instructive to start from a more straightforward case of moderate coupling $g\sqrt{\mathcal{N}_m} = 0.1$. Figure 3.4 shows the composition of the unstable mode (lower panels), frequencies of all system eigenmodes (upper panels), and gain of the unstable mode along three fixed pumping cuts across the top left phase diagram Fig. 3.3. In Fig. 3.4(a), at low pumping $\Gamma_\uparrow = 0.4\Gamma_\downarrow$, we can see polaritonic splitting where photon[1] resonates with the excitonic $(0-0)$ transition (which does not involves phonons), i.e. where $\omega_c = \varepsilon$. There is one more anti-crossing point at higher photon frequency due to a transition involving a phonon. However, corresponding anti-crossing is much smaller because this molecular transition is much more weakly coupled to a photon[2], and emission

[1] here we use effective photon frequency, which comes from the diagonalisation of a photonic part of the Hamiltonian (3.1), which gives effective frequency $\omega_c^{\text{eff}} = \sqrt{\omega_c(\omega_c + 4g^2\mathcal{N}_m/\varepsilon)}$ and effective coupling $g^{\text{eff}} = g\sqrt{\omega_c/\omega_c^{eff}}$.

[2] in the second order perturbation theory for a transition involving n phonons in the electronically excited state, it is $g^2 S^n e^{-S}/n!$

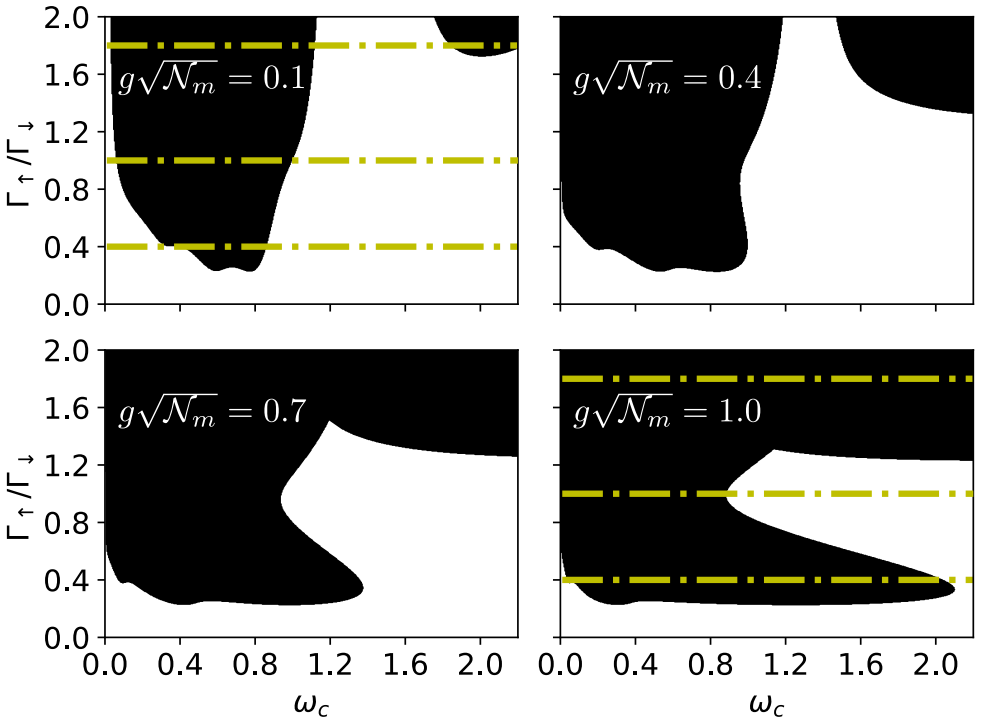

Figure 3.3: Evolution of phase diagrams with increasing coupling, $g\sqrt{\mathcal{N}_m}$ (values as shown). Dash-dotted (yellow) lines indicate the cuts shown in Fig. 3.4,3.6. Parameters as in Fig. 2.1.

from this state is very weak due to fast relaxation to the lowest energy state in the excited electronic state manifold. There is no anti-crossing at smaller photon frequency because ground electronic state with finite number of phonons is not activated at low temperatures, so there is no absorption from this state. As pumping increases — panels (b,c) — polaritonic splitting goes away due to extra effective dephasing caused by stronger pumping. At weak pumping, $\Gamma_\uparrow = 0.4\Gamma_\downarrow$, lasing develops when photon frequency ω_c crosses the $(1-0)$ or $(2-0)$ transitions, as expected. Indeed, as can be seen from the Fig. 3.4(d), the unstable mode mostly involves $(1-0)$ transition, evolving to $(0-0)$ transition as ω_c approaches the zero-phonon line. As pumping increases, lasing becomes possible over a wider range of photon frequencies. When excitonic pumping $\Gamma_\uparrow$ exceeds decay rate $\Gamma_\downarrow$, electronic transition becomes inverted, so lasing becomes possible at $\omega_c = \varepsilon$. As pump power increases further, lasing can be achieved even in the region of ω_c where absorption is stronger than emission. However, as can be seen in the Fig. 3.4(c), high-frequency lasing develops in the region of the smallest absorption-emission ratio first. At even stronger pumping, low- and high-frequency lasing regions finally merge. This can be clearly seen in the full $g\sqrt{\mathcal{N}_m} = 0.1$ phase diagram in the Fig. 3.5, which clearly shows low-pumping peaks due to local maxima of emission, and

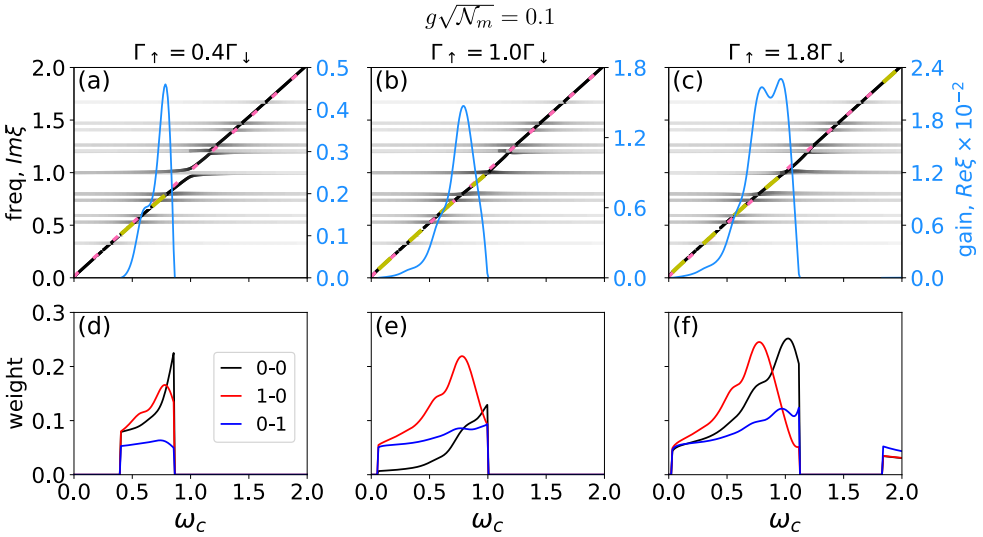

Figure 3.4: Nature of lasing instability at $g\sqrt{\mathcal{N}_m} = 0.1$. Top (a–c): Real (right, solid cyan) and imaginary (left, grayscale) parts of linearized eigenvalues ξ. The grayscale indicates the photon component of that mode. The yellow dashed line highlights which imaginary part corresponds to the mode that is unstable (has a positive real part). The pink dotted line shows the effective photon frequency, ω_c^{eff}. Bottom (d–f): Vibrational composition of unstable mode. Parameters as in Fig. 2.1.

high-pumping anti-peaks due to absorption maxima.

At stronger coupling, $g\sqrt{\mathcal{N}_m}$, the physics changes considerably. First, in the low-pumping regime $\Gamma_\uparrow = 0.4\Gamma_\downarrow$, Fig. 3.6(a), we have a very strong anti-crossing, which now involves many transitions, in contrast to mostly $(0-0)$ for $g\sqrt{\mathcal{N}_m} = 0.1$. In addition, Fig. 3.6(a) shows a a new feature: a self-tuning effect, where the unstable polaritonic mode locks with a $(1-0)$ vibrational sideband driving lasing. Therefore, in spite of a strong exciton-photon detuning, frequency locking allows lasing at a wide range of photon frequencies in the strong-coupling regime because of self-tuning of the lower polariton to allow feeding by the $(1-0)$ molecular transition.

As pumping goes up, Fig. 3.6(b), frequency locking reduces due to effectively reduced matter-light coupling by extra dephasing caused by stronger pumping. Another notable feature is that now the unstable mode frequency pins to the $(0-0)$ transition. As pumping increases further, Fig. 3.6(c), polaritonic splitting gets smaller. At the same time, in contrast to previous cases, we get frequency pinning with the $(0-1)$ transition, which is also clear from the Fig. 3.6(f). Moreover, as frequency pinning goes away at high enough bare photon frequency, the system still supports lasing, but at a bare photon frequency — Fig. 3.7. Therefore, in the strong coupling and pumping regime the system demonstrates a transition from polariton to photon lasing as a

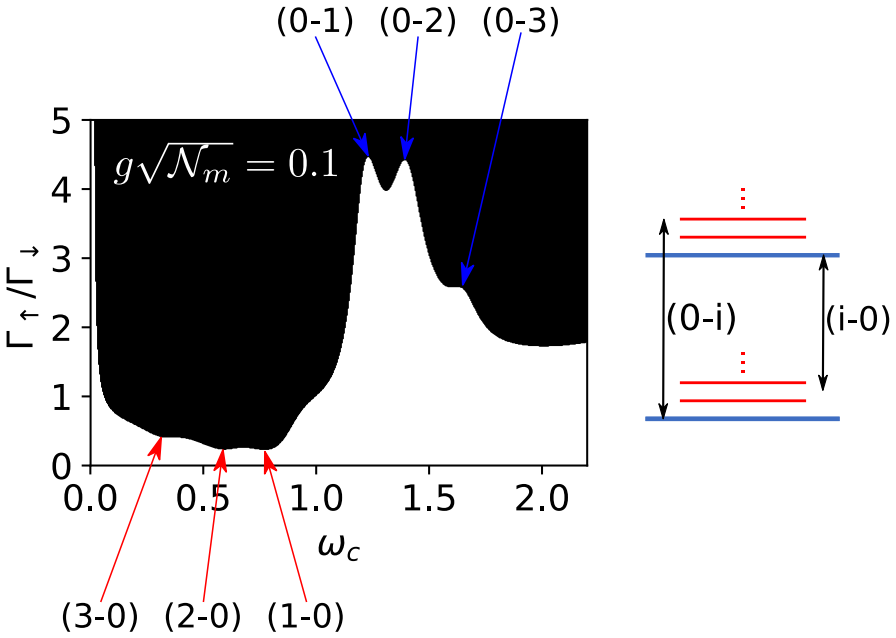

Figure 3.5: Full $g\sqrt{\mathcal{N}_m} = 0.1$ phase diagram

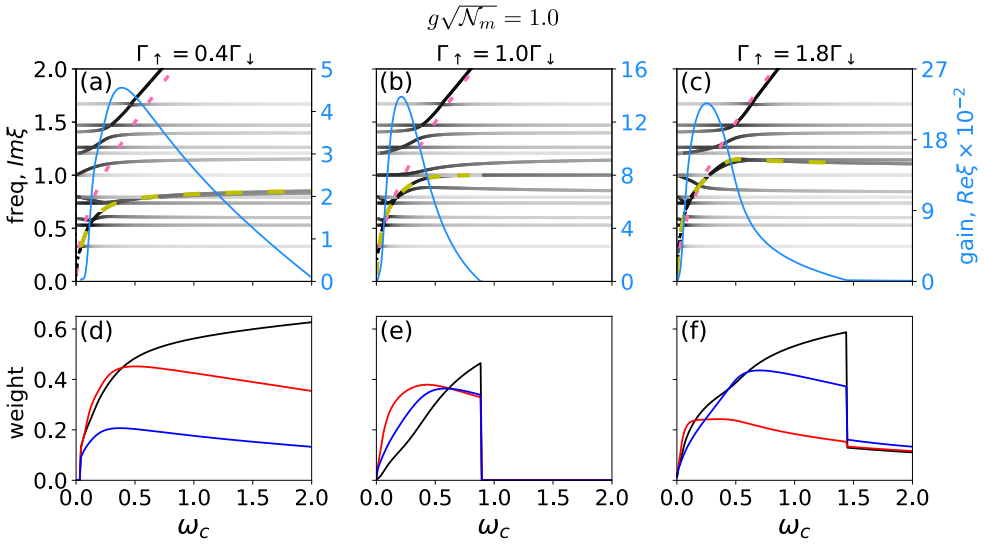

Figure 3.6: Nature of lasing instability at $g\sqrt{\mathcal{N}_m} = 1.0$

detuning does up.

To check the effect of stronger dephasing on a phase diagram, in Fig. 3.8 phase diagrams with increased coupling of vibrational mode to bath phonons γ_v and with increased electronic dephasing rate are demonstrated. Clearly, increased dephasing rate Γ_z has the strongest effect on a phase diagram reducing the effect of strong matter-light coupling. This makes sense because enhancing

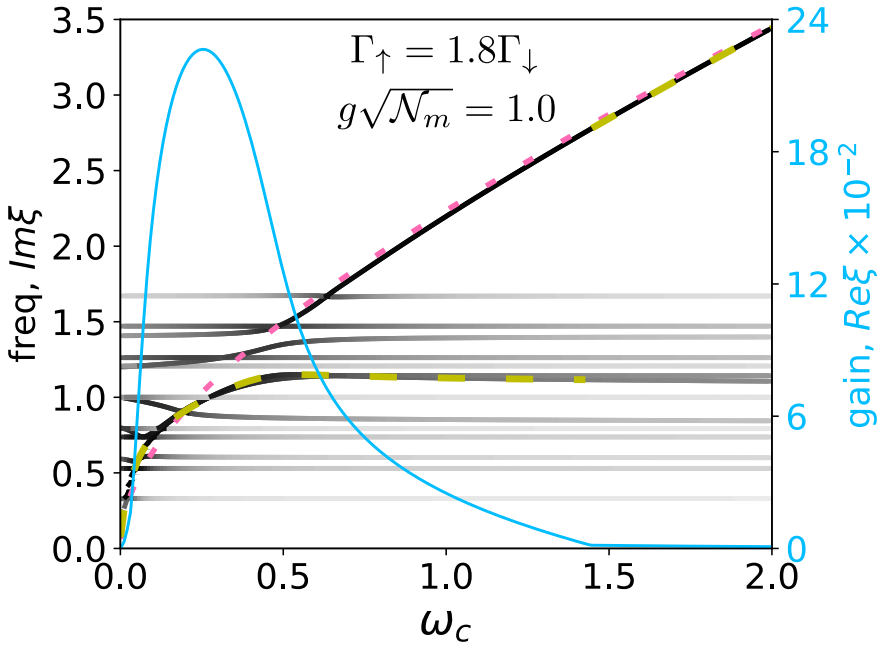

Figure 3.7: Transition from polariton to photon lasing

Γ_z increases affects excitonic linewidth, which reduces effective exciton-photon coupling.

3.3.3 Pumping threshold versus matter-light coupling strength & optimal cavity frequency ω_c

Having understood the effect of strong matter-light coupling on a lasing phase diagram, we can now address the questions of whether strong coupling is a direct route to low-threshold lasing, in other words whether polariton laser outperforms an ordinary molecular one in terms of lasing threshold. Fig. 3.9(a-c) show $(\Gamma_\uparrow, g\sqrt{\mathcal{N}_m})$ phase diagrams when photon resonates with $(1-0)$, $(0-0)$ and $(0-1)$ transitions respectively. In the regime of a "good molecular laser", where $\omega_c = \varepsilon - \omega_v$ ($\omega_c = 0.8$ in our case), strong-coupling phase boundary matches weak-coupling results (red dashed line) up to a unimportant normal region where coupling is strong and pumping is relatively high. This suggests that strong coupling does not improve a frequency-optimised molecular laser. If we go beyond optimal photon frequency and tune ω_c to $(0-0)$ or $(0-1)$ transition, Fig. 3.9(b,c), where $\Gamma_\uparrow > \Gamma_\downarrow$ is necessary (but not sufficient) for lasing in the weak-coupling theory, strong coupling does lead to reduced threshold. Therefore, strongly-coupled polaritonic lasing outperforms a weakly-coupled molecular laser if cavity frequency is not optimised, i.e. when $\omega_c \neq \varepsilon - \omega_v$.

To see how lasing threshold pumping depends on the strength of matter-light coupling, in Fig. 3.9(d) I plot threshold $\Gamma_\uparrow/\Gamma_\downarrow$ optimised over a bare

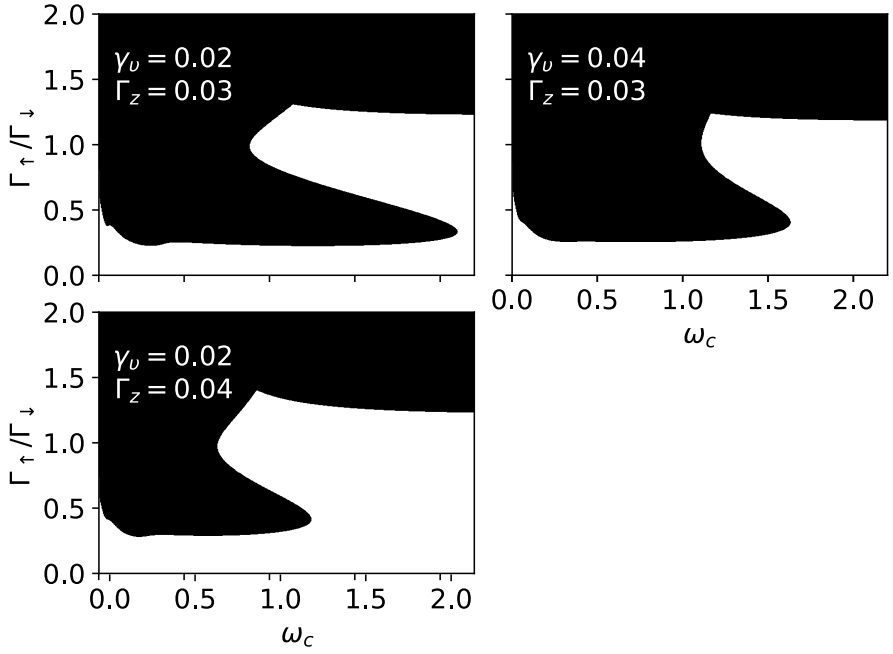

Figure 3.8: Dependence of phase diagram at $g\sqrt{\mathcal{N}_m} = 1.0$ on varying vibrational damping γ_v and excitonic dephasing rate Γ_z

cavity frequency ω_c versus bare Rabi splitting $g\sqrt{\mathcal{N}_m}$. These results suggest that stronger coupling does lead to lower-threshold lasing. However, as soon as the system enters the strong-coupling regime, not much threshold reduction can be achieved (only a few per cent) upon increasing coupling further if ω_c is optimised.

While Fig. 3.9(d) shows how lasing threshold depends on coupling at optimised frequency, it doesn't show how to choose optimal frequency, which is an essential experimental parameter. So, Fig. 3.10 shows bare photon frequencies at which lasing threshold has local minima versus matter-light coupling. Firstly, there is no lasing below critical coupling strength, which is around $g\sqrt{\mathcal{N}_m} \approx 0.0024$ in our model. As coupling becomes strong enough to allow lasing, due to very inefficient coupling to $(n-0)$ transitions, the lasing is driven $(0-0)$ transition. As coupling increase further, another minimum due to $(1-0)$ transition arises, which soon becomes a global minimum (standard molecular laser case). At even stronger coupling, local minima due to higher-order transitions $(2-0)$ and $(3-0)$ (which can be also seen in Fig. 3.3) arise.

Increasing coupling further into the strong-coupling regime leads to quite non-trivial evolution of the positions of local minima. The behaviour of the $(1-0)$ branch can be associated with the self-tuning at strong coupling, which allows lasing threshold for this transition to move to higher photon frequency.

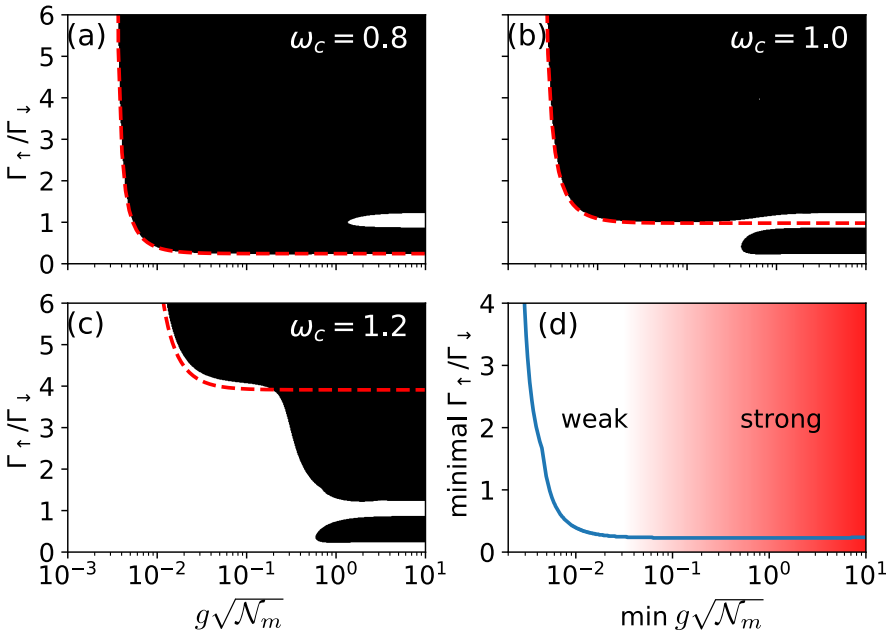

Figure 3.9: (a)–(c) Phase diagrams at different cavity frequencies. The red dashed line shows the weak-coupling theory phase boundary [27]. Panel (d) shows how minimal critical pumping strength (optimized over cavity frequency) depends on matter-light coupling. The red shading highlights the crossover from the weak- to strong-coupling region (where light-matter coupling exceeds rates of incoherent processes)

In contrast, the $(2-0)$ and $(3-0)$ transitions do not show any self-tuning effect because they are not strongly coupled to a photon, which may be seen (although not rigorously) from the lowest-order perturbation theory, which gives corresponding emission (absorption) matrix element $g^2 S^n e^{-S}/n!$. At the same time, upon increasing matter-light coupling, effective photon frequency goes up $\omega_c^{\text{eff}} = \sqrt{\omega_c(\omega_c + 4g^2\mathcal{N}_m/\varepsilon)}$. Therefore, for a photon to resonate with $(2-0)$ or $(3-0)$ transitions, its bare frequency should be reduced in the strong-coupling region to cope with effective photon frequency growth.

To sum up, although strong matter-light coupling does not reduce molecular laser pumping threshold, it does increase the range of photon frequencies at which low-threshold lasing can be achieved, as Fig. 3.3 clearly demonstrates.

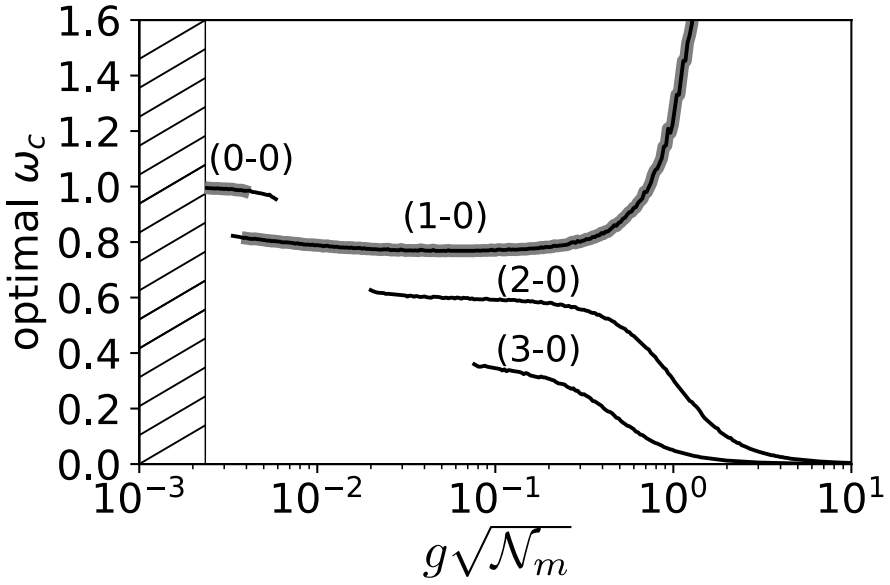

Figure 3.10: Optimal photon frequency vs matter-light coupling. Shaded region highlights global minimum.

Chapter 4

Imbalanced polariton condensates

The ground state of a non-interacting bosonic system is a simple condensate, which is described by a wave-function $\psi = \sqrt{\rho}e^{i\phi}$, where ρ is a condensate density and ϕ — its phase. Due to Pauli exclusion principle, the fermionic ground state is drastically different from a bosonic one, and it is described by a Fermi sea, which is a Slater determinant, which in the second quantized notation — for a single flavor of fermions — is simply $|FS\rangle = \prod_{k<k_F} c_k^\dagger |0\rangle$, where $|0\rangle$ is a vacuum state and k_F — Fermi momentum. However, in the presence of attractive interaction between fermions, they may form pairs — so-called composite bosons — and condense. For two flavors of fermions a and b the corresponding mean-field wavefunction is $\prod_k \left(\cos\theta_k + \sin\theta_k a_k^\dagger b_{-k}^\dagger\right)|0\rangle$ (where θ_k is a system–dependent function). Composite boson condensation is the origin of such effects as superfluidity and superconductivity. In the following discussion, we refer to several results for superconductors. As discussed in Section 1.3.1, these can be translated to properties of excitonic insulators directly, by means of a particle-hole transformation[1].

Usually, the numbers of fermions of each flavour (N_a and N_b) are the same, so each fermion may pair up. However, under some circumstances, $N_a \neq N_b$, which frustrates the system and may bring it to a normal (non-condensed) state. For example, when the Zeeman energy $\frac{1}{2}g\mu_B H$ exceeds the superconducting gap Δ, pairs break down and a superconductor turns into a metal, i.e. it loses any coherence. However, as was proposed in the sixties [72, 73], in order to accommodate density difference and still restore some coherence, a simple uniform superconducting state may be replaced by state with finite center-of-mass momentum Q Cooper pairs and finite density of

[1] it is worth mentioning that in contrast to previous chapters where localized intramolecular electronic excitations were considered, in this section delocalized electrons and holes potentially forming so-called Wannier-Mott excitons in semiconductors will be discussed

unpaired fermions:

$$|\psi_Q\rangle = \prod_{l\in \mathrm{U}} a_l^\dagger \prod_{l'\in \mathrm{U}'} b_l^\dagger \prod_{k\in \mathrm{P}} \left(\cos\theta_k + \sin\theta_k a_{Q/2+k}^\dagger b_{Q/2-k}^\dagger\right)|0\rangle, \tag{4.1}$$

where P corresponds to paired and U/U' — to unpaired fermions. The idea is that the smaller (minority particles) Fermi surface shifts to contact the larger one, and pairs are formed in the vicinity of the touching point. If energy gain due to pair formation exceeds kinetic energy penalty, then $|\psi_Q\rangle$ has lower energy than the normal state, thus describes the ground state. This state with a single center of mass pair momentum is called an FF state (Fulde Ferrel [72]) and a superposition of states with opposite momenta — LO (Larkin Ovchinnikov [73]), which is also sometimes called a Pair Density Wave (PDW) state [107]. However, there is no consensus on whether such a state has ever been observed in superconducting (or cold atom) systems, although there is some evidence discussed in, e.g. Ref. [107]. Probably, in superconductors the problem comes from weak attractive interaction (making the imbalanced condensate region rather small in parameter space), while in cold atoms — from ubiquitous phase separation accompanying the first–order phase transition from a zero- to a finite-momentum condensate.

In contrast, a semiconductor is not expected to have these problems. First, electrons and holes are charged particles, which, as in a superconductor, prevents phase separation. Second, electrons and holes interact via long-range Coulomb rather then weak phonon-mediated potential, thus one may expect an excitonic condensed state to be more robust to variations of external parameters. Indeed, exciton binding energy E_b in 2D TMDC materials [108] is of the order of 0.1 eV (e.g. in a monolayer of WS_2 $E_b = 0.71 \pm 0.01$eV, while gap energy $E_g = 2.73$eV [109]), which means that, in principle, condensed excitonic states may be stable even at room temperature. Moreover, when taking into account strong exciton-photon coupling, the critical temperature of condensation is known to be much higher due to small polaritonic mass, thus leading to room T_c polariton condensation. For these reason, a 2D TMDC semiconductor in a microcavity serves an ideal playground for exploring the physics of imbalanced polaritonic condensates.

Although polariton condensation has been widely explored since its first observation [63], almost exclusively balanced systems, with equal densities of electrons and holes, have been studied so far. However, recent experimental works on imbalanced electron-hole systems (due to applied bias voltage) in TMDC monolayers strongly coupled to a cavity photon [80–84], demonstrated control over charge density in polaritonic systems, thus opening an experimental avenue for studying imbalanced polaritonic condensates. This leads to an easy–to–formulate question: can a combination of strong matter-light coupling and electric field biasing promote novel imbalanced condensed states, which do not exist otherwise?

Indeed, on the one hand electron hole density imbalance promotes finite centre of mass momentum Q (FFLO) condensation, but on the other, steep photon dispersion facilitates $Q \approx 0$ pairing, so this is where the competition comes from. Depending on the system parameters, this competition may bring the system to an FFLO state or to an ordinary polariton condensate. However, there is a chance that new phases will emerge from this competition or otherwise unstable states (e.g. a so-called breached–pair state [110] or a deformed–fermi–surface state [111], which are discussed below) will be stabilized by a photon. Moreover, due to the existence of a cavity photon, these new states may have no counterparts in the physics of superconductors or cold atoms, which makes the imbalanced polariton system so unique.

The aim of this chapter is to find which states are realized in the system of imbalanced polaritons at the mean-field level. Section 4.1 describes the simplest model of a two-band semiconductor with effectively free electrons and holes coupled to cavity photons. Section 4.2 introduces self-consistent mean-field variational approach used to find the lowest energy state of the system and so to extract a phase diagram versus tunable parameters such as temperature, charge density, photon cut-off frequency. Section 4.3 discusses the nature of the states found in this system. Section 4.4 discusses prospects of experimental observations.

4.1 Model

Fig. 4.1 shows a cartoon of the system consisting of a biased semiconductor layer in a microcavity. The Hamiltonian reads:

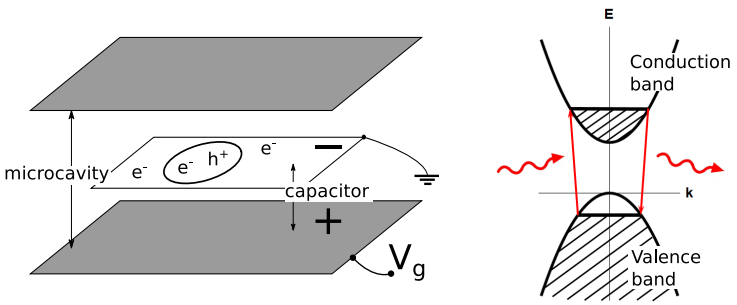

Figure 4.1: Cartoon illustrating the model: the upper and the lower mirrors form a microcavity, while the lower mirror and a system (a single layer of a semiconductor) form a capacitor

$$H = H_0 + H_c + H_{lm} + H_{es}, \tag{4.2}$$

where the bare Hamiltonian

$$H_0 = \sum_k \left[\left(\frac{k^2}{2m_e} + E_G \right) e_k^\dagger e_k + \frac{k^2}{2m_h} h_k^\dagger h_k + \omega_k a_k^\dagger a_k \right], \tag{4.3}$$

where E_G is an electron-hole gap energy, $m_{e/h}$ - effective mass of an electron or a hole, e_k, h_k, a_k are electron, hole and photon annihilation operators respectively, and ω_k is photon dispersion. The next term describes Coulomb interaction:

$$H_c = \frac{1}{2S} \sum_{kk'q} V(q) \left\{ e_{k+q}^\dagger e_{k'-q}^\dagger e_{k'} e_k + h_{k+q}^\dagger h_{k'-q}^\dagger h_{k'} h_k - 2 e_{k+q}^\dagger h_{k'-q}^\dagger h_{k'} e_k \right\}, \tag{4.4}$$

where S is the quantization (sample) area, $V(q) = 2\pi e^2/\varepsilon q$, ε is a background dielectric permittivity. The light-matter interaction term — written in the Coulomb gauge — for simplicity using rotating wave approximation, is

$$H_{lm} = \frac{g}{\sqrt{S}} \sum_{k,q} \left(e_k^\dagger h_{q-k}^\dagger a_q + a_q^\dagger h_{q-k} e_k \right). \tag{4.5}$$

The remaining terms describe externally controlled quantities: system excitation density and electric charge density. The first one — the level of system excitation in a thermal equilibrium — is modeled by introducing an excitation chemical potential, which couples to the conserved total number of excitations:

$$\tilde{H} = H - \mu_{ex} \sum_k \left(a_k^\dagger a_k + \frac{1}{2} \left[e_k^\dagger e_k + h_k^\dagger h_k \right] \right). \tag{4.6}$$

In the following, to find the state of the system, $\tilde{H}$ will be minimized. Also, from now H is identified with $\tilde{H}$. Electrical charging of the system may be performed using the principles of Field Effect Transistor operation. Consider a capacitor with two parallel plates (gate and "system"), one of which is grounded (system), and the other one has some externally fixed potential (gate). The energy of such a capacitor is $q^2/2C$, where $n_0 = CV$ is a fixed charge on a gate plate and $C \approx S/4\pi d$ is capacitance (S — plate area, d — distance between plates, V — gate potential; CGS). Fluctuations of the system charge lead to electrostatic energy penalty, which is quadratic in charge deviation. Assuming that the system layer is very thin, such that its surface is equivalent to its body, so extra electrons occupy the entire piece of material (rather than staying exponentially close to a surface), the last term of the Hamiltonian (4.2) describing external electrostatic biasing reads:

$$H_{es} = \alpha \int d^2x (n_c(x) - n_0)^2, \tag{4.7}$$

where α and n_0 are an experimentally tunable parameters, which describe energy penalty for charge deviation and target charge density set by external voltage respectively; $n_c(x)$ is charge density in real space, i.e. $n_c(x) =$

$e^\dagger(x)e(x) - h^\dagger(x)h(x)$. The assumption of an atomically thin layer is valid for the materials of interest — TMDC monolayers, with which the described setup has already been experimentally realized in optical experiments [80–84].

This term (4.7) is quite different from a term usually used to model imbalance:

$$H_{imb} = h\sum_k (n_e(k) - n_h(k)). \tag{4.8}$$

A term, similar to (4.8), was originally used to describe a superconductor in magnetic field. It is also widely used to describe polarisation of cold atomic systems in effective magnetic field in some pseudo-spin space. However, its application is not well justified in modeling biased charged systems. Indeed, the term (4.8) promotes maximum imbalance, i.e. it pushes the system to a state with as high particle number difference as possible $(n_e - n_h) \to \max$, while the term (4.7), in contrast, drives the system to a state with externally fixed value of imbalance. Given that energy penalty α for the deviation of imbalance from a target value n_0 is an experimentally controlled parameter, and it can be made big compared to the system internal energy scales, n_0 basically sets the system imbalance charge) for large enough α, i.e. $n_c \simeq n_0$.

4.2 Variational approach

4.2.1 Why variational?

Applications of the approach of Green's functions and subsequent iterative solutions of gap equations or some approximate "proof-of-principle" calculations led to a lot of controversy in the field of imbalanced condensates. A potential reason of these problems probably lies in difficulty of choosing the correct solution of out potentially multiple solutions of a gap equation. Just as an example, in 1963, in the context of superconductivity G. Sarma proposed a state with both paired and unpaired electrons, which was later called a Sarma state [112]. Forty years later, in 2003, in the context of QCD this state was rediscovered [110] and then called a breached–pair (BP) state. In the same year it was shown that this state is unstable [113]. Two years later, in 2005, in response to this paper, a paper [114] showed how to amend the model presented in [110] such that the resulting BP state becomes stable. Then, e.g. in [115] it was suggested that a BP state is stable only at large enough mass imbalance (the proposed value was $m_1/m_2 > 10$). Then, in [116, 117] a BP state was theoretically found for mass ratios corresponding to electrons and holes in GaAs. However, in a recent paper [118] devoted to resolve these issues, a BP state was not found for similar mass ratios.

Another proposal for an imbalanced condensed state was a deformed–Fermi–surface (dFS) state [111, 119]. However, the existence of this state has never been supported by other theoretical calculations or experimental measurements.

Therefore, it seems that obtaining a phase diagram by directly solving the gap equation is a very challenging task. In contrast, a variational approach is free of such problems. Indeed, even if minimization of ground state energy $\langle\psi|H|\psi\rangle$ leads to multiple local minima or saddle points, one should just choose the solutions with the lowest energy. Therefore, beyond choosing an adequate variational state, nothing else is needed. Moreover, while Green's function approaches are based on weak–coupling expansions and thus are not always well–controlled when coupling is strong, a variational approach contains clear intuitive ingredients and the criterion of accuracy of a variational method is straightforward: the lower the resulting energy, the better physics is described. For these reasons to obtain a phase diagram of a system of interacting electrons, holes and photons, a variational approach will be used. On the other hand, if possible [120], extension of a variational approach beyond mean-field is not straightforward. This is left for future work.

4.2.2 Zero temperature

At zero temperature, a variational wave-function approach can be employed to find the system ground state. The mean-field variational wavefunction describing pair condensation of fermions e and h is

$$\prod_k (u_k + \upsilon_k e_k^\dagger h_{-k}^\dagger)|0\rangle \tag{4.9}$$

with a normalisation condition $u_k^2 + \upsilon_k^2 = 1$, which means that the probability to find or not to find a pair is 1. This wavefunction is known to describe both BEC and BCS limits well [59]. It may be obtained by mean-field decoupling of an interacting Hamiltonian, diagonalising it and then constructing a vacuum state of resulting quasiparticles [121]. To consider an imbalanced system, one can add extra parameters to introduce finite density of unpaired electrons and/or holes:

$$\prod_k (\alpha_k e_k^\dagger + \beta_k h_k^\dagger + u_k + \upsilon_k e_{Q/2+k}^\dagger h_{Q/2-k}^\dagger)|0\rangle, \tag{4.10}$$

where another variational parameter — pair center of mass wavevector Q — is added to also allow for a possibility of a Fulde-Ferrel (FF) state. Therefore, all the possible imbalanced states, including a usual uniform condensate, proposed FF, BP and dFS states, can be found in a unified approach by minimizing ground state energy using a single wavefunction (4.10).

While the wavefunction (4.9) can be derived from the mean-field decoupling of an interacting Hamiltonian, it can be also guessed by constructing a coherent state of pairs $\exp(\phi_k e_k^\dagger h_{-k}^\dagger)|0\rangle$ and then expanding the exponent, which then results in (4.9). In analogy to the BCS theory of superconductivity, this variational wavefunction was used by Keldysh and Kopaev [122]

to study exciton condensation in semiconductors. In the very same way a polaritonic wavefunction can be constructed. Indeed, a polariton is a superposition of an exciton and a photon, so its creation operator is given by $P_Q^\dagger = \lambda_Q a_Q^\dagger + \phi_k e_{Q/2+k}^\dagger h_{Q/2-k}^\dagger$. Exponentiation of this operator then leads to

$$e^{\lambda_Q a_Q^\dagger} \prod_k (u_k + e_{Q/2+k}^\dagger h_{Q/2-k}^\dagger)|0\rangle, \tag{4.11}$$

which was used in, e.g. Ref. [123] for a balanced condensate with zero center of mass moment pairing $Q = 0$.

The fact that an exponentiated wavefunction and one obtained by dioganalising mean-field Hamiltonian match is not a coincidence. Indeed, mean-field decoupling is based on the assumption that the system state is Gaussian, while a constructed state (4.9) is Gaussian as well. Therefore, this approaches originate from the same assumption of a Gaussian state.

In spite of advantages of a variational approach described above, it has an important drawback: it is difficult to go beyond mean-field approximation. While there are available approaches for few-body systems, e.g. for describing the physics of polarons [124–126], there is no established way of adding the physics of quantum fluctuations to the usual BCS ansatz (4.9). While there is a well-established field-theoretical technique of dealing with quantum fluctions based on including Gaussian fluctuations and going beyond with an RG analysis [121], it is highly desirable to obtain robust results for a mean-field phase diagram first, which can be reliably done variationally. On the other hand, the mean-field physics of thermal fluctuations can be well captured within the variational density matrix approach, which is the topic of the next section.

4.2.3 Finite temperature

While the wavefunction (4.10) (with a photonic coherent state) can be used to study ground state of an imbalanced polaritonic condensate, it does not allow to explore finite-temperature regime, the importance of which is apparent. To understand the role of temperature, one may use a variational density matrix approach. Again, the idea is to introduce a Gaussian thermal state and then minimize the resulting free energy $F = E - TS$ (rather than just energy $\langle H \rangle$ as above). As shown in Ref. [127], one can obtain an upper bound for an exact free energy:

$$F \leq F_0 + \langle H - H_0 \rangle_0, \tag{4.12}$$

where H is the original Hamiltonian, H_0 — any other Hamiltonian, $\langle O \rangle_0 = \mathrm{Tr}\left[e^{-\beta H_0}\hat{O}\right]/Z_0$, and $\beta = 1/T$ is inverse temperature ($k_B \equiv 1$). Also, $F_0 = -T \ln Z_0$ and $Z_0 = \mathrm{Tr}\left(\exp\{-\beta H_0\}\right)$. The right hand side of this expression may be associated with a variaional free energy $\mathcal{F}_v$. Therefore, the search for system lowest energy state comes down to minimization of $\mathcal{F}_v$. To introduce a variational Gaussian (mean-field) state, one just needs to write

the most general quadratic Hamiltonian, which can be diagonalised to then find any expectation values. Such an approach was used, e.g. in Ref. [128] to study bi-polariton condensate formation. The advantage of the quadratic Hamiltonian is that it allows to calculate all expectations in a closed form. However, apparently in (4.12) one can choose any non-quadratic Hamiltonian as well, but it then requires using other numerical techniques, e.g. exact diagonalisation of a variational Hamiltonian [120], to calculate the free energy.

4.2.4 Variational mean-field free energy

In the calculations below, a variational mean-field free energy will be used

$$\mathcal{F}_{\mathrm{vMF}} = F_{\mathrm{MF}} + \langle H - H_{\mathrm{MF}} \rangle_{\mathrm{MF}}, \tag{4.13}$$

where F_{MF} is the free energy corresponding to a variational mean-field Hamiltonian H_{MF}. The most general variational quadratic (mean-field) Hamiltonian reads:

$$\begin{aligned} H_{MF} = T_Q(a_Q^\dagger + a_Q) + \sum_k \Bigg[& \nu_k a_k^\dagger a_k + \eta_k^h + \\ & + \begin{pmatrix} e_{Q/2+k}^\dagger & h_{Q/2-k} \end{pmatrix} \begin{pmatrix} \eta_k^e & \Delta_k \\ \Delta_k & -\eta_k^h \end{pmatrix} \begin{pmatrix} e_{Q/2+k} \\ h_{Q/2-k}^\dagger \end{pmatrix} \Bigg]. \end{aligned} \tag{4.14}$$

This Hamiltonian contains three variational functions η_k^e, η_k^h, Δ_k (all defined in 2D), and two variaional scalar parameters T_Q and Q (setting $\nu_k = \omega_k$ because the original Hamiltonian does not contain photon-photon interaction terms). The variational parameters η_k^e and η_k^h are introduced to describe band renormalisation due to repulsive electron-electron and hole-hole interaction, which reduces a semiconductor band gap and renormalises bare masses. Excitonic pairing is described by a gap–function Δ_k. Exciton center of mass momentum is introduced by a single variable Q. Due to a spontaneously chosen direction of Q, one can always associate x–axis with the direction of Q, thus one needs only a single x–component of a Q–vector. The coherent state of a photon with a momentum Q is modeled by a displacement parameter T_Q. The coherent photon momentum is the same as the exciton momentum due to momentum conservation.

To calculate (4.13), the variational Hamiltonian (4.14) should be diagonalised. First, the photonic field may be displaced $\tilde{a}_Q = a_Q + T_Q/\omega_Q$ to remove the linear term. The fermionic part may be diagonalised by a unitary transformation

$$\begin{pmatrix} \alpha_k \\ \gamma_k^\dagger \end{pmatrix} = \begin{pmatrix} u_k & -v_k \\ v_k & u_k \end{pmatrix} \begin{pmatrix} e_{Q/2+k} \\ h_{Q/2-k}^\dagger \end{pmatrix}, \tag{4.15}$$

which leads to

$$H_{\rm MF} = \sum_k \Big(\eta_k^h + \varepsilon_1(k)\alpha_k^\dagger\alpha_k + \varepsilon_2(k)(1+\gamma_k^\dagger\gamma_k)\Big) + \omega_Q\tilde{a}_Q^\dagger\tilde{a}_Q + \sum_{k\neq Q}\omega_k a_k^\dagger a_k - T_Q^2/\omega_Q, \tag{4.16}$$

where $\varepsilon_{1,2}(k) = E_k \pm (\eta_k^e - \eta_k^h)/2$, $E_k = \sqrt{(\eta_k^e+\eta_k^h)^2/4 + \Delta_k^2}$ and

$$u_k = \sqrt{\frac{1}{2}\left(1 + \frac{\eta_k^e+\eta_k^h}{2E_k}\right)},$$
$$\upsilon_k = -\operatorname{sign}(\Delta_k)\sqrt{\frac{1}{2}\left(1 - \frac{\eta_k^e+\eta_k^h}{2E_k}\right)}.$$

Using this Hamiltonian, any expectations can be easily calculated. For example,

$$\langle e_k^\dagger e_k\rangle = u_{k-Q/2}^2 n_F[\varepsilon_1(k-Q/2)] + \upsilon_{k-Q/2}^2(1 - n_F[\varepsilon_2(k-Q/2)])$$

and

$$\langle a_p^\dagger h_{p-k} e_k\rangle = \frac{-T_Q\delta_{p,Q}}{\nu_Q} u_{k-Q/2}\upsilon_{k-Q/2}\Big\{1 - n_F[\varepsilon_1(k-Q/2)] - n_F[\varepsilon_2(k-Q/2)]\Big\}$$

or one of the Coulomb terms $\langle e_{k+p}^\dagger e_{k'-p}^\dagger e_{k'} e_k\rangle = -\delta_{p,k'-k}\langle e_{k'}^\dagger e_{k'}\rangle\langle e_k^\dagger e_k\rangle$. In this expression the infinite Hartree term $p = 0$, which describes interaction of an electron with charge background, is excluded because electrostatic (charging) energy is already included in (4.7).

To rewrite free energy in term of dimensionless quantities, it is convenient to introduce 2D binding energy $E_0 = 2\hbar^2/\mu a_B^2$, 2D exciton Bohr radius $a_B = \varepsilon\hbar^2/\mu e^2$, reduced mass $\mu = m_e m_h/(m_e+m_h)$ and $k_0 = 1/a_B$ (ε - the background dielectric permittivity) and introducing an ansatz $T_Q = \sqrt{S}k_0\nu_Q\phi$ (so ϕ is intensive and dimensionless). Dividing the total free energy by Sk_0^2, and introducing a dimensionless wave-vector $k \equiv k/k_0$, and defining $f \equiv \mathcal{F}/Sk_0^2$ for the free energy and $h = H/Sk_0^2$ for all the parts of the Hamiltonian, the total free energy reads:

$$\frac{1}{Sk_0^2}\mathcal{F}_{\rm vMF} \equiv f_{\rm vMF} = f_{\rm MF} - \langle h_{\rm MF}\rangle + \langle h_{\rm lm}\rangle + \langle h_{\rm eh}\rangle + \langle h_{\rm ee/hh}\rangle, \tag{4.17}$$

where

$$f_{\rm MF} - \langle h_{\rm MF}\rangle = -\int\frac{d^2k}{(2\pi)^2}\left\{\varepsilon_1(k)n_F[\varepsilon_1(k)] + \frac{1}{\beta}\ln\left(1+e^{-\beta\varepsilon_1(k)}\right) + (1\to 2)\right\}. \tag{4.18}$$

Defining $\tilde{g} \equiv \frac{k_0 g}{\sqrt{S}}$, the matter-light term reads

$$\langle h_{\rm lm} \rangle = 2\tilde{g}\phi \int \frac{d^2k}{(2\pi)^2} u_k \upsilon_k \Big[n_F[\varepsilon_1(k)] + n_F[\varepsilon_2(k)] - 1 \Big]. \tag{4.19}$$

Electron-hole interaction term:

$$\langle h_{\rm eh} \rangle = - \int \frac{d^2k d^2k'}{(2\pi)^4} C_k C_{k'} V(k-k'), \tag{4.20}$$

where a coherence function is $C_k = u_k \upsilon_k \left(1 - n_F[\varepsilon_1(k)] - n_F[\varepsilon_2(k)]\right)$, where $n_F[x]$ is Fermi distribution. The last term reads

$$\begin{aligned} \langle h_{\rm ee/hh} \rangle = \phi^2(\omega_Q - \mu_{ex}) + \int \frac{d^2k}{(2\pi)^2} \Big\{ E_b^e(k,q) N_e(k) + E_b^h(k,Q) N_k(k) \Big\} - \\ - \frac{1}{2} \int \frac{d^2k d^2k'}{(2\pi)^4} \Bigg(N_{e/h}(k) N_{e/h}(k') \left[V(k-k') - 2\alpha \right] + 4\alpha N_e(k) N_h(k') \Bigg), \end{aligned} \tag{4.21}$$

where electron/hole bare energy

$$E_b^{e/h}(k,Q) = \frac{1}{4} \frac{m_{h/e} E_0}{m_e + m_h} \left(k \pm \frac{Q}{2} \right)^2 - \frac{1}{2} \mu_{ex} \mp 2 n_0 \alpha + \zeta E_G \tag{4.22}$$

with $\zeta = 1$ for electrons and $\zeta = 0$ for holes, and

$$\begin{aligned} N_e(k) &= u_k^2 n_F[\varepsilon_1(k)] + \upsilon_k^2 \left(1 - n_F[\varepsilon_2(k)]\right), \\ N_h(k) &= \upsilon_k^2 \left(1 - n_F[\varepsilon_1(k)]\right) + u_k^2 n_F[\varepsilon_2(k)]. \end{aligned} \tag{4.23}$$

To obtain a phase diagram, the resulting free energy should be minimized with respect to variational parameters $\eta_k^{e/h}$, Δ_k, ϕ and q. Let us first consider the normal state solution (this means setting $\Delta_k = 0$ and $\phi = 0$), which is a possible local minimum of the free energy. Minimizing with respect to $\eta_k^{e/h}$ readily leads to coupled equations:

$$\eta_k^{e/h} = E_b^{e/h}(k,q) \pm 2\alpha(n_c - n_0) - \Sigma_{ex}^{e/h}(k), \tag{4.24}$$

where the second term is an electrostatic band renormalisation, while the last one is a familiar exchange self-energy (Fock term) given by $\Sigma_{ex}^{e/h}(k) = \frac{1}{2} \int \frac{d^2k}{(2\pi)^2} N_{e/h}(k) N_{e/h}(k') V(k-k')$. Another simple limit occurs if one neglects electrostatic energy, photon and Coulomb repulsion. In this case, minimization readily leads to a familiar BCS-like gap equation:

$$\Delta_k = \int \frac{d^2p}{(2\pi)^2} \frac{V(k-p)\Delta_p}{2E_p} (1 - n_F[\varepsilon_1(p)] - n_F[\varepsilon_2(p)]), \tag{4.25}$$

which can be rewritten symbolically as $\Delta_k = -\Sigma_{eh}(k)$. Inclusion of a photon increases coherence leading to the following "polaritonic" gap equation $\Delta_k = -[\Sigma_{eh}(k) + g\phi]$, which shows that coupling to a photon increases coherence between conduction and valence bands. Minimization of the free energy over all variational parameters leads to a rather lengthy set of coupled equations, which are difficult to solve, and which solution problems has been discussed above. However, variational free energy may be efficiently minimized numerically, thus gap-like equations following analytical minimization are redundant in this approach.

While single 2D k-integrals appearing in non-interacting terms are numerically tractable, double k-integrals (which are thus 4D integrals) do not allow to do calculations on any reasonable 2D grid because the number of operations for a single integral evaluation scales as N^4 (where N is a number of grid points), and it should be evaluated hundreds or even thousands of times in an optimization routine for one realization of physical parameters. However, calculations may be sped up enormously by using Fast Fourier Transform, which requires $O(N^2 \ln^2 N)$ operations. Indeed, all 4D integrals above have the same form $I = \int \frac{d^2k d^2k'}{(2\pi)^4} f(k) f(k') v(k - k')$, which may be rewritten in real space as $I = \int d^2x |\tilde{f}(x)|^2 \tilde{v}(x)$, where $\tilde{f}(x) = \int \frac{d^2k}{(2\pi)^2} f(k) e^{ikx}$. This real space integral requires N^2 operations. Therefore, all interacting terms can be computed approximately within N^2 operations rather than N^4. This then allows to do full 2D optimization on a reasonable grid.

The other — more fundamental — problem comes from the fact that the Hamiltonian is unbound from below. Indeed, for simplicity considering only $Q = 0$, integrating photons out generates electron-hole interaction term of the form $-g^2 \sum_k e_k^\dagger e_k h_{-k}^\dagger h_{-k}$, which in real space reads $-g^2 \int d^2x P_e(x) P_h(x)$ with, e.g., $P_e(x) = \frac{1}{S} \int dy e^\dagger(y + \frac{x}{2}) e(y - \frac{x}{2})$, i.e. it is infinitely long-range electron-hole interaction, which drives the system into a state with an infinite number of electrons and holes and so diverges as a system size goes to infinity. Therefore, this term makes the results of numerical calculations grid size dependent, which was not discussed in earlier papers, e.g. [64, 129]. In the study of polariton ground state, Kamide and Ogawa [130, 131] used an exponential UV momentum cut-off $\tilde{g} \to \tilde{g}_0 \exp(-k/\kappa)$ to regularise exciton-photon interaction (with κ roughly given by a lattice spacing of a material of interest). While this approach does help to avoid technical difficulties in a very simple and physically well motivated way, it breaks gauge invariance. Indeed, consider adding a constant vector-potential (for brevity assuming $e/c \equiv 1$)

$$\sum_k \frac{k^2}{2m} (e_k^\dagger e_k + h_k^\dagger h_k) \to \sum_k \frac{1}{2m} \left\{ (k + A)^2 e_k^\dagger e_k + (k - A)^2 h_k^\dagger h_k \right\}. \quad (4.26)$$

Relabeling operators $e_k \to e_{k+A}$ and $h_k \to h_{k-A}$ clearly leads to the original Hamiltonian, i.e. to the left hand side of Eq. 4.26. While this relabeling

does not affect the Coulomb term (4.4), this does change the matter-light interaction term (4.5) if a momentum cutoff is imposed:

$$\sum_k g_k e_k^\dagger h_{q-k}^\dagger a_q \to \sum_k g_k e_{k+A}^\dagger h_{q-k-A}^\dagger a_q = \sum_k g_{k-A} e_k^\dagger h_{q-k}^\dagger a_q \tag{4.27}$$

While for a single polariton solution a better approach — based on a renormalised theory — exists [132], a proper gauge-invariant description of a ground state without introducing artificial cutoffs remains a challenge and is left for the future work. Below an exponential cutoff will be used.

4.3 Results

While the details of numerical implementation are discussed in Appendix C.1, this section is devoted to the discussion of results. Unless specified separately, below the set of parameters presented in Table 4.1 will be used. All quantities above, which have units of energy, e.g. E_0, $\tilde{g}_0$, T, μ_{ex}, are in units of E_g by the definition.

Parameter	Meaning	Value
E_0	binding energy	0.5
E_g	band gap	1.0
ω_0	photon cut-off frequency	1.53
κ	matter-light interaction momentum cut-off	5.0
$\tilde{g}_0$	"bare" matter-light coupling	0.2
m_e/m_h	electron to hole mass ratio	1.0
ε	background dielectric permittivity	1.0
T	temperature	0.02
μ_{ex}	excitation chemical potential	1.5
α	electrostatic term prefactor	8.0

Table 4.1: System parameters used in calculations

Below the fact that a photon has a very low mass compared to electron mass will play an important role. For this reason, let us show how these masses are related. Considering only a fundamental mode of a 2D microcavity and supposing that a photon 2D wavevector (in the plane on a microcavity) is small compared to π/L (L is the distance between cavity mirrors), photon energy reads $\omega_k \simeq \omega_0(1 + c^2k^2/2\omega_0^2)$, where ω_0 is a photon cutoff frequency. After some algebra, it is easy to get

$$\omega_k = \omega_0 \left[1 + \frac{1}{8}\left(\frac{\varepsilon}{\alpha}\right)^2 \left(\frac{E_0}{\hbar\omega_0}\right)^2 \left(\frac{k}{k_0}\right)^2\right], \tag{4.28}$$

where α is the fine structure constant. Identifying the denominator of $(k/k_0)^2$ with two masses of a photon, one can find the ratio of photon and electron

masses:

$$\frac{m_{ph}}{m_e} = \frac{\hbar\omega_0}{E_0}\alpha^2 \tag{4.29}$$

which clearly shows that a photon is around $10^3 - 10^4$ times lighter than an electron.

4.3.1 Almost zero and finite pairing momentum imbalanced condensates

With regards to finite-momentum Q pairing in the presence of a photon, there are two classes of coherent (with $\Delta_{\boldsymbol{k}} \neq 0$) solutions: $Q \approx 0$ bright polaritonic states and $Q = Q_{FF} \neq 0$ dark FF-like condensed state.

We can understand why the FF state is dark as follows. The FF state becomes stable (i.e. a global minimum) at high enough density n_0, where q_{FF} is roughly given by electron and hole Fermi surface mismatch divided by a Fermi velocity. The typical momentum of the FF state is of the order of $1/a_B$, where a_B is an exciton Bohr radius. Photons at this momentum have energy of the order of $\omega_0/\alpha^2 \simeq 10^4$ — see Eq. 4.28. This photon energy is far higher than the Rabi splitting, so the state is dark (i.e. creation of a photon with such energy leads to a huge energy penalty, so it is energetically unfavourable to have photons). For this reason, photon density in the FF state is negligible (although, formally, finite).

Fig. 4.2(a) shows the results of minimization of the free energy at different

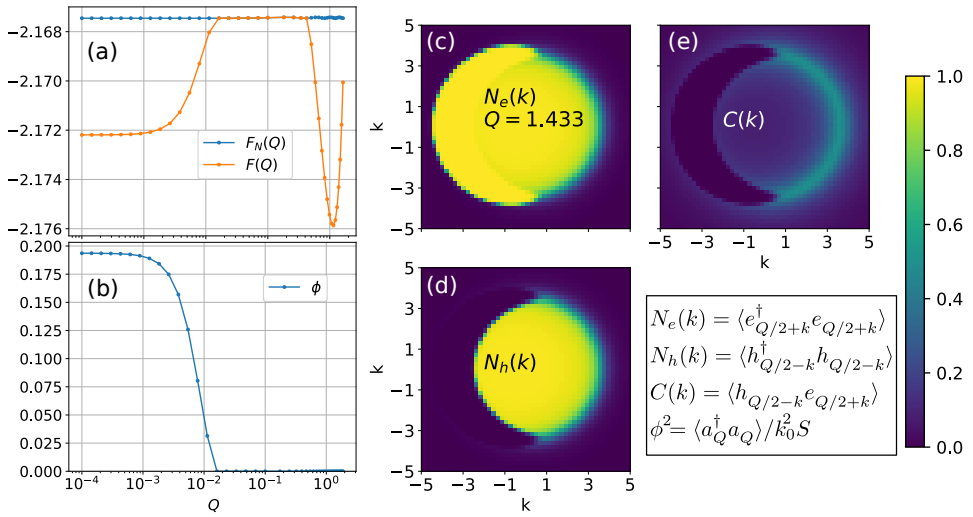

Figure 4.2: (a) Dependence of the free energy on pairing vector Q, (b) Photon density versus pairing vector Q, (c-e) Electron $N_e(k)$, hole $N_h(k)$ mode population and coherence $C(k)$ at the minimum of free energy corresponding to an FF state; $\omega_0 = 1.6$, $\kappa = 5.0$, $n_0 = 0.5$; k-grid: $k \in [-10, 10]a_B$, 100 by 100 points; Other physical parameters are summarised in Table 4.1.

values of center of mass pairing momentum Q — which for brevity will be denoted by $F(Q)$ for a free energy (using the full ansatz 4.14, i.e. allowing finite Δ_k) and $F_N(Q)$ for a normal state free energy (forcing $\Delta_k = 0$ and $\phi = 0$) — at target density $n_0 = 0.5$. As expected, $F(Q)$ contains two minima: one at $Q \approx 0$ due to photon-driven polariton condensation and another one at finite $Q = Q_{FF}$. While the $Q \approx 0$ solution will be extensively discussed in the next sections, let us now concentrate on the finite Q result. This finite $Q = Q_{FF}$ state will be referred to as an FF state. Panels (c–e) of Fig. 4.2 show mode population of electrons $N_e(k)$, holes $N_h(k)$ as in Eq. 4.23, and coherence $C(k) \equiv \langle h_{Q/2-k} e_{Q/2+k} \rangle = u_k v_k (1 - n_F[\varepsilon_1(k)] - n_F[\varepsilon_2(k)])$ at the $Q = Q_{FF}$ minimum, which clearly show the physics of this state. The distribution of majority (here electrons) and minority (holes) species shifts opposite to each other in momentum space allowing interspecies pairing at the intersection of their Fermi surfaces. Next, Fig. 4.2(b) shows photon density at each Q-point. Photon density is highest at small Q-vectors as it is energetically favourable to excite low-energy photons. Due to low mass of a photon, its energy goes up rapidly with Q, which explains low photon population at higher Q-vectors. The photon density in the FF region is non-zero, but so small that it cannot be accurately extracted from the variational approach. We know that it is non-zero because of finite coherence, which is related to photon density as

$$\phi = \frac{1}{\omega_Q - \mu_{ex}} \int \frac{d^2k}{(2\pi)^2} g_k C(k) \tag{4.30}$$

as can be seen from minimizing free energy with respect to ϕ. Therefore, formally FF state is not completely dark.

Next, the pairing vector Q is approximately given by the difference of Fermi vectors of minority and majority species, thus Q_{FF} goes up (and Fermi surfaces overlap goes down) as target density n_0 increases. In contrast to the first order phase transition from $Q = 0$ to the FFLO $Q \neq 0$ condensate predicted using the term (4.8) in, e.g. [118], the term (4.7) leads to a second order phase transition, which can be seen from the continuous evolution of a pairing wavevector Q — Fig. 4.3. To facilitate the understanding of the results of the next sections, it is helpful to plot electron and hole mode populations, coherence and a gap function Δ_k at relatively small value of imbalance without a photon. Fig. 4.4 shows corresponding results at $n_0 = 0.1$. From these results it is clear how the FFLO state emerges and then continuously evolves to the FFLO state at larger imbalance — Fig. 4.2.

While the finite $Q = Q_{FF}$ FF state is promoted by density imbalance n_0 (and electrostatic prefactor α – see eq. 4.7), $Q = 0$ condensation is favoured by the photonic component due to low photon mass. Reducing cut-off frequency ω_0 or increasing matter-light coupling $\tilde{g}_0$ tunes the physics and may lead to a transition from the $Q = Q_{FF}$ FF to the $Q \approx 0$ polaritonic state. In Fig. 4.5 the $Q \approx 0$ and $Q = Q_{FF}$ state energies cross as ω_0 changes showing that tuning of ω_0 leads to a quantum first-order phase transition between these

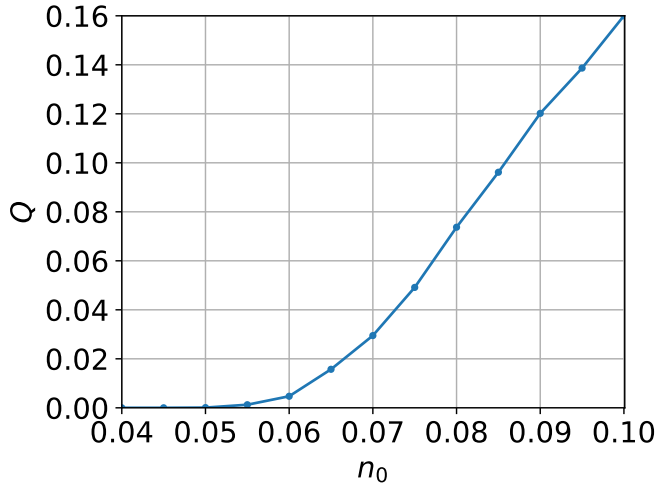

Figure 4.3: Dependence of the position Q of a minimum of the free energy on the target charge density n_0

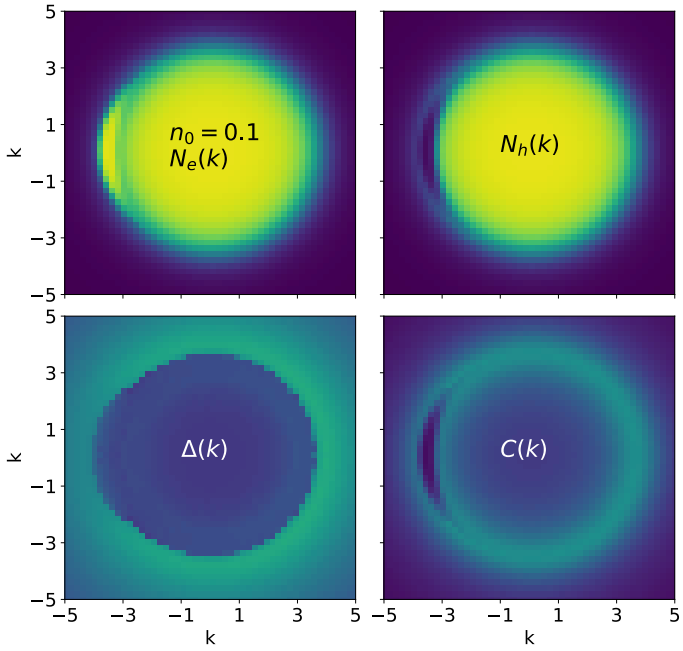

Figure 4.4: Electron and hole mode populations, coherence and a gap function Δ_k corresponding to the FFLO state at $n_0 = 0.1$; colorscale is the same as in Fig. 4.2

two states. The fact that lowering ω_0 promotes $Q \approx 0$ polaritonic state can be easily understood. Indeed, it is energetically favourable to have more photons if their energy is lower. Also, integrating photons out leads to an electron-hole

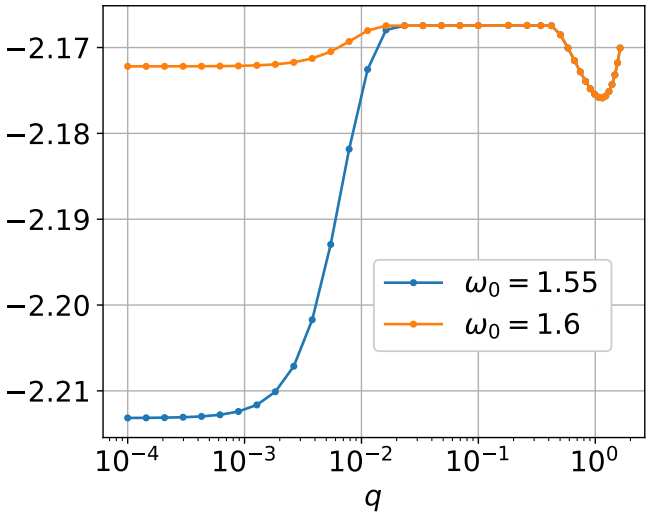

Figure 4.5: $F(Q)$ at $\omega_0 = 1.6$ and $\omega_0 = 1.55$; $n_0 = 0.5$

interaction term $\sum \frac{g^2}{\omega_k - \mu_{ex}} e_p^\dagger h_{k-p}^\dagger h_{k-p'} e_{p'}$ (in a static approximation), which rapidly goes up as ω_0 approaches μ_{ex} thus favouring $Q \approx 0$ condensation.

4.3.2 Almost zero pairing momentum imbalanced condensates

Having found two classes of solutions and identified a finite pairing momentum solution with a familiar FF condensate, let us now look at the $Q \approx 0$ class of solutions in more detail. Surprisingly, this class turns out to be very rich containing four distinct condensed imbalanced phases in addition to a familiar balanced polaritonic condensate and an FFLO state.

Evolution of state under increasing charge density Figure 4.6 summarises the results of calculations at different target densities n_0[2]. At small enough target charge density $n_0 < 0.1$, the system stays in the balanced isotropic state, which is a usual polariton condensate. At higher n_0, the system enters an imbalanced isotropic state IC(I) without unpaired electrons (i.e. coherence is finite in the whole region of non-zero electron mode population). Increasing n_0 further, we can see a transition to an imbalanced anisotropic state IC(A) without unpaired electrons and then with unpaired electrons at even higher n_0, e.g. $n_0 = 0.45$ in Fig. 4.6. Before transforming into an FFLO state at higher n_0, the IC(A) turns back into isotropic state IC(I), but with

[2]these results combine a few solutions doing calculations with memory of a solution increasing and reducing n_0

a ring of unpaired electrons in momentum space. This state is similar to the previously proposed Sarma or breached–pair state [110, 112].

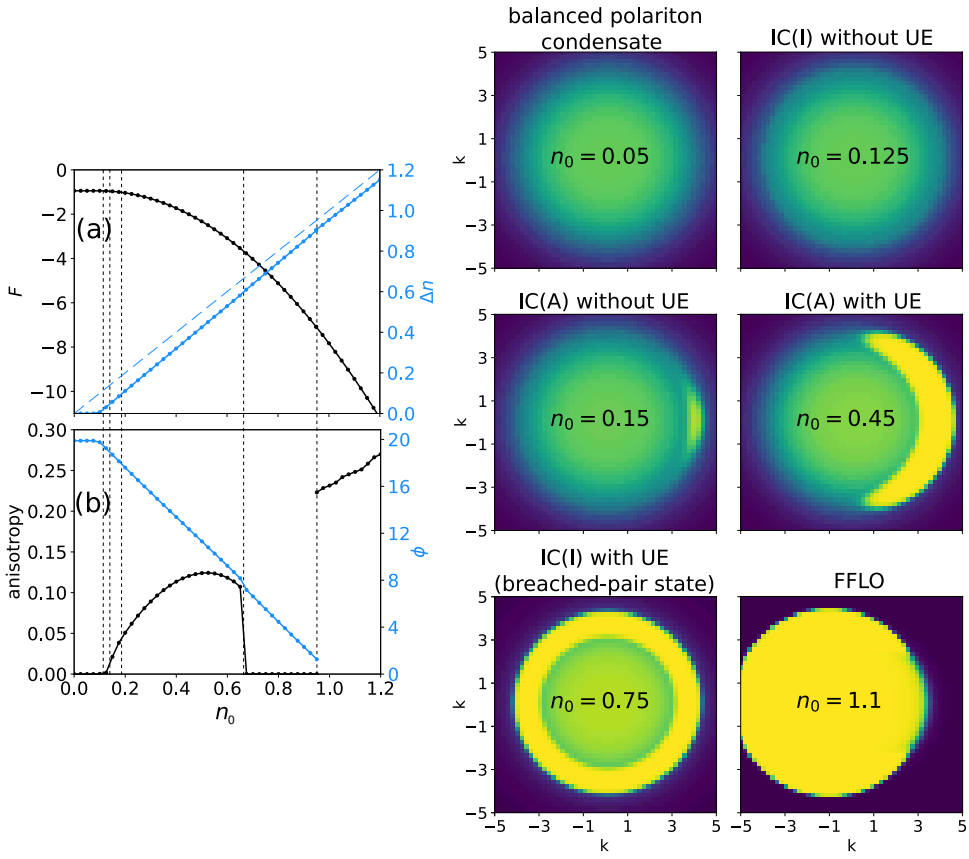

Figure 4.6: (a) Free energy F (black line), charge density $\Delta n = n_e - n_k$ (blue line) and n_0 (light blue dashed line) versus target charge density n_0, (b) Anisotropy parameter (black line) defined as $\sum_k N_e(\boldsymbol{k})(k_x/|\boldsymbol{k}|)/\sum_k N_e(\boldsymbol{k})$, and photon field ϕ versus n_0; other figures show characteristic electron mode populations in different regimes. Electron-hole (charge) imbalance drives a transiton from a balanced condensate to a series of imbalanced condensates IC (separated by vertical dashed lines), which are either isotropic IC(I) or anisotropic IC(A) and contain or do not contain unpaired electrons (UE). Momentum grid: $k_{max} = 10a_B$, 100 by 100 points; photon cut-off frequency $\omega_0 = 1.53$; colorscale is the same as in Fig. 4.2

The most surprising result of these calculations is the imbalanced anisotropic condensed state IC(A), which features coexisting polariton condensate and — on top of this — finite density of unpaired electrons to accommodate finite imbalance. This state is similar to a proposed breached–pair state [110] in a sense that finite density of unpaired fermions on top of the majority species Fermi surface and paired fermions below and above this region in the mo-

mentum space. However, unpaired electrons fill a "broken-ring" rather than a full-ring region, which extends to a full-ring region as the charge density goes up.

These results are straightforward to understand considering the combination of a finite density imbalance promoting the FFLO condensation and a photon favouring $Q = 0$ polaritonic condensation. Indeed, we can notice that the FFLO state at relatively small imbalance presented in Fig. 4.4 is not much different from the IC(A) state. Moreover, calculations with a reduced Coulomb attraction showed that anisotropy disappears at some critical value of electron hole attraction. Therefore, we can conclude that an anisotropic solution is the result of a Coulomb attraction and has the same origin as the FFLO state. However, due to a steep dispersion, a photon does not favour large Q FFLO pairing and so it brings Q to very small values (as an example, see Fig. 4.7), therefore strongly reducing the shift of electron and hole

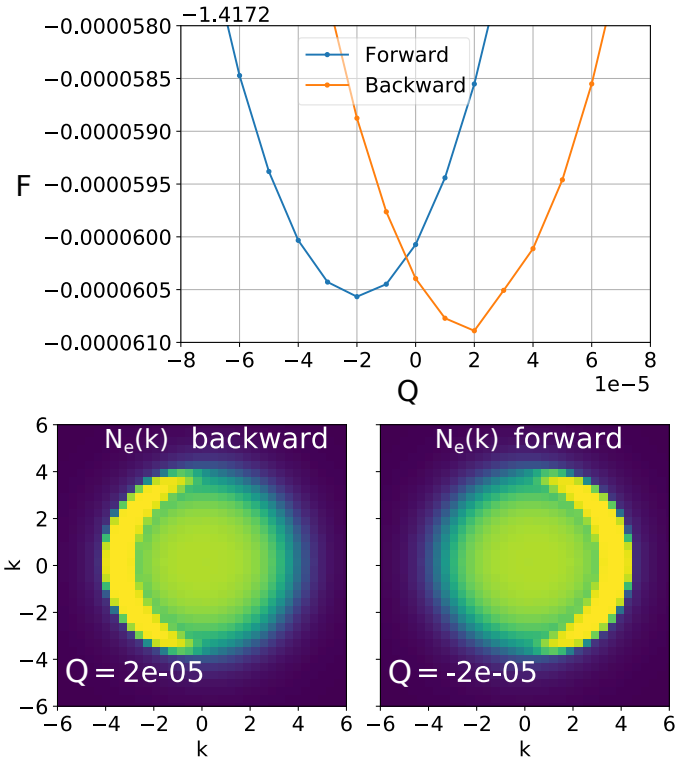

Figure 4.7: $F(Q)$ corresponding to an IC(A) state running calculations increasing Q-vector (forward) and reducing it (backward); colorscale is the same as in Fig. 4.2

Fermi mode populations with respect to each other. This leads to a different from the FFLO state evolution, which ends up in a breached-pair state before entering the FFLO regime. The nature of the breached-pair state is easy to

understand. Due to a large density imbalance, holes — which are minority species — pair up with electrons inside the Fermi sea leaving electrons with higher energies unpaired.

All the results presented in this thesis are obtained using an artificially imposed matter-light coupling momentum cutoff $\kappa = 5.0$. While we do not yet know how to do proper renormalised calculations without a cutoff, we can ask how increasing a cutoff affects the results. The main effect of a larger cutoff is the spreading of polaritonic bright $Q \approx 0$ condensed states to larger values of a target charge density n_0 and temperatures T, so increasing a cutoff increases the effect of a photon. This makes sense because higher cutoff leads to bigger absolute value of a photon self-energy [132], so to lower effective photon energy and — according to Eq. 4.30 — to larger photon density. At the same time, the results (e.g. electron mode population, coherence) do not change qualitatively, i.e. the form of the results remains basically the same. These considerations suggest that, in spite of an artificially imposed momentum cutoff, the results obtained in this chapter are feasible.

Evolution of state under reducing temperature Varying charge density, in the previous paragraph isotropic anisotropic IC(A) and IC(I) imbalanced condensed states were found. The isotropic state found is analogous to an elusive breached–pair state [110, 114], while anisotropic state is quite different from a regular FF state. This paragraph aims to check the fate of these $Q \approx 0$ states as temperature varies. The charge density $n_0 = 0.3$ is chosen such that the finite $Q = Q_{FF}$ FF state energy is much higher than energy of bright $Q \approx 0$ states, thus only transitions between new $Q \approx 0$ will be found. The full phase diagram will be presented in the next section.

Fig. 4.8(a-d) shows how charge density $\Delta n = (n_e - n_h)$, free energy F, photon density and anisotropy parameter change with temperature, while fig. 4.8(e-l) shows examples of electron, hole and coherence distribution (a $k_y = 0$ slice) of different states. Region (I) at approximately $T \in (0.43, \infty)$ corresponds to a normal state, which is clear from zero coherence in fig. 4.8(e,f), from matching normal and coherent state energies and charge densities — fig. 4.8(a,b), and from zero photon density fig. 4.8(c). State (II) spans a region $T \in (0.055, 0.43)$ and it is characterized by finite coherence for all momentum k-points fig. 4.8(e,i) and by different electron and hole densities. As temperature goes down, this state transforms to an isotropic BP-like state, but without unpaired electrons, i.e. with non-zero coherence $C(k) \neq 0\ \forall k$. As temperature reduces further, this state transforms to an anisotropic but still fully-coherent ($C(k) \neq 0\ \forall k$) state (III). Below the critical temperature — which is around $T = 0.03$ — the system enters an anisotropic state with a region of zero coherence, i.e. it contains unpaired electrons. No other states are found at lower temperatures. 2D electron distributions in these states are presented in Fig. 4.9.

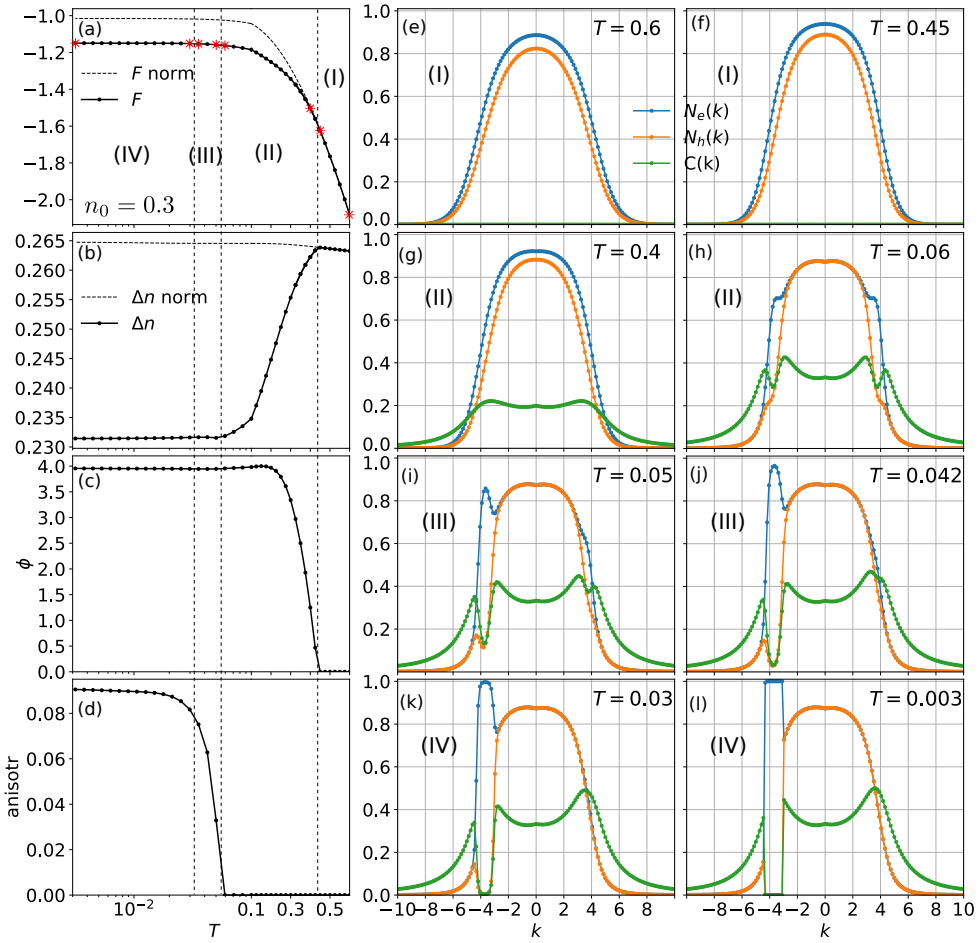

Figure 4.8: Evolution of state with temperature. (a) Shows free energies of normal (zero coherence and zero photon field) and coherent states, (b) Shows total charge density $\Delta n = n_e - n_h$ in the normal and coherent states, (c) Shows evolution of a photon field (d) Shows evolution of an anisotropy parameter, (e-l) Shows electron, hole and coherence distributions at $k_y = 0$ at different temperatures corresponding to four different regimes: (I) normal state, (II) isotropic imbalanced condensed state without unpaired electrons, (III) anisotropic imbalanced condensed state without unpaired electrons, (IV) anisotropic imbalanced condensed state with unpaired electrons

4.3.3 Phase diagrams (ω_0, n_0) and (T, n_0)

In the previous sections seven states were identified:

1. NS — normal state — with zero coherence $\Delta_k = 0$

2. FF — Fulde-Ferrel state — with finite center of mass momentum pairing

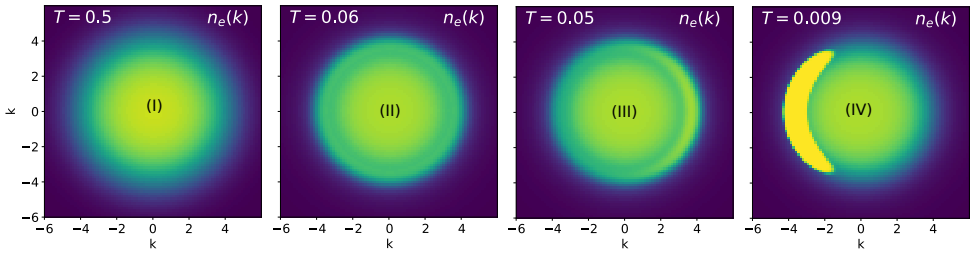

Figure 4.9: $2D$ electron distributions at different temperatures corresponding to the results presented in Fig. 4.8; colorscale is the same as in Fig. 4.2

3. IC(A) wUE — anisotropic imbalanced condensate with unpaired electrons
4. IC(A) nUE — anisotropic imbalanced condensate without unpaired electrons
5. IC(I) wUE — isotropic imbalanced condensate with unpaired electrons — which is similar to previously proposed Breach-Pair state
6. IC(I) nUE — isotropic imbalanced condensate without unpaired electrons
7. BC — balanced condensate (equivalent to a usual polaritonic condensate)

To get a broader view of competition between different phases, this section presents phase diagrams (ω_0, n_0) and (T, n_0) of the system.

Figure 4.10 shows a (ω_0, n_0) phase diagram. Clearly, a slice at $\omega_0 = 1.53$ matches the results of Fig. 4.6 up to a narrow region of the IC(I) without unpaired electrons between a fully balanced condensate and IC(A) region due to lower resolution of Fig. 4.10. To clarify notations, let us mention that a region k_{UE} with unpaired electrons is defined as k_{UE} : $|C(k)| < 10^{-2}$ and $\sum_k (n_e(k) - n_h(k)) > 0$, $k \in k_{UE}$. As cavity cutoff frequency goes down and approaches excitation chemical potential μ_{ex}, effect of a photon increases proportionally to $(\omega_0 - \mu_{ex})^{-1}$, which leads to spreading of a bright condensate to a higher charge density region. Therefore, a photon strongly widens the region of bright condensed imbalanced states, thus increases chances of observation of these states. Moreover, the region of large charge density may be more stable with respect to quantum fluctuations, thus making mean-field results potentially more reliable. On top of this, strong lowering of the coherent state energy with respect to the normal state due to a photon may make this state more robust with respect to fluctuations which break coherence (and so promote the normal state).

Figure 4.11 shows the (n_0, T) phase diagram with a photon fixing $\omega_0 = 1.55$. Without a photon (not shown) the bright imbalanced states shrink

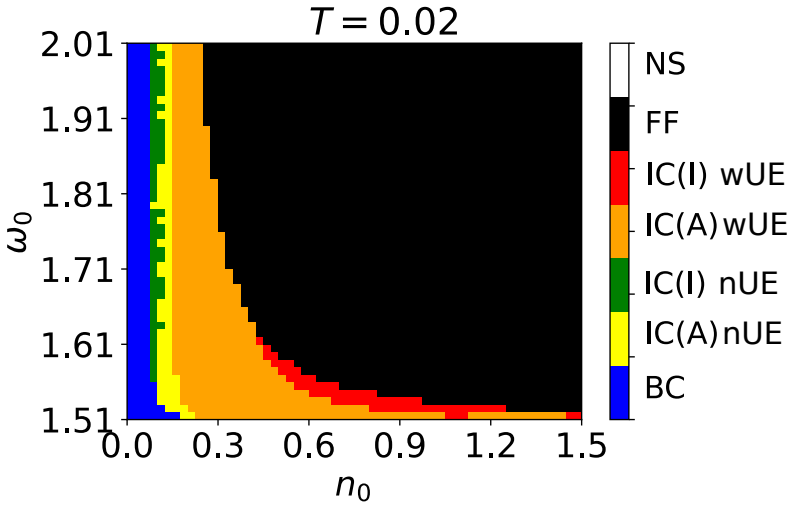

Figure 4.10: (ω_0, n_0) phase diagram at $T = 0.02$; $\mu_{ex} = 1.5$, $\omega_0 = 1.53$

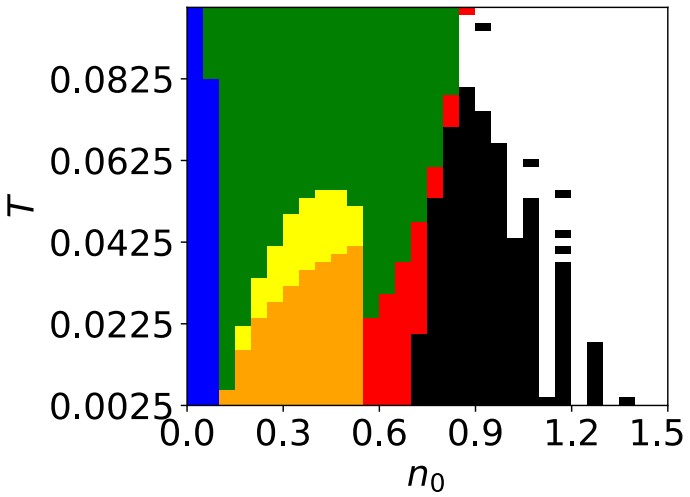

Figure 4.11: (n_0, T) phase diagram with a photon $\omega_0 = 1.55$; noise is due to not high enough numerical accuracy

significantly, but the boundary between the FFLO and normal state is not affected as expected from negligible density of a photon in the FFLO state.

4.4 Prospects of experimental observation

While polariton condensation can be simply deduced from emission spectrum (narrowing of emission linewidth, blueshift, jump in intensity of emitted ligth at the lowest energy mode), the experimental tests of the states described in this chapter are a bit more challenging and require different probes. Indeed,

as charge of the system increases, coherent light emission intensity goes down — Fig. 4.6(c) — which does not provide enough information about the type of the condensed state. However, there are established experimental techniques allowing to directly reveal the matter state of the system.

For example, the experiment [133] demonstrated simultaneous strong and weak coupling of light of orthogonal polarisations to excitons, thus allowing to trace a usually hidden matter part of excitons in exciton-polariton condensation experiments. Another approach to study the matter part of polaritons is to do terahertz spectroscopy of 1s-2p excitonic transition [134].

However, the most striking evidence of the existence of probably the most intriguing imbalanced anisotropic condensed state with free electrons would be transport measurements. Due to the existence of free electrons, the sample should conduct current. At the same time, due to strong Fermi surface anisotropy, current response should be anisotropic (with variable degree of anisotropy) in such a state. While such measurements have never been done, an experiment combining exciton-polaritons and current of free electrons is already available [135]. There is another experiment [136] where charged interlayer exciton motion was demonstrated using Ohmic-contacted devices. From the theoretical point of view, in the presence of a U(1) symmetry-breaking condensate, conductivity cannot be inferred from simple linear response analysis, but must be calculated self-consistently to maintain the gauge invariance as has recently been done for pair density waves [137].

Therefore, combination of existing experimental techniques makes it possible to check the result of presented theoretical analysis and hopefully to detect novel exotic states proposed in this chapter.

Chapter 5

Conclusion and future directions

This chapter briefly summarises the main conclusions of this dissertation and outlines potential extensions of the projects discussed.

5.1 Raman scattering with strongly coupled vibron-polaritons

As was shown, strong coupling between an infrared photon and a molecular vibron, resulting in the formation of vibron-polaritons, naturally leads to redistribution of Raman scattering (RS) signal between the upper and the lower vibron-polariton modes. At the same time, the signals are not the same. Indeed, due to mode softening, RS scattering to the lower polariton mode increases as coupling strength goes up, while RS to the upper polariton — reduces. However, the net effect of strong coupling on RS is that the total RS signal increases by up to four times in the ultra-strong coupling regime, which contradicts to the experiment [1], while supports and extends the results of independent theoretical calculations presented in Ref. [26]. Next, due to symmetry, it is clear that there can be no RS to a state with a single dark state. However, surprisingly there is finite Raman transition probability to the double-excited dark state (with zero total momentum), which has the same order of magnitude as a transition probability to one of single excited polariton modes.

Given the existence of two independent theoretical papers on vibron-polariton RS with similar results, which contradict to a single existing experimental paper [1], it seems that more experimental measurements would help to clarify the story and guide further theoretical modeling. For example, it would help to make sure whether the RS signal enhancement is really associated with the vibronic strong coupling or with some other mirror (e.g. plasmonic) effects. Also, measurements of the detuning and coupling strength dependence of up-

per and lower polariton RS amplitudes would be of great use for checking theoretical predictions.

5.2 Organic polariton lasing

The phase diagram of an ordinary (weakly coupled) dye laser was obtained and explained. It was shown that increasing the strength of matter-light coupling leads to a smooth transition from a dye laser to a strongly-coupled polariton. However, in contrast to common beliefs, at optimised cavity frequency, there is no significant lasing threshold reduction as the system enters a strong coupling regime. On the other hand, in the polariton laser regime, low-threshold lasing can be achieved over a wider range of bare cavity photon frequencies compared to a weakly-coupled laser due to a self-tuning effect. Also, the method developed in this project allows to answer a lot of other related questions.

Firstly, to study the emission and absorption spectrum below the lasing threshold, one may go one step beyond the mean-field approach using a so-called cumulant expansion [106, 138], i.e. writing equations for higher-order expectations such as $\langle aa \rangle$, $\langle a^\dagger a \rangle$, $\langle a\lambda_i \rangle$ and $\langle \lambda_i^m \lambda_j^k \rangle$ (m, k refer to the index of a molecule).

Secondly, taking into account many photon modes, one can study mode populations to describe a process of thermalisation and condensation, to understand how the physics of weakly coupled photon BEC [46, 101, 102, 139, 140] changes as one enters the strong coupling regime, or to understand the effect of relatively high temperature on the bottleneck effect observed in, e.g. [22]. This may require to write a better master equation to allow transitions between different polariton momentum states caused by some low-energy degrees of freedom (which in the current model are responsible for dephasing Γ_z only), for example adopting the approach developed in Ref. [141].

Another direction is to study effects of multiple vibrational modes (for example, to start with, one strongly and one weakly coupled to an electronic transition vibrational mode), or to explore the effect of structured baths using Redfield theory with the true system eigenstates [141].

5.3 Imbalanced polariton condensates

Within a mean-field approach, there are six ordered states (with a finite region of non-zero expectation $\langle h_{Q/2-k} e_{Q/2+k} \rangle$) found: a usual balanced polariton condensate with equal densities of electrons and holes, imbalanced isotropic and anisotropic condensed state with and without uncoupled electrons, and the FFLO state. It is shown that imbalanced condensed states with almost zero center of mass exciton momentum are promoted by a photon as its cutoff frequency goes down. Moreover, due to small photon mass the resulting polaritonic states are expected to be stable at high temperatures akin to usual

polariton condensates. These mean-filed results form a firm foundations for many other directions.

The most straightforward extension of this project is to consider other phases, such as, e.g. superconductivity or magnetic orders, to understand how they interact with other phases found at the mean-field level.

Another obvious question is how to formulate a gauge-independent renormalised cutoff-free theory, which though is not so obvious how to do.

An interesting direction would be to explore the effects of topological band structure of real materials, to find new phases emerging from topology, Coulomb and a cavity-photon mediated interactions. The first step in this direction has recently been made in Ref. [142] considering polariton condensation in topological materials. However, the physics of imbalanced polariton condensates and the effect of other tunable parameters, such as band inversion and band-coupling strength [143], remains unexplored. All these calculations can be done using a variational mean-field approach developed in this thesis updating the form of the bare Hamiltonian to include topological band structure.

An apparent but not so straightforward direction is to go beyond mean-field to study the physics of fluctuations. Firstly, it is interesting to understand the effects of dressing of polaritons by itinerant electrons, to understand the connection between Fermi-polaron-polaritons and trions in regimes of high and low electron doping, to understand how screening affects the phase diagrams in different regimes. Another related question is how fluctuations reshape the phase diagram, how they affect different ordered states and whether they may induce new ordered states near quantum critical points akin to superconductivity induced by critical fluctuations discussed in, e.g. Ref. [144, 145]. While it is difficult to include the physics of fluctuations within a variational many-body approach, there are well-established field-theoretical methods, which can now be relatively safely used given the existence of a variational mean-field solution.

While the discussion above implicitly assumed thermal equilibrium calculations, in practice all polaritonic systems are essentially non-equilibrium because photons leave a cavity and so an external pumping is always required. Therefore, predictions of an equilibrium theory should be considered with a pinch of salt because non-equilibrium effects may wash out some phases or bring a system to some particular metastable state, which is not necessarily the global free energy minimum state as has been recently shown in Ref. [146]. Therefore, non-equilibrium theory is a natural and necessary extension of this project.

Appendix A

Calculation details for the Raman scattering

A.1 A^2-term for an harmonical oscillator and a two-level system

In this section I show how a prefactor of an A^2-term is derived starting from a QED Hamiltonian in the Coulomb gauge.

A Hamiltonian of a system of charged particles (CGS) reads

$$H = \sum_i \frac{1}{2m_i}\left(\boldsymbol{p}_i - \frac{q_i}{c}\boldsymbol{A}(\boldsymbol{r}_i)\right)^2 + \sum_{\boldsymbol{k},n} \hbar\omega_{\boldsymbol{k}} a^\dagger_{\boldsymbol{k},n} a_{\boldsymbol{k},n} + V_{Coulomb} \tag{A.1}$$

In the Coulomb gauge, the longitudinal part of a vector potential is zero $\boldsymbol{A}(t) \equiv \boldsymbol{A}_\perp(r)$, thus $\boldsymbol{pA} = \boldsymbol{Ap}$, so expanding brackets and supposing that we deal with equivalent particles ($m_i = m$, $q_i = e$) we get

$$H = \sum_i \left[\frac{\boldsymbol{p}_i^2}{2m} - \frac{e}{mc}\boldsymbol{A}(\boldsymbol{r}_i)\boldsymbol{p}_i + \frac{e^2}{2mc^2}\boldsymbol{A}^2(\boldsymbol{r}_i)\right] \tag{A.2}$$

A.1.1 Two-level system

Making a two-level system approximation, i.e. taking into account only ground $|g\rangle$ and the first excited $|e\rangle$ state with energy difference ε, one can get $\langle e|p|g\rangle = \frac{i\varepsilon m}{e\hbar} d_{eg}$ with d_{eg} - dipole matrix element, thus within this approximation we get

$$\frac{e}{mc} pA \to \frac{ie\varepsilon d}{\hbar ec}\sigma_i^x A = \frac{ie\varepsilon d}{\hbar ec}\sqrt{\frac{2\pi\hbar c^2}{\omega_c V}}\sigma_i^x (a^\dagger e^{-i\boldsymbol{kr}_i} + a e^{i\boldsymbol{kr}_i}) \equiv g\sigma_i^x (a^\dagger + a) \tag{A.3}$$

for a single lowest-energy photon mode in a 2D cavity (so that $\boldsymbol{k} \equiv \boldsymbol{k}_\parallel = 0$). For transition dipole matrix elements there is a sum rule, called the Thomas-Reiche-Kuhn sum rule, which reads

$$\sum_b |d_{ab}|^2 (E_b - E_a) = \frac{\hbar e^2}{2m} \tag{A.4}$$

which for a two-level systems has a simple form $d_{eg}^2 \varepsilon = \hbar^2 e^2 / 2m$. Supposing that light wavelength is much larger than particle separation, we can approximately set $\boldsymbol{A}(\boldsymbol{r}_i) \approx \boldsymbol{A}$. Therefore, combining all the expressions above, the last part of the Hamiltonian A.2 may be rewritten as follows:

$$\frac{e^2}{2mc^2} \sum_i \boldsymbol{A}^2(\boldsymbol{r}_i) = \frac{g^2 N}{\varepsilon} (a^\dagger + a)^2 \tag{A.5}$$

where N is a total number of particles.

A.1.2 Harmonic oscillator

The matter-light part of the Hamiltonian reads $-\frac{e}{mc} A \sum p_i + \frac{e^2 N}{2mc^2} A^2$, where $A = \sqrt{\frac{2\pi\hbar c^2}{\omega_c V}}$. Momentum operator is $p = i\sqrt{m\hbar\omega_v/2}(b^\dagger - b)$. To get the desired form $(b^\dagger + b)$, we can make a unitary transformation $b \to e^{i\pi} b$. Identifying then a prefactor of the term $(b^\dagger + b)(a^\dagger + a)$ with matter-light coupling G, one can readily see that the prefactor of the term $(a^\dagger + a)^2$ equals to $G^2 N / \omega_v$.

A.2 n-th polariton excitation

In this appendix I show how to generalize the expression 2.17, describing the Raman transition amplitude to a single excited polariton mode, to describe the transition to n-th excited bright mode.

For, definiteness, let us do it for UP. As we have shown

$$\mathcal{M}_{int,0} = \beta_1^{p_1} \beta_2^{p_2} (\beta_{n,3}^*)^{p_3} \dots (\beta_{n,N+1}^*)^{p_{N+1}}, \tag{A.6}$$

so we only need to calculate the second matrix element $\mathcal{M}_{f_k,int}$ for the transition to m-th excited UP:

$$\begin{aligned} \mathcal{M}_{f_k,int} &= \langle 0 | (\eta_1 + \beta_1)^{p_1} \dots (\eta_{N+1} + \beta_{n,N+1})^{p_{N+1}} e^{-\sum_i \beta_{n,i}^* \eta_i} \frac{\eta_1^{\dagger m}}{\sqrt{m!}} |0\rangle = \\ &= \sum_l \frac{(-\beta_1)^l}{l!} \langle 0 | (\eta_1 + \beta_1)^{p_1} \dots (\eta_{N+1} + \beta_{n,N+1})^{p_{N+1}} \eta_1^l | m, 0, ..., 0 \rangle. \end{aligned} \tag{A.7}$$

Then noticing that $\eta^k|n\rangle = \sqrt{\frac{n!}{(n-k)!}}|n-k\rangle$, we get

$$\mathcal{M}_{f_k,int} = \sum_{l=0}^{m} \frac{(-\beta_1)^l\sqrt{m!}}{l!\sqrt{(m-l)!}}\langle 0|(\eta_1+\beta_1)^{p_1}\dots(\eta_{N+1}+\beta_{n,N+1})^{p_{N+1}}|m-l,0,...,0\rangle =$$
$$= \beta_2^{p_2}...\beta_{n,N+1}^{p_{N+1}} \sum_{l=0}^{m} \frac{(-\beta_1)^l\sqrt{m!}}{l!\sqrt{(m-l)!}}\langle 0|\sum_k C_{p_1}^k \eta_1^{p_1-k}\beta_1^k|m-l\rangle. \tag{A.8}$$

The sum over k has only nonzero term at $k = p_1 - m + l$, so

$$\langle 0|\sum_k C_{p_1}^k \eta_1^{p_1-k}\beta_1^k|m-l\rangle = \sqrt{(m-l)!}\beta_1^{p_1-m+l}C_{p_1}^{p_1-m+l}, \tag{A.9}$$

thus we clearly get

$$\mathcal{M}_{f_k,int} = \sqrt{m!}\,\mathcal{M}^*_{int,0}\sum_{l=0}^{m}\frac{(-1)^l}{l!}C_{p_1}^{p_1-m+l}\beta_1^{2l-m}. \tag{A.10}$$

Although, it is impossible to simplify it further, it is possible to calculate an expression similar to (2.15) (for polaritonic states $\sum_n \to N$):

$$M = \sqrt{m!}\,N\sum_{\{p_i\}}\prod_i e^{-|\beta_{n,i}|^2}\frac{|\beta_{n,i}|^{2p_i}}{p_i!}\frac{1}{\Delta+\sum_j p_j\omega_j}\sum_{l=0}^{m}\frac{(-1)^l}{l!}C_{p_1}^{p_1-m+l}\beta_1^{2l-m}. \tag{A.11}$$

Skipping evident from previous derivation steps, now we need to calculate (like in (2.15))

$$\sqrt{m!}\sum_{l=0}^{m}\frac{(-1)^l}{l!}\beta_1^{2l-m}\prod_{j\neq 1}e^{|\beta_{nj}|^2\left(e^{-z\omega_j}-1\right)}\sum_p\frac{x^p}{p!}C_p^{p-m+l}e^{-\beta_1^2}, \tag{A.12}$$

where $x = \beta_1^2 e^{-z\omega_1}$. First,

$$\sum_p\frac{x^p}{p!}C_{p_1}^{p_1-m+l} = \sum_p\frac{x^p}{p!}\frac{p!}{(p-m+l)!(m-l)!} = ... = \frac{1}{(m-l)!}e^x x^{m-l}. \tag{A.13}$$

Next, the sum over l:

$$\sqrt{m!}\sum_{l=0}^{m}\frac{(-1)^l}{l!}\beta_1^{2l-m}\frac{x^{m-l}}{(m-l)!} = \sqrt{m!}\,\beta_1^{-m}x^m\sum_{l=0}^{m}\frac{(-x^{-1}\beta_1^2)^l}{l!(m-l)!} =$$
$$= \beta_1^{-m}x^m\frac{1}{\sqrt{m!}}\sum_{l=0}^{m}\frac{\theta^l m!}{l!(m-l)!} = \beta_1^{-m}x^m\frac{1}{\sqrt{m!}}\sum_{l=0}^{m}\theta^l C_m^l = \beta_1^{-m}x^m\frac{1}{\sqrt{m!}}(1+\theta)^m. \tag{A.14}$$

Now we only need to collect all the terms together. For the sum over l from (A.14) we get:

$$\frac{1}{\sqrt{m!}}\beta_1^m \left(e^{-z\omega_1}-1\right)^m \tag{A.15}$$

and so on, eventually getting the desired expression (in resonance):

$$M_k^n = N\frac{\beta_k^n}{\sqrt{2^n n!}}\int ds e^{-s\Delta}\left(e^{-s\omega_k}-1\right)^n \exp\left[-\frac{1}{2}\sum_i |\beta_i|^2\left(1-e^{-s\omega_i}\right)\right], \tag{A.16}$$

where β was defined in the main text.

A.3 N to three modes transformation

In this appendix I show how to transform the description of the model to replace N-mode problem by 3-mode one.

In order to get a three mode description as in (2.20) we can just chose the following basis: $|\psi_a^{(m)}\rangle = (1;0,0,...0)$ for a cavity mode and $|\psi_b^{(m)}\rangle = (0;0,...,0,1,0,...,0)$ (where nonzero element means vibrationally excited m-th molecule), $|\psi_c^{(m)}\rangle = \frac{1}{\sqrt{N-1}}(0;1,...,1,0,1,...,1)$ (zero for m-th molecule) for molecular modes. So, we can clearly see that if we change now $b \to b_m$ and $c \to \frac{1}{\sqrt{N-1}}\sum_{j\neq m} b_j$ in (2.20), we reproduce an original Hamiltonian (2.19). In terms of these basis state, the eigenmodes are: upper and lower polaritons

$$|LP/UP\rangle = |\psi_a\rangle \pm \frac{1}{\sqrt{N}}\left(|\psi_b\rangle + \sqrt{N-1}|\psi_c\rangle\right) \tag{A.17}$$

and dark states

$$|D^{(m)}\rangle = \frac{1}{\sqrt{N}}\left(\sqrt{N-1}|\psi_b\rangle - |\psi_c\rangle\right). \tag{A.18}$$

The form of the dark mode depends on the number of the excited molecule, so if we calculate the transition to the dark state and consequently sum up over all molecules, we should always take a different dark mode, corresponding to the molecule which gets excited. However, it turns out that there is no transition to the dark state, so we can neglect it and consider Raman transition only to the bright states. This statement was proven after the Eq. 2.16 for a different set of basis states. Let us prove it for a basis discussed in the current context.

To prove it, let us calculate the transition probability P_X from some state $|\psi\rangle$ to some reference eigenstate $|X\rangle$. So, $P_X = |\sum_m \langle\psi|D_m\rangle\langle D_m|X\rangle|^2 = |\sum_m \theta_m\langle D_m|X\rangle|^2$, where the amplitude $\langle\psi|D_m\rangle = \theta_m$ does not depend on the molecule number as was shown in the main text. Let us choose a reference eigenstate to be a dark state $|X\rangle = |D_1\rangle$, which is an eigenmode. If so, $\langle D_1|D_{m\neq 1}\rangle = \frac{1}{N}\left(-2+\frac{N-2}{N-1}\right) = \frac{-1}{N-1}$. Then summing it over all molecules

gives $|\sum_m \langle X|D_m\rangle|^2 = 0$. This means that due to destructive interference we do not have scattering to the dark mode.

A.4 Transition amplitude in non RWA and $\delta\omega_v \neq 0$

In this appendix I show how to calculate the transition amplitude beyond RWA and including $\delta\omega_v \neq 0$ effect.

In order to calculate (2.26), we can define $\mathbf{X} \equiv \mathbf{X}_\uparrow$ and rewrite connection relation for two (upper and lower) bases:

$$\mathbf{X}_\downarrow = \mathbf{U}_\downarrow^\dagger \left(\mathbf{U}_\uparrow \mathbf{X} - \mathbf{V}_\uparrow^{-1}\mathbf{h}_\uparrow\right) = \mathbf{U}_\downarrow^\dagger \mathbf{U}_\uparrow \left(\mathbf{X} - \mathbf{l}\right), \tag{A.19}$$

where we introduced $\mathbf{l} = \mathbf{U}_\uparrow^\dagger \mathbf{V}_\uparrow^{-1}\mathbf{h}_\uparrow = \Omega_\uparrow^{-2}\mathbf{U}_\uparrow^\dagger \mathbf{h}_\uparrow$. Then using, for example, the result of harmonic oscillator density matrix calculation, we can compute the sum (which is a weighted sum of the product of Hermite polynomials)

$$\begin{aligned}\sum_m \psi_m\left(\sqrt{\omega}X\right)\psi_m\left(\sqrt{\omega}X'\right)e^{-sm\omega} = \\ = \frac{1}{\sqrt{\pi}}\frac{1}{\sqrt{1-e^{-2s\omega}}}\exp\left[-\frac{\omega}{2}\left(\frac{X^2+X'^2}{\tanh(s\omega)} - \frac{2XX'}{\sinh(s\omega)}\right)\right],\end{aligned} \tag{A.20}$$

so with this expression for the sum over intermediate states and definition (2.26) we get

$$\begin{aligned}M_k = \frac{\sqrt{2\omega_{k,\downarrow}}}{\pi^3}\left[\mathbf{U}_\downarrow^\dagger\mathbf{U}_\uparrow\right]_{kr}\int ds e^{-s\Delta}\int\prod_i\left(d^3x_i d^3x_i'\sqrt{\omega_{i,\uparrow}\omega_{i,\downarrow}}\right)(\mathbf{x}_r - \mathbf{l}_r) \\ \exp\left[-\frac{1}{2}\Big((\mathbf{x}-\mathbf{l})^\intercal \mathbf{U}_\uparrow^\intercal \mathbf{U}_\downarrow \mathbf{\Omega}_\downarrow \mathbf{U}_\downarrow^\intercal \mathbf{U}_\uparrow (\mathbf{x}-\mathbf{l}) + (\mathbf{x}'-\mathbf{l})^\intercal \ldots (\mathbf{x}'-\mathbf{l})\Big)\right] \\ \prod_i \frac{1}{\sqrt{1-e^{-2s\omega_{i,\uparrow}}}}\exp\left[-\frac{\omega_{i,\uparrow}}{2}\left(\frac{X_i^2+X_i'^2}{\tanh(s\,\omega_{i,\uparrow})} - \frac{2X_iX_i'}{\sinh(s\,\omega_{i,\uparrow})}\right)\right] \equiv \\ \equiv \frac{\sqrt{2\omega_{k,\downarrow}}}{\pi^3}\left[\mathbf{U}_\downarrow^\dagger\mathbf{U}_\uparrow\right]_{kr}\int ds e^{-s\Delta}\prod_i\left(\sqrt{\frac{\omega_{i,\uparrow}\omega_{i,\downarrow}}{1-e^{-2s\omega_{i,\uparrow}}}}\right)O_r(s),\end{aligned} \tag{A.21}$$

where, defining $\mathbf{R} \equiv \mathbf{U}_\uparrow^\intercal \mathbf{U}_\downarrow \mathbf{\Omega}_\downarrow \mathbf{U}_\downarrow^\intercal \mathbf{U}_\uparrow$, $P_i \equiv \frac{\omega_{i,\uparrow}}{\tanh(s\omega_{i,\uparrow})}$ and $Q_i \equiv \frac{\omega_{i,\uparrow}}{\sinh(s\omega_{i,\uparrow})}$, for the vector $O_r(s)$ we have

$$\begin{aligned}O_r(s) = \int d^3x d^3x' \exp\Bigg[-\frac{1}{2}(\mathbf{x}-\mathbf{l})^\intercal\mathbf{R}(\mathbf{x}-\mathbf{l}) + \\ +(\mathbf{x}'-\mathbf{l})^\intercal\mathbf{R}(\mathbf{x}'-\mathbf{l}) - \frac{1}{2}\sum_i\Big(P_i(X_i^2+X_i'^2) - \\ -2Q_iX_iX_i'\Big)\Bigg](X_r - l_r).\end{aligned} \tag{A.22}$$

To proceed further, we can notice that this is a 6 dimensional Gaussian integral, so it can be calculated analytically. Defining then $\mathbf{z}^\intercal \equiv (\mathbf{x}^\intercal, \mathbf{x}'^\intercal)$ for convenience, we get

$$O_r(s) = \int d^6 z (z_r - l_r) \exp\left(-\frac{1}{2}\mathbf{z}^\intercal \mathbf{A}\mathbf{z} + \mathbf{q}^\intercal \mathbf{z} - c\right), \tag{A.23}$$

where

$$\mathbf{A} = \left(\begin{array}{c|c} \mathbf{P}+\mathbf{R} & -\mathbf{Q} \\ \hline -\mathbf{Q} & \mathbf{P}+\mathbf{R} \end{array}\right), \tag{A.24}$$

where $\mathbf{P}, \mathbf{Q}$ - diagonal matrixes (defined in the main text), $\mathbf{q}^\intercal = (\mathbf{l}^\intercal\mathbf{R}, \mathbf{l}^\intercal\mathbf{R})$, $c = \mathbf{l}^\intercal\mathbf{R}\mathbf{l}$. Thus, computing Gaussian integral, we eventually obtain

$$\mathbf{O}_r(s) = \left(\mathbf{A}^{-1}\mathbf{q} - \mathbf{l}\right)_r \frac{(2\pi)^3}{\sqrt{\det(\mathbf{A})}} \exp\left(\frac{1}{2}\mathbf{q}^\intercal \mathbf{A}^{-1}\mathbf{q} - \mathbf{l}^\intercal\mathbf{R}\mathbf{l}\right), \tag{A.25}$$

and eventually we obtain the final expression (2.27).

Appendix B

Calculation details for the Organic polariton lasing

B.1 Molecular transition weights calculation

In this appendix I show how to obtain the compositions of molecular transitions involved in lasing, which were presented in Fig. 3.1(d), Fig. 3.4(d-f), Fig. 3.6(d-f).

To determine the weights of molecular transitions corresponding to a given unstable mode, we need to construct a molecular density matrix, which can be built from the eigenvector $\upsilon = (\delta\alpha, \delta\alpha^*, \delta\ell)^\intercal$ of the stability matrix $\mathcal{M}$. We can then extract the matter part $\delta\ell_i$ and so construct the corresponding molecular density matrix, $\rho(t) = \rho_{\rm ns} + \mathcal{A}(\delta\ell_i e^{\xi t} + \delta\ell_i^* e^{\xi^* t})\lambda_i/2$ where $\mathcal{A}$ is an arbitrary amplitude and $\rho_{\rm ns}$ is the normal state density matrix, which form is not important now. (For simplicity of notation, we neglect the superscripts on $\delta\ell$ and ξ labeling eigenmodes.) The complex conjugates are required in order to guarantee Hermiticity (because the Gell Mann matrices are chosen to be Hermitian). This is crucial since the equations of motion mix ℓ_i and ℓ_i^*. To find the amplitude of the oscillatory component of a given element of the density matrix ρ_{ij}, we first define the matrix $r = \delta\ell_i\lambda_i/2$ and then note the oscillatory component of ρ_{ij} takes the form $\delta\rho_{ij} = r_{ij}e^{\xi t} + r_{ji}^* e^{\xi^* t}$ (because Gell Mann matrices λ_i are Hermitian).

The diagonal components of a density matrix give the molecular state populations. Defining $Re(\xi) = \xi'$ and $Im(\xi) = \xi''$, for the diagonal components of the density matrix we can get $\delta\rho_{ii} = 2|r_{ii}|\cos\big(\xi'' t + \mathrm{Arg}(r_{ii})\big)e^{\xi' t}$. The nondiagonal ones correspond to coherences. In particular, the block of the density matrix which is off-diagonal in terms of electronic states gives the weights of molecular transitions involved in lasing.

For the off diagonal components, in general $|r_{ij}| \neq |r_{ji}|$; we thus expect that the quantity $\delta\rho_{ij}$ traces an elliptical spiral in the Argand plane, $\delta\rho_{ij} = [r_A\cos(\xi'' t + \phi) + i r_B \sin(\xi'' t + \phi)]e^{i\theta + \xi' t}$. The semi-major and semi-

minor axes of this ellipse are given by $r_{A,B} = |r_{ij}| \pm |r_{ji}|$, while $\phi, \theta = [\mathrm{Arg}(r_{ij}) \pm \mathrm{Arg}(r_{ji})]/2$. Given this behavior, we define the amplitude of a given component by the semi-major axis. The contribution (weight) of a given molecular transition $(n-m)$ to the lasing mode thus corresponds to the amplitude $|r_{n\downarrow,m\uparrow}| + |r_{m\uparrow,n\downarrow}|$.

Appendix C

Imbalanced polariton condensates

C.1 Numerical implementation

In this appendix I discuss details of numerical solution of the model discussed in the main text.

To obtain the solution, one need to optimize the functional (4.17) over $4N + 1$ (N is the number of momentum grid points, which is, e.g. 10^4 for a 100 by 100 momentum-space grid) variables $l_{\boldsymbol{k}} \equiv \{\eta^e_{\boldsymbol{k}}, \eta^h_{\boldsymbol{k}}, \Delta_{\boldsymbol{k}}, \phi, \boldsymbol{Q}\}$. First, to simplify a solution, we may choose a direction of spontaneous symmetry breaking $\boldsymbol{Q} = (Q_x, 0)$ and so to remove $N - 1$ variables. Secondly, given that we expect to have asymmetry in the direction of $\boldsymbol{Q} = (Q_x, 0)$, we may restrict our ansatz to have variables symmetric with respect to reflection $k_y \to -k_y$, which leaves us around $1.5N$ rather than original $4N$ variables.

Nevertheless, even with this reduction of the number of variables, we are still left with of order of $10^3 - 10^4$ variables for a physically reasonable momentum-grid size. Unfortunately, starting from arbitrary initial conditions for $l_{\boldsymbol{k}}$, minimization routine often ends up in some local minimum, which may be far away from the global minimum, so it fails to find a system lowest free energy state. This requires to provide good initial conditions for minimization. However, even before this, one should provide a gradient of (4.17) for minimization. While the derivatives over $\{\eta^e_k, \eta^h_k, \Delta_k, \phi\}$ can be calculated analytically, there is no closed form of $\delta\mathcal{F}/\delta Q$. This is why the variable Q is treated separately from the others. For this reason, to minimize with respect to Q, free energy functional is optimized at some fixed Q, then this calculation is repeated for many values of Q and eventually one can find which Q minimizes the free energy. Therefore, hereafter some fixed Q will be assumed.

Let us discuss how to provide good initial conditions for minimization. First, the simplest thing to do is to build a system normal state (i.e. $\Delta_k \equiv 0$ and $\phi \equiv 0$) solution. Without the electrostatic term ($\alpha = 0$), normal state

equations (4.24) may well be solved iteratively, which can be symbolically written as $x^{new} = x^{old} + F[x^{old}]$. However, with arbitrary α, the iterative procedure turns out to be unstable. This problem may be fixed by introducing some small admixing parameter $\zeta \ll 1$ ($x^{new} = x^{old} + \zeta F[x^{old}]$). Although this trick stabilises the solution, it does not guarantee that the resulting state is the lowest energy state. For these reasons a different successive minimization approach was used. The problem is that minimization does not work well at low temperature, where there is a sharp Fermi surface. To tackle the problem of arbitrary α and at low temperature, the following algorithm is used:

1. Find normal state at $\alpha = 0$ and at high temperature, where a Fermi surface is smooth
2. Use the previous solution as an initial condition for minimization at higher α
3. Repeat the previous step until reaching the target value of α
4. After this slightly reduce temperature and then repeat it going to lower temperature using a previous step solution as an initial condition for the next step

This allows to overcome the problem of rather large α and low temperature T and so to find a normal state solution ($\Delta_{\boldsymbol{k}} = 0$ and $\phi = 0$). Next, the solution for $\eta^{e/h}_{\boldsymbol{k}}$ is used as an initial condition for a full ansatz optimization, i.e. allowing finite gap function $\Delta_{\boldsymbol{k}}$ and photon density ϕ. To obtain a good initial condition for $\Delta_{\boldsymbol{k}}$, a gap equation (4.25) is solved iteratively using normal state solutions for $\eta^{e/h}_{\boldsymbol{k}}$. A solution obtained in this way is then used as an initial condition for optimization.

Bibliography

[1] A. Shalabney, J. George, H. Hiura, J. A. Hutchison, C. Genet, P. Hellwig, and T. W. Ebbesen, *Enhanced Raman Scattering from Vibro-Polariton Hybrid States*, Angew. Chem., Int. Ed. **54**, 7971–7975 (2015).

[2] V. Stanev, C. Oses, A. G. Kusne, E. Rodriguez, J. Paglione, S. Curtarolo, and I. Takeuchi, *Machine learning modeling of superconducting critical temperature*, Npj Comput. Mater. **4**, 29 (2018).

[3] M. König, S. Wiedmann, C. Brüne, A. Roth, H. Buhmann, L. W. Molenkamp, X.-L. Qi, and S.-C. Zhang, *Quantum spin Hall insulator state in HgTe quantum wells*, Science **318**, 766–770 (2007).

[4] B. A. Bernevig, T. L. Hughes, and S.-C. Zhang, *Quantum spin Hall effect and topological phase transition in HgTe quantum wells*, Science **314**, 1757–1761 (2006).

[5] H. Onnes and W. Keesom, *Commun. Phys. Lab. Univ. Leiden. Suppl. 29* (1911).

[6] M. Somayazulu, M. Ahart, A. K. Mishra, Z. M. Geballe, M. Baldini, Y. Meng, V. V. Struzhkin, and R. J. Hemley, *Evidence for Superconductivity above 260 K in Lanthanum Superhydride at Megabar Pressures*, Phys. Rev. Lett. **122**, 027001 (2019).

[7] K. v. Klitzing, G. Dorda, and M. Pepper, *New Method for High-Accuracy Determination of the Fine-Structure Constant Based on Quantized Hall Resistance*, Phys. Rev. Lett. **45**, 494–497 (1980).

[8] D. C. Tsui, H. L. Stormer, and A. C. Gossard, *Two-Dimensional Magnetotransport in the Extreme Quantum Limit*, Phys. Rev. Lett. **48**, 1559–1562 (1982).

[9] T. Oka and S. Kitamura, *Floquet Engineering of Quantum Materials*, Annu. Rev. Condens. Matter Phys. **10**, 387–408 (2019), .

[10] M. Mitrano, A. Cantaluppi, D. Nicoletti, S. Kaiser, A. Perucchi, S. Lupi, P. Di Pietro, D. Pontiroli, M. Riccò, S. R. Clark *et al.*, *Possible light-induced superconductivity in K 3 C 60 at high temperature*, Nature **530**, 461 (2016).

[11] A. Cantaluppi, M. Buzzi, G. Jotzu, D. Nicoletti, M. Mitrano, D. Pontiroli, M. Riccò, A. Perucchi, P. Di Pietro, and A. Cavalleri, *Pressure tuning of light-induced superconductivity in K 3 C 60*, Nat. Phys. **14**, 837 (2018).

[12] I. Carusotto and C. Ciuti, *Quantum fluids of light*, Rev. Mod. Phys. **85**, 299–366 (2013).

[13] H. Deng, H. Haug, and Y. Yamamoto, *Exciton-polariton bose-einstein condensation*, Rev. Mod. Phys. **82**, 1489 (2010).

[14] J. A. Hutchison, T. Schwartz, C. Genet, E. Devaux, and T. W. Ebbesen, *Modifying chemical landscapes by coupling to vacuum fields*, Angew. Chem., Int. Ed. **51**, 1592–1596 (2012).

[15] S. Wang, A. Mika, J. A. Hutchison, C. Genet, A. Jouaiti, M. W. Hosseini, and T. W. Ebbesen, *Phase transition of a perovskite strongly coupled to the vacuum field*, Nanoscale **6**, 7243–7248 (2014).

[16] J. Feist, J. Galego, and F. J. Garcia-Vidal, *Polaritonic chemistry with organic molecules*, ACS Photonics **5**, 205–216 (2017).

[17] G. L. Paravicini-Bagliani, F. Appugliese, E. Richter, F. Valmorra, J. Keller, M. Beck, N. Bartolo, C. Rössler, T. Ihn, K. Ensslin *et al.*, *Magneto-transport controlled by Landau polariton states*, Nat. Phys. **15**, 186 (2019).

[18] N. Bartolo and C. Ciuti, *Vacuum-dressed cavity magnetotransport of a two-dimensional electron gas*, Phys. Rev. B **98**, 205301 (2018).

[19] E. Orgiu, J. George, J. Hutchison, E. Devaux, J. Dayen, B. Doudin, F. Stellacci, C. Genet, J. Schachenmayer, C. Genes *et al.*, *Conductivity in organic semiconductors hybridized with the vacuum field*, Nature Materials (2015).

[20] X. Zhong, T. Chervy, S. Wang, J. George, A. Thomas, J. A. Hutchison, E. Devaux, C. Genet, and T. W. Ebbesen, *Non-Radiative Energy Transfer Mediated by Hybrid Light-Matter States*, Angew. Chem., Int. Ed. **55**, 6202–6206 (2016).

[21] X. Zhong, T. Chervy, L. Zhang, A. Thomas, J. George, C. Genet, J. A. Hutchison, and T. W. Ebbesen, *Energy transfer between spatially separated entangled molecules*, Angew. Chem., Int. Ed. **56**, 9034–9038 (2017).

[22] J. D. Plumhof, T. Stöferle, L. Mai, U. Scherf, and R. F. Mahrt, *Room-temperature Bose–Einstein condensation of cavity exciton–polaritons in a polymer*, Nat Mater. **13**, 247 (2014).

[23] S. Kéna-Cohen and S. Forrest, *Room-temperature polariton lasing in an organic single-crystal microcavity*, Nat. Phot. **4**, 371 (2010).

[24] G. Lerario, A. Fieramosca, F. Barachati, D. Ballarini, K. S. Daskalakis, L. Dominici, M. De Giorgi, S. A. Maier, G. Gigli, S. Kéna-Cohen *et al.*, *Room-temperature superfluidity in a polariton condensate*, Nat. Phys. **13**, 837 (2017).

[25] A. Strashko and J. Keeling, *Raman scattering with strongly coupled vibron-polaritons*, Phys. Rev. A **94**, 023843 (2016).

[26] J. del Pino, J. Feist, and F. Garcia-Vidal, *Signatures of vibrational strong coupling in Raman scattering*, J. Phys. Chem. C **119**, 29132–29137 (2015).

[27] A. Strashko, P. Kirton, and J. Keeling, *Organic Polariton Lasing and the Weak to Strong Coupling Crossover*, Phys. Rev. Lett. **121**, 193601 (2018).

[28] C. N. Banwell, E. M. McCash *et al.*, *Fundamentals of molecular spectroscopy*, vol. 851 (McGraw-Hill New York, 1994).

[29] M. Klein and S. Dierker, *Theory of Raman scattering in superconductors*, Phys. Rev. B **29**, 4976 (1984).

[30] V. Berestetskii, E. Lifshitz, and L. Pitaevskii, *Relativistic Quantum Theory part 1* (Pergamon Press, 1971).

[31] W. Demtröder, *Laser spectroscopy: basic concepts and instrumentation* (Springer Science & Business Media, 2013).

[32] S. Nie and S. R. Emory, *Probing Single Molecules and Single Nanoparticles by Surface-Enhanced Raman Scattering*, Science **275**, 1102–1106 (1997), .

[33] A. Campion and P. Kambhampati, *Surface-enhanced Raman scattering*, Chem. Soc. Rev. **27**, 241–250 (1998).

[34] M. Moskovits, *Surface-enhanced spectroscopy*, Rev. Mod. Phys. **57**, 783 (1985).

[35] A. Shalabney, J. George, J. Hutchison, G. Pupillo, C. Genet, and T. W. Ebbesen, *Coherent coupling of molecular resonators with a microcavity mode*, Nat Commun. **6** (2015).

[36] J. George, A. Shalabney, J. Hutchison, C. Genet, and T. Ebbesen, *Liquid-Phase Vibrational Strong Coupling*, J. Phys. Chem. Lett. **6**, 1027–1031 (2015).

[37] M. Muallem, A. Palatnik, G. Nessim, and Y. Tischler, *Strong light-matter coupling between a molecular vibrational mode in a PMMA film and a low-loss mid-IR microcavity*, Annalen der Physik (2015).

[38] B. S. Simpkins, K. Fears, W. Dressick, B. Spann, A. Dunkelberger, and J. Owrutsky, *Spanning Strong to Weak Normal Mode Coupling between Vibrational and Fabry-Perot Cavity Modes through Tuning of Vibrational Absorption Strength*, ACS Photonics **2**, 1460–1467 (2015).

[39] J. Long and B. Simpkins, *Coherent Coupling between a Molecular Vibration and Fabry-Perot Optical Cavity to Give Hybridized States in the Strong Coupling Limit*, ACS Photonics **2**, 130–136 (2015).

[40] L. Pitaevskii and S. Stringari, *Bose-Einstein condensation and superfluidity*, vol. 164 (Oxford University Press, 2016).

[41] S. Demokritov, V. Demidov, O. Dzyapko, G. Melkov, A. Serga, B. Hillebrands, and A. Slavin, *Bose–Einstein condensation of quasi-equilibrium magnons at room temperature under pumping*, Nature **443**, 430 (2006).

[42] T. Giamarchi, C. Rüegg, and O. Tchernyshyov, *Bose–Einstein condensation in magnetic insulators*, Nat. Phys. **4**, 198 (2008).

[43] M. H. Anderson, J. R. Ensher, M. R. Matthews, C. E. Wieman, and E. A. Cornell, *Observation of Bose-Einstein condensation in a dilute atomic vapor*, Science **269**, 198–201 (1995).

[44] A. Kogar, M. S. Rak, S. Vig, A. A. Husain, F. Flicker, Y. I. Joe, L. Venema, G. J. MacDougall, T. C. Chiang, E. Fradkin *et al.*, *Signatures of exciton condensation in a transition metal dichalcogenide*, Science **358**, 1314–1317 (2017).

[45] J. Eisenstein and A. H. MacDonald, *Bose–Einstein condensation of excitons in bilayer electron systems*, Nature **432**, 691 (2004).

[46] J. Klaers, J. Schmitt, F. Vewinger, and M. Weitz, *Bose–Einstein condensation of photons in an optical microcavity*, Nature **468**, 545 (2010).

[47] K. Daskalakis, S. Maier, R. Murray, and S. Kéna-Cohen, *Nonlinear interactions in an organic polariton condensate*, Nat Mater. **13**, 271 (2014).

[48] K. G. Lagoudakis, M. Wouters, M. Richard, A. Baas, I. Carusotto, R. André, L. S. Dang, and B. Deveaud-Plédran, *Quantized vortices in an exciton–polariton condensate*, Nat Phys. **4**, 706 (2008).

[49] T. Yagafarov, D. Sannikov, A. Zasedatelev, K. Georgiou, A. Baranikov, O. Kyriienko, I. Shelyk, L. Gai, Z. Shen, D. G. Lidzey *et al.*, *On the origin of blueshifts in organic polariton condensates*, arXiv preprint arXiv:1905.02573 (2019).

[50] S. Betzold, M. Dusel, O. Kyriienko, C. P. Dietrich, S. Klembt, J. Ohmer, U. Fischer, I. A. Shelykh, C. Schneider, and S. Höfling, *Coherence and Interaction in confined room-temperature polariton condensates with Frenkel excitons*, arXiv preprint arXiv:1906.02509 (2019).

[51] T. Cookson, K. Georgiou, A. Zasedatelev, R. T. Grant, T. Virgili, M. Cavazzini, F. Galeotti, C. Clark, N. G. Berloff, D. G. Lidzey *et al.*, *A yellow polariton condensate in a dye filled microcavity*, Adv Opt Mater. **5**, 1700203 (2017).

[52] K. S. Daskalakis, S. A. Maier, and S. Kéna-Cohen, *Spatial Coherence and Stability in a Disordered Organic Polariton Condensate*, Phys. Rev. Lett. **115**, 035301 (2015).

[53] F. Scafirimuto, D. Urbonas, U. Scherf, R. F. Mahrt, and T. Stoferle, *Room-temperature exciton-polariton condensation in a tunable zero-dimensional microcavity*, ACS Photonics **5**, 85–89 (2017).

[54] S. K. Rajendran, M. Wei, H. Ohadi, A. Ruseckas, G. A. Turnbull, and I. D. Samuel, *Low Threshold Polariton Lasing from a Solution-Processed Organic Semiconductor in a Planar Microcavity*, Adv Opt Mater. p. 1801791 (2019).

[55] M. Wouters and I. Carusotto, *Excitations in a Nonequilibrium Bose-Einstein Condensate of Exciton Polaritons*, Phys. Rev. Lett. **99**, 140402 (2007).

[56] A. Amo, J. Lefrère, S. Pigeon, C. Adrados, C. Ciuti, I. Carusotto, R. Houdré, E. Giacobino, and A. Bramati, *Superfluidity of polaritons in semiconductor microcavities*, Nat. Phys. **5**, 805 (2009).

[57] H. Breuer and F. Petruccione, *The Theory of Open Quantum Systems* (Oxford University Press, Oxford, 2002).

[58] W. Kohn and J. M. Luttinger, *New Mechanism for Superconductivity*, Phys. Rev. Lett. **15**, 524–526 (1965).

[59] P. Nozieres and S. Schmitt-Rink, *Bose condensation in an attractive fermion gas: From weak to strong coupling superconductivity*, Journal of Low Temperature Physics **59**, 195–211 (1985).

[60] I. Bloch, J. Dalibard, and W. Zwerger, *Many-body physics with ultracold gases*, Rev. Mod. Phys. **80**, 885 (2008).

[61] D. Vollhardt and P. Wolfle, *The superfluid phases of helium 3* (Courier Corporation, 2013).

[62] M. G. Alford, A. Schmitt, K. Rajagopal, and T. Schäfer, *Color superconductivity in dense quark matter*, Rev. Mod. Phys. **80**, 1455–1515 (2008).

[63] J. Kasprzak, M. Richard, S. Kundermann, A. Baas, P. Jeambrun, J. Keeling, F. Marchetti, M. Szymańska, R. André, J. Staehli *et al.*, *Bose–Einstein condensation of exciton polaritons*, Nature **443**, 409 (2006).

[64] T. Byrnes, T. Horikiri, N. Ishida, and Y. Yamamoto, *BCS Wave-Function Approach to the BEC-BCS Crossover of Exciton-Polariton Condensates*, Phys. Rev. Lett. **105**, 186402 (2010).

[65] B. Keimer, S. A. Kivelson, M. R. Norman, S. Uchida, and J. Zaanen, *From quantum matter to high-temperature superconductivity in copper oxides*, Nature **518**, 179 (2015).

[66] L. Li, E. Ofarrell, K. Loh, G. Eda, B. Özyilmaz, and A. C. Neto, *Controlling many-body states by the electric-field effect in a two-dimensional material*, Nature **529**, 185 (2016).

[67] D. Fausti, R. Tobey, N. Dean, S. Kaiser, A. Dienst, M. C. Hoffmann, S. Pyon, T. Takayama, H. Takagi, and A. Cavalleri, *Light-induced superconductivity in a stripe-ordered cuprate*, Science **331**, 189–191 (2011).

[68] M. A. Sentef, M. Ruggenthaler, and A. Rubio, *Cavity quantum-electrodynamical polaritonically enhanced electron-phonon coupling and its influence on superconductivity*, Science advances **4**, eaau6969 (2018).

[69] J. B. Curtis, Z. M. Raines, A. A. Allocca, M. Hafezi, and V. M. Galitski, *Cavity Quantum Eliashberg Enhancement of Superconductivity*, Phys. Rev. Lett. **122**, 167002 (2019).

[70] X. Wang, E. Ronca, and M. A. Sentef, *Cavity Quantum-Electrodynamical Chern Insulator: Route Towards Light-Induced Quantized Anomalous Hall Effect in Graphene*, arXiv preprint arXiv:1903.00339 (2019).

[71] F. Schlawin, A. Cavalleri, and D. Jaksch, *Cavity-mediated electron-photon superconductivity*, Phys. Rev. Lett. **122**, 133602 (2019).

[72] P. Fulde and R. A. Ferrell, *Superconductivity in a Strong Spin-Exchange Field*, Phys. Rev. **135**, A550–A563 (1964).

[73] A. Larkin and I. Ovchinnikov, *Inhomogeneous state of superconductors(Production of superconducting state in ferromagnet with Fermi surfaces, examining Green function)*, Soviet Physics-JETP **20**, 762–769 (1965).

[74] R. Casalbuoni and G. Nardulli, *Inhomogeneous superconductivity in condensed matter and QCD*, Reviews of Modern Physics **76**, 263 (2004).

[75] L. Radzihovsky and D. E. Sheehy, *Imbalanced feshbach-resonant fermi gases*, Reports on Progress in Physics **73**, 076501 (2010).

[76] M. M. Parish, F. Marchetti, A. Lamacraft, and B. Simons, *Finite-temperature phase diagram of a polarized Fermi condensate*, Nat. Phys. **3**, 124 (2007).

[77] M. M. Parish, F. M. Marchetti, and P. B. Littlewood, *Supersolidity in electron-hole bilayers with a large density imbalance*, EPL (Europhysics Letters) **95**, 27007 (2011).

[78] L. Radzihovsky and A. Vishwanath, *Quantum Liquid Crystals in an Imbalanced Fermi Gas: Fluctuations and Fractional Vortices in Larkin-Ovchinnikov States*, Phys. Rev. Lett. **103**, 010404 (2009).

[79] P. Strack and P. Jakubczyk, *Fluctuations of Imbalanced Fermionic Superfluids in Two Dimensions Induce Continuous Quantum Phase Transitions and Non-Fermi-Liquid Behavior*, Phys. Rev. X **4**, 021012 (2014).

[80] M. Sidler, P. Back, O. Cotlet, A. Srivastava, T. Fink, M. Kroner, E. Demler, and A. Imamoglu, *Fermi polaron-polaritons in charge-tunable atomically thin semiconductors*, Nat. Phys. **13**, 255 (2017).

[81] A. Chernikov, A. M. van der Zande, H. M. Hill, A. F. Rigosi, A. Velauthapillai, J. Hone, and T. F. Heinz, *Electrical tuning of exciton binding energies in monolayer WS 2*, Phys. Rev. Lett. **115**, 126802 (2015).

[82] B. Chakraborty, J. Gu, Z. Sun, M. Khatoniar, R. Bushati, A. L. Boehmke, R. Koots, and V. M. Menon, *Control of Strong Light–Matter Interaction in Monolayer WS2 through Electric Field Gating*, Nano Lett. **18**, 6455–6460 (2018).

[83] A. M. Dibos, Y. Zhou, L. A. Jauregui, G. Scuri, D. S. Wild, A. A. High, T. Taniguchi, K. Watanabe, M. D. Lukin, P. Kim *et al.*, *Electrically Tunable Exciton–Plasmon Coupling in a WSe2 Monolayer Embedded in a Plasmonic Crystal Cavity*, Nano Lett. (2019).

[84] H. A. Fernandez, F. Withers, S. Russo, and W. L. Barnes, *Electrically Tuneable Exciton-Polaritons through Free Electron Doping in Monolayer WS2 Microcavities*, Adv Opt Mater. p. 1900484 (2019).

[85] K. Nash, M. Skolnick, J. Rorison, S. Bass, and A. Pitt, *Many-electron edge singularity at the Fermi cutoff in the photoluminescence spectrum of modulation-doped quantum wells*, Superlattices and Microstructures **4**, 553–554 (1988).

[86] W. Chen, M. Fritze, W. Walecki, A. V. Nurmikko, D. Ackley, J. M. Hong, and L. L. Chang, *Excitonic enhancement of the Fermi-edge singularity in a dense two-dimensional electron gas*, Phys. Rev. B **45**, 8464–8477 (1992).

[87] A. Gabbay, Y. Preezant, E. Cohen, B. M. Ashkinadze, and L. N. Pfeiffer, *Fermi Edge Polaritons in a Microcavity Containing a High Density Two-Dimensional Electron Gas*, Phys. Rev. Lett. **99**, 157402 (2007).

[88] S. Smolka, W. Wuester, F. Haupt, S. Faelt, W. Wegscheider, and A. Imamoglu, *Cavity quantum electrodynamics with many-body states of a two-dimensional electron gas*, Science **346**, 332–335 (2014).

[89] K. Kheng, R. T. Cox, M. Y. d' Aubigné, F. Bassani, K. Saminadayar, and S. Tatarenko, *Observation of negatively charged excitons X^- in semiconductor quantum wells*, Phys. Rev. Lett. **71**, 1752–1755 (1993).

[90] A. Esser, E. Runge, R. Zimmermann, and W. Langbein, *Photoluminescence and radiative lifetime of trions in GaAs quantum wells*, Phys. Rev. B **62**, 8232–8239 (2000).

[91] K. F. Mak, K. He, C. Lee, G. H. Lee, J. Hone, T. F. Heinz, and J. Shan, *Tightly bound trions in monolayer MoS 2*, Nat Mater. **12**, 207 (2013).

[92] J. Yang, T. Lu, Y. W. Myint, J. Pei, D. Macdonald, J.-C. Zheng, and Y. Lu, *Robust excitons and trions in monolayer MoTe2*, ACS Nano **9**, 6603–6609 (2015).

[93] O. Cotlet, D. S. Wild, M. D. Lukin, and A. Imamoglu, *Rotons in Optical Excitation Spectra of Monolayer Semiconductors*, arXiv preprint arXiv:1812.10494 (2018).

[94] F. P. Laussy, A. V. Kavokin, and I. A. Shelykh, *Exciton-Polariton Mediated Superconductivity*, Phys. Rev. Lett. **104**, 106402 (2010).

[95] P. Skopelitis, E. D. Cherotchenko, A. V. Kavokin, and A. Posazhennikova, *Interplay of Phonon and Exciton-Mediated Superconductivity in Hybrid Semiconductor-Superconductor Structures*, Phys. Rev. Lett. **120**, 107001 (2018).

[96] M. Matuszewski, T. Taylor, and A. V. Kavokin, *Exciton Supersolidity in Hybrid Bose-Fermi Systems*, Phys. Rev. Lett. **108**, 060401 (2012).

[97] O. Cotleţ, S. Zeytinoğlu, M. Sigrist, E. Demler, and A. Imamoğlu, *Superconductivity and other collective phenomena in a hybrid Bose-Fermi mixture formed by a polariton condensate and an electron system in two dimensions*, Phys. Rev. B **93**, 054510 (2016).

[98] T. Hümmer, J. Noe, M. S. Hofmann, T. W. Hänsch, A. Högele, and D. Hunger, *Cavity-enhanced Raman microscopy of individual carbon nanotubes*, Nat Commun. **7**, 12155 (2016).

[99] R. Chikkaraddy, B. De Nijs, F. Benz, S. J. Barrow, O. A. Scherman, E. Rosta, A. Demetriadou, P. Fox, O. Hess, and J. J. Baumberg, *Single-molecule strong coupling at room temperature in plasmonic nanocavities*, Nature **535**, 127 (2016).

[100] r. e. edited by F. P. Schäfer, *Dye Lasers* (SpringerVerlag, Berlin, 1990).

[101] P. Kirton and J. Keeling, *Nonequilibrium Model of Photon Condensation*, Phys. Rev. Lett. **111**, 100404 (2013).

[102] P. Kirton and J. Keeling, *Thermalization and breakdown of thermalization in photon condensates*, Phys. Rev. A **91**, 033826 (2015).

[103] J. del Pino, F. A. Y. N. Schröder, A. W. Chin, J. Feist, and F. J. Garcia-Vidal, *Tensor network simulation of polaron-polaritons in organic microcavities*, Phys. Rev. B **98**, 165416 (2018).

[104] J. del Pino, F. A. Y. N. Schröder, A. W. Chin, J. Feist, and F. J. Garcia-Vidal, *Tensor Network Simulation of Non-Markovian Dynamics in Organic Polaritons*, Phys. Rev. Lett. **121**, 227401 (2018).

[105] M. Stone and P. Goldbart, *Mathematics for Physics: A Guided Tour for Graduate Students* (Cambridge University Press, Cambridge, England, 2009).

[106] P. Kirton and J. Keeling, *Suppressing and Restoring the Dicke Superradiance Transition by Dephasing and Decay*, Phys. Rev. Lett. **118**, 123602 (2017).

[107] D. F. Agterberg, J. Davis, S. D. Edkins, E. Fradkin, D. J. Van Harlingen, P. A. Lee, L. Radzihovsky, J. M. Tranquada, Y. Wang *et al.*, *The Physics of Pair Density Waves*, arXiv preprint arXiv:1904.09687 (2019).

[108] G. Wang, A. Chernikov, M. M. Glazov, T. F. Heinz, X. Marie, T. Amand, and B. Urbaszek, *Colloquium: Excitons in atomically thin transition metal dichalcogenides*, Rev. Mod. Phys. **90**, 021001 (2018).

[109] B. Zhu, X. Chen, and X. Cui, *Exciton binding energy of monolayer WS 2*, Sci Rep. **5**, 9218 (2015).

[110] W. V. Liu and F. Wilczek, *Interior gap superfluidity*, Phys. Rev. Lett. **90**, 047002 (2003).

[111] H. Müther and A. Sedrakian, *Spontaneous Breaking of Rotational Symmetry in Superconductors*, Phys. Rev. Lett. **88**, 252503 (2002).

[112] G. Sarma, *On the influence of a uniform exchange field acting on the spins of the conduction electrons in a superconductor*, Journal of Physics and Chemistry of Solids **24**, 1029–1032 (1963).

[113] S.-T. Wu and S. Yip, *Superfluidity in the interior-gap states*, Phys. Rev. A **67**, 053603 (2003).

[114] M. M. Forbes, E. Gubankova, W. V. Liu, and F. Wilczek, *Stability criteria for breached-pair superfluidity*, Phys. Rev. Lett. **94**, 017001 (2005).

[115] K. Yamashita, K. Asano, and T. Ohashi, *Quantum Condensation in Electron–Hole Bilayers with Density Imbalance*, J. Phys. Soc. Jpn. **79**, 033001 (2010).

[116] P. Pieri, D. Neilson, and G. Strinati, *Effects of density imbalance on the BCS-BEC crossover in semiconductor electron-hole bilayers*, Phys. Rev. B **75**, 113301 (2007).

[117] A. Subası, P. Pieri, G. Senatore, and B. Tanatar, *Stability of Sarma phases in density imbalanced electron-hole bilayer systems*, Phys. Rev. B **81**, 075436 (2010).

[118] J. Varley and D. Lee, *Structure of exciton condensates in imbalanced electron-hole bilayers*, Phys. Rev. B **94**, 174519 (2016).

[119] A. Sedrakian, J. Mur-Petit, A. Polls, and H. Müther, *Pairing in a two-component ultracold Fermi gas: Phases with broken-space symmetries*, Phys. Rev. A **72**, 013613 (2005).

[120] M. Schüler, M. Rösner, T. O. Wehling, A. I. Lichtenstein, and M. I. Katsnelson, *Optimal Hubbard Models for Materials with Nonlocal Coulomb Interactions: Graphene, Silicene, and Benzene*, Phys. Rev. Lett. **111**, 036601 (2013).

[121] A. Altland and B. D. Simons, *Condensed Matter Field Theory* (Cambridge University Press, 2010).

[122] L. Keldish and Y. V. Kopaev, *Fiz, Tverd, Tela, Leningard 6 (1964) 2791*, Sov. Phys. Solid State **6**, 2219 (1965).

[123] P. Littlewood, P. Eastham, J. Keeling, F. Marchetti, B. Simons, and M. Szymanska, *Models of coherent exciton condensation*, J. Phys. Condens. Matter **16**, S3597 (2004).

[124] F. Chevy, *Universal phase diagram of a strongly interacting Fermi gas with unbalanced spin populations*, Phys. Rev. A **74**, 063628 (2006).

[125] R. Combescot, A. Recati, C. Lobo, and F. Chevy, *Normal State of Highly Polarized Fermi Gases: Simple Many-Body Approaches*, Phys. Rev. Lett. **98**, 180402 (2007).

[126] C. Mora and F. Chevy, *Ground state of a tightly bound composite dimer immersed in a Fermi sea*, Phys. Rev. A **80**, 033607 (2009).

[127] R. P. Feynman, *Statistical Mechanics : A Set Of Lectures* (Westview Press, 1998).

[128] F. M. Marchetti and J. Keeling, *Collective Pairing of Resonantly Coupled Microcavity Polaritons*, Phys. Rev. Lett. **113**, 216405 (2014).

[129] F. Xue, F. Wu, M. Xie, J.-J. Su, and A. H. MacDonald, *Microscopic theory of equilibrium polariton condensates*, Phys. Rev. B **94**, 235302 (2016).

[130] K. Kamide and T. Ogawa, *What Determines the Wave Function of Electron-Hole Pairs in Polariton Condensates?*, Phys. Rev. Lett. **105**, 056401 (2010).

[131] K. Kamide and T. Ogawa, *Ground-state properties of microcavity polariton condensates at arbitrary excitation density*, Phys. Rev. B **83**, 165319 (2011).

[132] J. Levinsen, G. Li, and M. M. Parish, *Microscopic description of exciton-polaritons in microcavities*, arXiv preprint arXiv:1902.07966 (2019).

[133] J. Hu, Z. Wang, S. Kim, H. Deng, S. Brodbeck, C. Schneider, S. Höfling, N. H. Kwong, and R. Binder, *Signatures of a Bardeen-Cooper-Schrieffer Polariton Laser*, arXiv preprint arXiv:1902.00142 (2019).

[134] J.-M. Ménard, C. Pöllmann, M. Porer, U. Leierseder, E. Galopin, A. Lemaître, A. Amo, J. Bloch, and R. Huber, *Revealing the dark side of a bright exciton–polariton condensate*, Nat Commun. **5**, 4648 (2014).

[135] D. Myers, B. Ozden, J. Beaumariage, L. Pfeiffer, K. West, and D. Snoke, *Pushing Photons with Electrons: Observation of the Polariton Drag Effect*, arXiv preprint arXiv:1808.07866 (2018).

[136] L. A. Jauregui, A. Y. Joe, K. Pistunova, D. S. Wild, A. A. High, Y. Zhou, G. Scuri, K. De Greve, A. Sushko, C.-H. Yu *et al.*, *Electrical control of interlayer exciton dynamics in atomically thin heterostructures*, arXiv preprint arXiv:1812.08691 (2018).

[137] Z. Dai and P. A. Lee, *Optical conductivity from pair density waves*, Phys. Rev. B **95**, 014506 (2017).

[138] P. Kirton and J. Keeling, *Superradiant and lasing states in driven-dissipative Dicke models*, New J. Phys. **20**, 015009 (2018).

[139] H. J. Hesten, R. A. Nyman, and F. Mintert, *Decondensation in Nonequilibrium Photonic Condensates: When Less Is More*, Phys. Rev. Lett. **120**, 040601 (2018).

[140] M. Radonjić, W. Kopylov, A. Balaž, and A. Pelster, *Interplay of coherent and dissipative dynamics in condensates of light*, New J. Phys. **20**, 055014 (2018).

[141] J. del Pino, J. Feist, and F. J. Garcia-Vidal, *Quantum theory of collective strong coupling of molecular vibrations with a microcavity mode*, New J. Phys. **17**, 053040 (2015).

[142] K. H. Lee, C. Lee, H. Min, and S. B. Chung, *Phase Transitions of the Polariton Condensate in 2D Dirac Materials*, Phys. Rev. Lett. **120**, 157601 (2018).

[143] F. Xue and A. H. MacDonald, *Time-Reversal Symmetry-Breaking Nematic Insulators near Quantum Spin Hall Phase Transitions*, Phys. Rev. Lett. **120**, 186802 (2018).

[144] G. J. Conduit, C. J. Pedder, and A. G. Green, *Fluctuation-induced pair density wave in itinerant ferromagnets*, Phys. Rev. B **87**, 121112 (2013).

[145] S. Lederer, Y. Schattner, E. Berg, and S. A. Kivelson, *Enhancement of Superconductivity near a Nematic Quantum Critical Point*, Phys. Rev. Lett. **114**, 097001 (2015).

[146] Z. Sun and A. J. Millis, *Transient trapping into metastable states in systems with competing orders*, arXiv preprint arXiv:1905.05341 (2019).